# ABSTRACT


| | |
|---|---|
| Title of dissertation | Functional roles of butyrophilin 1a1 and xanthine oxidoreductase in lactating mammary gland |
| | Jae Kwang Jeong, Doctor of Philosophy, 2011 |
| Dissertation directed by | Professor Ian H. Mather<br>Department of Animal and Avian Science |



Butyrophilin 1a1 (BTN) and xanthine oxidoreductase (XOR) are expressed in the lactating mammary gland and are secreted into milk in association with lipid droplets. Disruption of either the BTN or XOR gene in mice causes the accumulation of large pools of lipid in the cytoplasm, thus suggesting that both proteins may function in the accretion and/or secretion of milk-lipid droplets during lactation. Therefore, we investigated the potential functions of BTN and XOR in the lactating mammary gland of mice by molecular and cell biological approaches. The cytoplasmic domain of BTN bound to XOR *in vitro* and *in vivo* with relative high affinity, through the B30.2 domain with a 1:1 binding ratio (one XOR dimer to two BTN monomers). BTN bound to XOR via the N-terminal $Fe_2S_2$ clusters and FAD domain. BTN/XOR complexes were concentrated in the apical plasma membrane, but XOR was a soluble cytoplasmic protein in the absence of BTN in *Btn1a1*$^{-/-}$ mice. Furthermore,

knock-out of BTN gene expression led to the accumulation of XOR protein and mRNA, thus indicating that BTN negatively regulates the amount of XOR in cells. Over-expression of the B30.2 domain as a soluble protein induced a similar phenotype as that of *Btn1a1*$^{-/-}$ mice, suggesting that the B30.2 domain acts in a dominant negative manner to inhibit binding of BTN to XOR *in vivo*. Based on these data, we postulate that BTN/XOR complexes may function in milk-lipid droplet secretion by acting as a structural scaffold protein.

# Functional roles of butyrophilin 1a1 and xanthine oxidoreductase in lactating mammary gland

By

Jae Kwang Jeong

Dissertation submitted to the Faculty of the Graduate School of the
University of Maryland, College Park in partial fulfillment
of the requirements for the degree of
Doctor of Philosophy
2011

Advisory Committee:

Professor Ian H. Mather, Chair
Associate Professor Leslie Pick
Associate Professor Wenxia Song
Associate Professor Iqbal Hamza
Associate Professor Carol L. Keefer

# DEDICATION

I dedicate this dissertation to my parents, brother, and Hanhee

# ACKNOWLEDGEMENT

I would like to thank all of the people who helped me and made my graduate life successful.

First of all, I really really thank my great advisor Ian Mather. He is a great mentor. He always gave me positive feedback, when I had language or academic troubles. He usually said his memory is gone, but I think he remembers everything in our field. Whenever I needed to talk with him, he made time for me, and discussed enough. I really feel lucky to have worked with him for my past four and half years. If I have a problem in the future, the best thing that I know is to get advice from him.

I also thank Jinling Xu and Anil Kadegowda. Jinling was our technician and whenever I needed her help, she tried to help me. We worked together for 4 years, and she was kind of an elder sister to me. I think if she had not joined our lab, our progress would have been slow. Anil was our post-doc, and we worked together for two years. We discussed our project a lot, and made good progress. After he joined, we started to move in the right direction.

I thank my committee members (Leslie Pick, Wenxia Song, Iqbal Hamza, and Carol L. Keefer) too. Whenever I had a committee meeting, they gave me good advice.

I want to thank members of the Hamza lab. They allowed me to use their instruments any time.

I also want to thank Drs. Jerry Schaack and Brian Daniels. Dr. Schaack provided us with all of the recombinant adenoviral vectors and Dr. Daniels analyzed the FRAP data for us.

I always thank my parents, brother and Hanhee. They always support and encourage me to do what I want. I met my wife Hanhee during my graduate

life, and we married. She always encourages me.

It is hard to remember everything, and I am really sorry to those I have left out. Anyway, thank you all for your help and for making my graduate experience a good one.

# TABLE OF CONTENTS

# LIST OF TABLES

# LIST OF FIGURES

# LIST OF ABBREVIATIONS

| | |
|---|---|
| ADPH | adipophilin |
| Adv-mB30.2+EGFP | a recombinant adenoviral vector separately encoding EGFP and the soluble mB30.2 domain |
| Adv-B30.2$\Delta_{10}$+EGFP | a recombinant adenoviral vector separately encoding EGFP and mB30.2$\Delta_{10}$ domain |
| Adv-EGFP | a recombinant adenoviral vector encoding EGFP |
| Adv-mBTN-ECFP | a recombinant adenoviral vector encoding mouse BTN fused to ECFP |
| Adv-mBTN-EGFP | a recombinant adenoviral vector encoding mouse BTN fused to EGFP |
| Adv-mBTN-EYFP | a recombinant adenoviral vector encoding mouse BTN fused to EYFP |
| Adv-mXOR-ECFP | a recombinant adenoviral vector encoding mouse XOR fused to ECFP |
| BCA | bicinchoninic acid |
| BSA | bovine serum albumin |
| BTN | represents cow, human, and mouse butyrophilin 1A1 regardless of species |
| BTN1A1 | human butyrophilin 1A1 |
| BTN2A1 | human butyrophilin 2A1 |
| BTN3A1 | human butyrophilin 3A1 |
| CD36 | Cluster of Differentiation 36 |
| CLA | trans-10, cis-12 conjugated linoleic acid |
| CLD | cytoplasmic lipid droplet |
| CS | bovine calf serum |
| ER | endoplasmic reticulum |
| EGF | epidermal growth factor |
| ECFP | enhanced cyan fluorescent protein |
| EYFP | enhanced yellow fluorescent protein |
| EGFP | enhanced green fluorescent protein |
| FAD- EYFP | FAD of mouse XOR with EYFP at the C-terminus |

| | |
|---|---|
| FeS-EYFP | $Fe_2S_2$ centers of mouse XOR with EYFP at the C-terminus |
| FeS/FAD-EYFP | $Fe_2S_2$/FAD of mouse XOR with EYFP at the C-terminus |
| Mo-Co-EYFP | Mo-Co of mouse XOR with EYFP at the C-terminus |
| FLIP | Fluorescence loss in photobleaching |
| FRAP | Fluorescence recovery after photobleaching |
| FPLC | fast protein liquid chromatography |
| GST | glutathione *S*-transferase |
| GST-bBTNcyto | N-terminal region of the cytoplasmic domain of bovine BTN conjugated to the C-terminus of GST |
| GST-Bb30.2 | N-terminal region of the B30.2 domain of bovine BTN conjugated to the C-terminus of GST |
| GST-hBTN1A1cyto | N-terminal region of the cytoplasmic domain of human BTN conjugated to the C-terminus of GST |
| GST-hBTN1A1-B30.2 | N-terminal region of the B30.2 domain of human BTN conjugated to the C-terminus of GST |
| GST-hBTN2A1cyto | N-terminal region of the cytoplasmic domain of human BTN2A1 conjugated to the C-terminus of GST |
| GST-hBTN3A1cyto | N-terminal region of the cytoplasmic domain of human BTN3A1 conjugated to the C-terminus of GST |
| GST-hRoRet (TRIM38)-B30.2 | N-terminal region of the B30.2 domain of human TRIM38 conjugated to the C-terminus of GST |
| GST-mBTNcyto | N-terminal region of the cytoplasmic domain of mouse BTN conjugated to the C-terminus of GST |
| IBMX | 3-isobutyl-1-methyxanthine |
| mBTN | mouse butyrophilin 1a1 |
| mXOR | mouse xanthine oxidoreductase |
| Mo-Co | molybdo-pterin cofactor |
| MUC1 | Mucin1 |
| MUC15 | Mucin15 |
| MLD | Micro-lipid droplet |
| MFGM | milk fat globule membrane |
| MFG-E8 | milk fat globule-EGF factor 8 protein |
| MS | multiple sclerosis |

| | |
|---|---|
| MOG | oligodendrocyte glycoprotein |
| OCT | optimal cutting temperature |
| PAS6/7 | periodic acid Schiff glycoprotein 6/7 |
| PMSF | phenyl methyl sulphonyl fluoride |
| PBS | phosphate-buffered saline |
| pECFP-mBTN | plasmid encoding mBTN signal sequence ligated to the 5' end of ECFP with the 3'-end of ECFP ligated to the mature form of mBTN |
| pmXOR-EYFP | plasmid encoding mouse XOR with EYFP at the C-terminus |
| pmADPH-EYFP | plasmid encoding mouse ADPH with EYFP at the C-terminus |
| RIPA | radio-immunoprecipitation assay |
| ROS | reactive oxygen species |
| SDS | sodium dodecyl sulphate |
| SPR | surface plasmon resonance |
| TAG | Triacylglycerol |
| TBS | Tris-buffered saline |
| TLCK | $N^{\alpha}$-*p*-tosyl-L-lysine chloromethyl ketone |
| TPCK | $N^{\alpha}$-*p*-tosyl-L-phenylalanine chloromethyl ketone |
| WGA | Wheat germ agglutinin |
| XOR | xanthine oxidoreductase |

# Chapter 1: Introduction

The primary goal of this research was to understand the mechanism of milk-lipid secretion in the lactating mammary gland at the cellular and molecular level. In this introductory section, the mammary gland system will be reviewed, especially with regard to gland structure, and the synthesis and secretion of milk constituents.

## 1. 1. Mammary gland and formation of milk

The mammary gland is a defining characteristic of mammals that undergoes terminal differentiation during pregnancy and lactation, and that provides the neonate with essential nutrients in the form of milk during lactation (1). Development of the gland begins at embryonic day 13 in the mouse, and following birth, it continues through puberty. During puberty, growth and development of mammary gland is influenced by changes in the hormonal environment, which accompany the onset of ovarian cycling in females. The mammary gland increases in size, and the ducts extend into a glandular fat pad, but no secretory epithelium is evident. (Fig. 1.1 a). During pregnancy, the gland undergoes rapid development, and an extensive ductular tree is formed within lobular-alveolar structures (1) (Fig. 1.1 b). Progesterone from the ovaries and prolactin from the pituitary are essential for side branching and alveolar formation (2). During transition from the end of pregnancy (day 21) to the lactating phase in the mouse, the gland begins to secrete large amounts of milk. The lactating gland consists of a branched

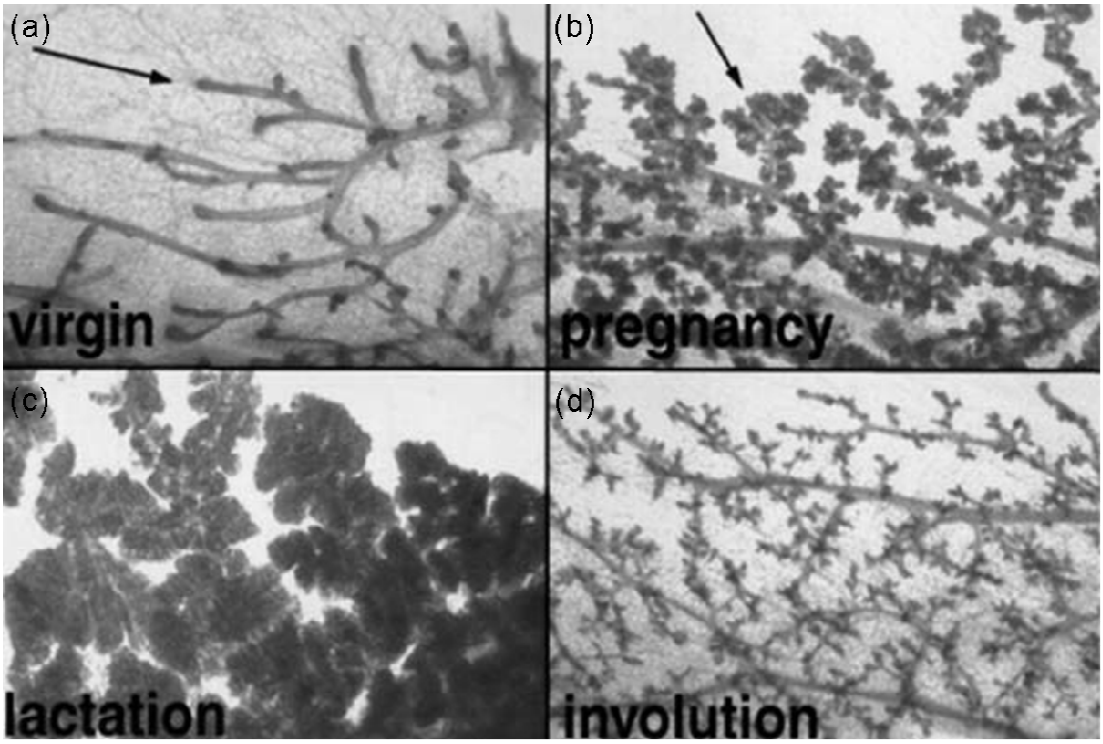


**Fig. 1.1. Mouse mammary gland development.** (a) At the onset puberty, the mammary gland increases in size, and the ducts penetrate into a glandular fat pad. (b) During pregnancy, alveolar and ductal epithelial cells proliferate and differentiate, and lobulo-alveolar structures are formed. (c) The lactating gland consists of extensive lobulo-alveolar clusters and secretes milk. (d) Involution returns the ductal structure to the non-pregnant state. Figure is from the website: http://mammary.nih.gov/atlas.

ductular network which is formed of epithelial cells ending in extensive lobulo-alveolar clusters (Fig 1.1 c) (1). Each alveolus is lined by polarized secretory epithelial cells and myoepithelial cells facing a central lumen (1) (Fig. 1.2 a). Milk is secreted from the secretory epithelial cell. The function of myoepithelial cells is to eject milk from the alveolar luminae following oxytocin-induced contraction during milk 'let-down' (Fig.1.2 a) (7). Following lactation, the mammary gland undergoes massive remodeling and the secretory cells undergo apoptosis, which results in involution of the mammary gland (Fig. 1.1 d).

Milk consists of essential constituents for neonatal survival including proteins, lipid [triacylglycerols (TAGs)], carbohydrate (lactose), ions ($K^+$, $Na^+$, $Cl^-$, and $Ca^{2+}$), water, immunoglobulins (IgG, sIgA, and sIgM), and cells (macrophages). The majority of protein in milk comprises the caseins, which are transported to the Golgi apparatus, packaged into secretory vesicles, and secreted into milk by exocytosis (6) (Fig. 1.2 b, mechanism E). However, milk-lipid is secreted by an entirely different mechanism, which is unique to the mammary gland. Synthesized lipid droplets from the endoplasmic reticulum (ER) are transported through the cytoplasm to the apex of the cell and enveloped with a layer of the apical plasma membrane (6) (Fig. 1.2 b, pathways I and II). Potential mechanisms for milk-lipid secretion will be discussed later. Milk constituents such as immunoglobulins, ions, and other proteins such as transferrin and prolactin are transported by transcytosis.

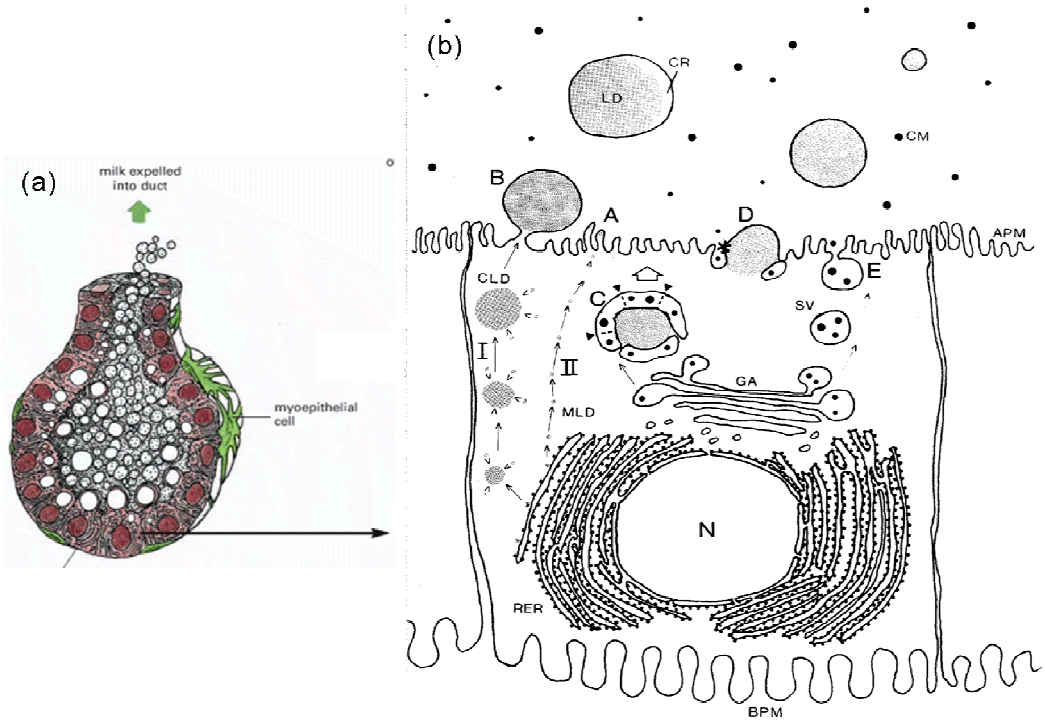


**Fig. 1.2. Mammary gland.** (a) The milk-secreting alveolus with a basket of contractile myoepithelial cells (green). Figure taken from reference (3). (b) Pathways for lipid droplet transit and secretion. MLDs (micro lipid droplets) formed in the ER fuse with each other and with larger CLDs. They are transported through cytoplasm to the apical plasma membrane, surrounded by the bilayer of the apical membrane (mechanism B), and secreted into the lumen (Pathway I). MLDs can be directly transported to the apex of the cell (Pathway II), surrounded by the apical membrane, and secreted into the lumen (mechanism A). Golgi-derived secretory vesicles surround lipid droplets, and fuse with each other to form vacuole-like structures. Subsequently, such vacuole-like structures fuse with the apical plasma membrane, and the lipid droplets are released from the cells by exocytosis (mechanism C and D) (4, 5). Caseins and other skim-milk proteins are secreted by exocytosis (mechanism E). Apical plasma membrane (APM); basal plasma membrane (BPM); cytoplasmic lipid droplet (CLD); casein micelle (CM); cytoplasmic crescent (CR); rough endoplasmic reticulum (rER); lipid droplet (LD); Golgi apparatus (GA); microlipid droplet (MLD); nucleus (N); secretory vesicle (SV) Figure taken from reference (6).

They are internalized from the basolateral membrane, sorted in endosomes, and transported to the apical plasma membrane either through specific vesicles or possibly from secretory vesicles formed in the Golgi apparatus (8, 9).

**1. 2. Origin and formation of lipid droplets**

The major lipids in milk are TAGs which comprise about 98% of the total. That the precursors of lipid droplets are formed in the ER (1, 10) is based on several lines of experimental evidence. Firstly, the activities of several acyltransferases, which esterify fatty acids in the *sn*- 1 and 2 positions of glycerol-3-phosphate were enriched in microsomal fractions from lactating rat mammary gland (11). Secondly, electron microscope radioautograpy showed that 95% of the radiolabeled fatty acids injected into rats was rapidly esterified into TAGs and that the radioautographic reactions were localized to the ER within 1 min after injection (12). No radioactivity was seen in the Golgi apparatus indicating that the formation of lipid droplets is different from the formation and secretion of casein micelles from Golgi-derived secretory vesicles (12). Interestingly, esterified fatty acids rapidly associated with visible lipid droplets suggesting either that newly synthesized TAGs rapidly associate with pre-existing lipid droplets, or that the formation of lipid droplets is very quick (12). Thirdly, in terms of phospholipid composition, surface coat materials on cytoplasmic lipid droplets (CLDs) resemble the phospholipid composition of the ER (13). Fourthly, rabbit antibody prepared against CLDs

binds to the ER as well as the surface of CLDs and micro-lipid droplets (MLDs) (precursors of CLDs, with diameters less than 0.5 μm), which suggests that the ER, MLDs, and CLDs share a number of common polypeptides, and that the formation of lipid droplets occurs in the ER (14). However, the purity of the CLD fraction used to immunize the rabbits, and specificity of the resulting antibody have been questioned. (13, 14). More convincingly, isolated MLDs from rat mammary gland have abundant ER resident proteins, such as protein disulfide isomerase, calreticulin, and immunoglobulin binding protein (Bip, GRP 78), which strongly suggests that precursors of lipid droplets are formed in the ER (15). Although the exit site of nascent droplets from the ER is controversial, the current consensus is that TAGs initially accumulate between the inner and outer bilayer halves of the ER membrane (16). This mechanism is based on the use of osmium tetroxide as a lipid stain and fixative, which highlights presumptive foci of lipid bilayer between the outer and inner halves of the ER, which are distinct from the staining characteristics of CLDs in the cytoplasm (17).

CLDs grow to more than 4 μm in diameter by the progressive fusion of MLDs (13, 14). In a cell-free system, fusion of MLDs, following release of lipid from the ER, required calcium ions at an optimal concentration of 2.5 mM and a protein complex from the cytosol (18). In addition, an exogenous supply of gangliosides enhanced fusion (18). The active protein fraction from the cytosol may be an aggregate or a complex comprising multi-subunit proteins,

because fusion of MLDs occurred with a protein fraction of more than 200 kDa prepared by gel permeation chromatography (18). This fraction comprised four polypeptides with molecular masses in a range between 15 – 20 kDa (18).

Fusion of MLDs is one possible mechanism to explain an increase in the volume of lipid droplets. However, there are other possibilities. For example, 4% or more of total neutral lipids and phospholipids are found in cytosolic fractions and much of these are associated with the fatty acid synthetase complex, which suggests that MLDs may acquire neutral lipids and phospholipids directly from the cytoplasm to form CLDs (19, 20). Interestingly, a group of GTP-binding proteins are found in the fatty acid synthase complex which suggests that GTP-binding proteins may function in the intracellular transit of lipid droplets (20). In addition, bovine fatty acid synthetase complex may contain butyrophilin 1a1, and xanthine oxidoreductase (two major proteins in the milk fat globule membrane (MFGM)) (20), but this observation does not agree with more recent immunohistochemical data on the intracellular distribution of these proteins (21-23).

### 1. 3. Intracellular trafficking of lipid droplets

As discussed above, lipid droplets are formed in the ER, and migrate from the ER to the apical plasma membrane, bypassing the Golgi apparatus. However, the mode of transit through the cell is unclear.

Microtubules are present in all mammary secretory cells, especially in the apical and medial cytoplasm in contact with small vesicles from 50 to 150 nm in diameter (24). Most of these microtubules are oriented perpendicularly to the apical plasma membrane, which suggests that they have important roles in guiding secretory vesicles and possibly lipid droplets toward the cell apex (25). Interestingly, when microtubule assembly was reversibly inhibited by the infusion of the plant alkaloids, colchicine and vincristine, into lactating goat mammary glands, both the synthesis and secretion of milk were inhibited (26). In another study, the milk fat content increased 36 – 48 hour after colchicine infusion into lactating goat mammary glands, and the diameter of the lipid droplets within the lactating cells was doubled, which suggests that colchicine does not inhibit the synthesis of milk-lipid per se, but milk-lipid secretion, such that large lipid droplets accumulate in the cells, until the effect of the inhibitor wears off (27). At this point, the accumulated lipid droplet is secreted in a wave; thus accounting for the transient rise in milk fat content and globule size following infusion (28). However, in other studies, the concentration of fat was not significantly affected by colchicine treatment, and treatment of colchicine in lactating goat mammary glands reduced the extraction of essential and non-essential amino acids, which are required for the synthesis of milk proteins (29). The drop in amino acid uptake paralleled the fall in milk protein yield, suggesting that colchicine may secondarily affect lipid secretion by affecting nutrient uptake or general cell metabolism (29). In addition,

incubation of mammary tissue fragments from lactating ewes and rabbits with colchicine did not inhibit lipid secretion, and after the immediate addition of prolactin, lipid secretion significantly increased suggesting that microtubule integrity is not required for lipid secretion (30). Incubation of lactating rat mammary explants with colchicine, *in vitro*, caused the accumulation of casein-containing secretory vesicles in the cytoplasm. However, there was little accumulation of lipid droplets. Thus, colchicine effects appear to be greater *in vivo* than *in vitro*. In summary, because of different observations and discrepancies between different studies, it is not clear what specific role microtubules may play in milk-lipid secretion.

With regard to microfilaments, skeletal muscle actin (42 kDa), clathrin, and cortactin-binding protein 1 (CortBP1) (180 kDa) are more abundant in alveolar milk-secreting cells than in contractile myoepithelial cells (31, 32). Treatment of lactating guinea pig mammary gland with cytochalasin B, a microfilament-altering drug, either inhibits lactose synthesis in the Golgi apparatus or secretion from the apical plasma membrane (33), suggesting that microfilaments are involved in the classical secretory pathway in lactation. Even though actin filaments can be identified with specific antibodies in apical regions of epithelial cells, they have not been detected on the surface of lipid globules and luminal areas of budding lipid droplets by immunofluorescence microscopy, which suggests that microfilaments may not function in lipid secretion (34). However, recent proteomic analysis of human MFGM has

shown that actin and actin-binding proteins are bound to the MFGM as well as the small GTP-binding protein RhoA, which is essential for secretory function and actin remodeling (35). Thus, the functional role of microfilaments in milk-lipid secretion is still not clear.

### 1. 4. Secretion of lipid droplets

As discussed in Fig. 1.2, the generally accepted mechanism for lipid droplet secretion in lactating mammary gland is that lipid droplets move directly toward the cell apex, and are surrounded by the apical plasma membrane, as they are released from the cell into the lumen (6, 34) (Fig. 1.2, mechanisms A and B). In an alternative mechanism, Wooding has proposed that Golgi-derived secretory vesicles containing casein micelles surround lipid droplets in the apex of the cell, and fuse with each other to form vacuole-like structures, which surround the lipid droplets. Subsequently, such vacuole-like structures fuse with the apical plasma membrane, and the lipid droplets are released from the cells by exocytosis (4, 5) (Fig. 1.2, mechanism C and D).

Most histochemical data support the apical route (34). Butyrophilin 1A1 (BTN[1]) is one of the major MFGM proteins, and is concentrated in the apical plasma membrane, not in secretory vesicles, the Golgi apparatus or the ER (34). The mucin, MUC1, is also concentrated in the apical plasma membrane

[1] Butyrophilin will be denoted as BTN for cow and human butyrophilin 1A1, and also for mouse butyrophilin 1a1.

and MFGM (22, 36). According to quantitative immunocytochemistry, analysis of guinea pig epithelial cells, the concentration of MUC1 on the apical plasma membrane and MFGM was approx. ten fold higher than on secretory vesicle membrane (36). The ratio of MUC1 on the apical plasma membrane to MUC1 on basal/lateral membranes was 99:1 (36). These data strongly suggest that milk-lipid droplets are directly enveloped by the apical plasma membrane rather than Golgi-derived secretory vesicles during secretion (4, 5).

The outer layer of the MFGM is directly derived from the apical plasma membrane (6) (Fig. 1.3 a). In electron micrographs, one face of isolated MFGM displays a membrane-like structure, but the other side of the membrane is coated with a thick layer of bound materials (37). In addition, in the process of secretion, the lipid droplet remains a constant distance of about 10-20 nm from the outer apical membrane bilayer (56). This layer is composed of proteins, and appears as a fuzzy electron dense coat in electron micrographs of isolated membrane (39, 40) (Fig. 1.3 c). Electron microscopy has shown that areas of the protein coat appear as a highly ordered paracrystalline structure with hexagonal symmetry in freeze-etched preparations (41) (Fig. 1.3 b), which suggests that integral and cytosolic proteins, resident in the apical plasma membrane, are recruited into highly ordered complexes**.**

**1. 5. MFGM proteins and their potential role in lipid droplet trafficking**

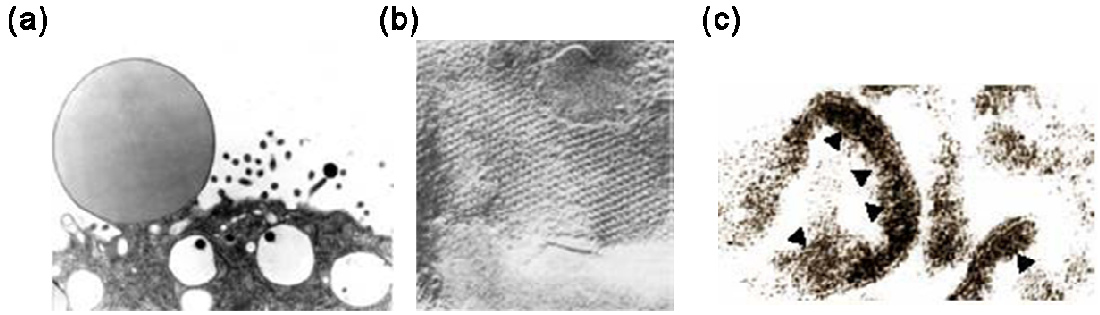


**Fig. 1.3. Electron microscopy of lipid secretion and MFGM formation.** (a) Budding lipid droplet from the apical surface of secretory cell (Mather, I. H., unpublished data). (b) Freeze-etch microscopy of inner surface of MFGM (41). (c) Electron micrograph of MFGM. Black arrowhead, dense coat on inner face of membrane (39).

**and milk-lipid secretion**

The protein composition of the MFGM has been the subject of intensive study (6), especially to identify proteins that may function in either lipid droplet trafficking or secretion. Several proteins were identified that are associated with both intracellular lipid droplets and the MFGM (42). As noted above, proteomics analysis has shown that ER resident proteins are found in both intracellular lipid droplets as well as the MFGM, which suggests either that these proteins are involved in transition from MLDs to CLDs or that they function in trafficking lipid droplets to the apical plasma membrane (42). In addition, cytoskeletal proteins were also found in intracellular lipid droplets suggesting that they may function in the transit of CLDs to the apical plasma membrane (42). The mechanisms involved in the release and scission of lipid droplets are not clear. Protein kinases, such as trimeric G protein β–subunit, may function in the secretion of lipid droplets, because the β–subunit of trimeric G proteins is enriched in MFGM, but not in CLDs (42). In addition, even though trimeric G protein is known generally as a modulator or transducer in transmembrane signaling systems, it is also involved in the calcium dependent exocytosis of secretory vesicles in pancreatic beta cells (42).

Several major MFGM proteins may play pivotal roles in the secretion of lipid droplets. Major proteins in bovine MFGM are the mucins MUC1 and MUC15, the redox enzyme, xanthine oxidoreductase (XOR), cluster of

differentiation 36 (CD36), BTN, adipophilin (ADPH), periodic acid Schiff glycoprotein 6/7 (PAS6/7), and fatty acid binding protein (FABP) (43) (Fig. 1.4).

MUC1 mucins have a type 1 orientation, and the exoplasmic domain is highly glycosylated (43). Depending upon species, they contain multiple tandem repeats, and short cytoplasmic tails (43). MUC1 is expressed in most simple secretory epithelial cells, and may protect the cell surface from physical damage and invasion by microorganisms (44). However, MUC1 deficient mice are healthy and fertile, and lactation appears to be normal, suggesting that MUC1 is not essential in the mechanism of milk secretion (44). MUC15 (formerly called PAS III) is a type 1 transmembrane protein, and like MUC1, has structural hallmarks of mucins such as a high content of serine, threonine, and proline and large quantities of carbohydrate (45, 46). The extracellular region has 11-15 sites for O or N-glycosylation (6, 46). Human and bovine MUC15 are expressed in most tissues, but the functional role of MUC15 in normal physiology is not clear (45, 47), and there is no evidence that it is involved in lipid secretion.

Xanthine oxidoreductase (XOR) is expressed in most cell types, but is expressed at very high levels in the lactating mammary gland (6). Many studies have focused on the functions and mechanisms of XOR regarding purine metabolism (48) and innate immunity (49), but the potential function of

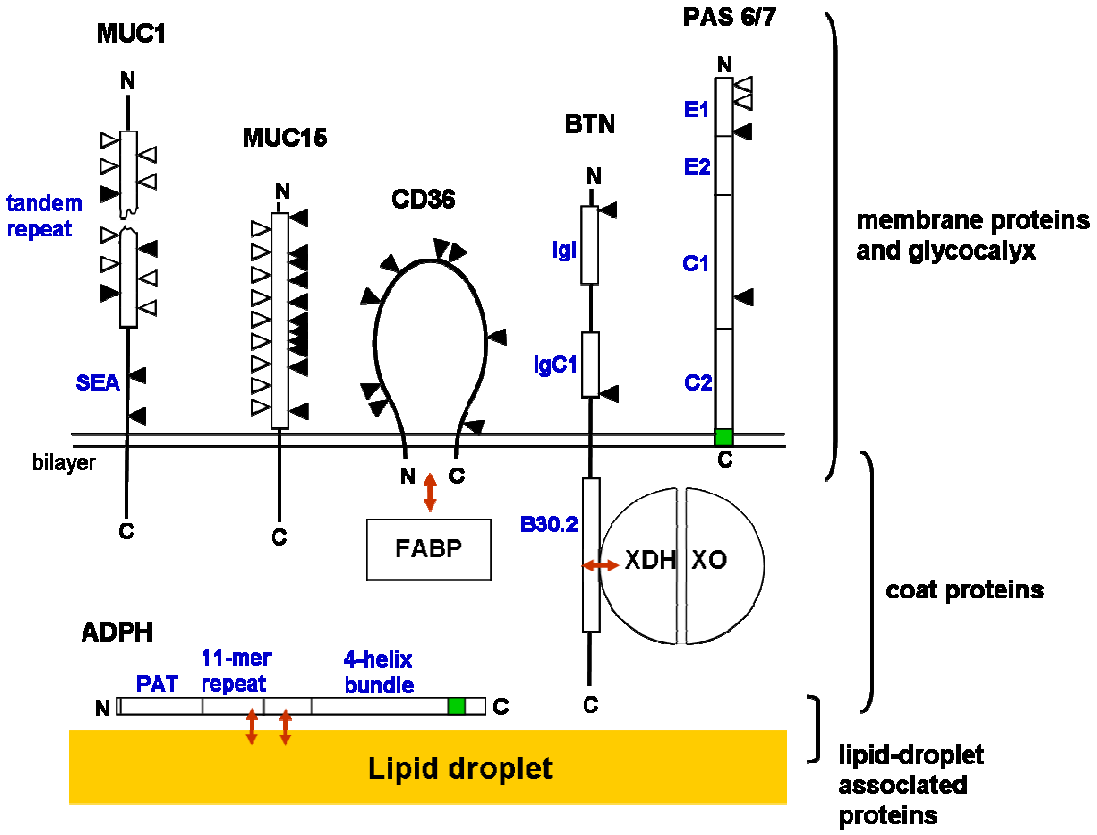


**Fig. 1.4. Predicted topology of major proteins in MFGM.** Integral proteins include MUC1, MUC15, CD36 and BTN. MUC1, MUC15 and BTN are type 1 membrane proteins. BTN is a member of the immunoglobulin superfamily with two immunoglobulin-like domains (IgI, IgC1) and a single cytoplasmic tail. XOR and adipophilin (ADPH) are peripheral membrane proteins that do not have membrane anchors. These two proteins are probably associated with the cytoplasmic face of MFGM (6). ADPH, adipophilin; BTN, butyrophilin 1A1; CD36, cluster of differentiation 36; FABP, fatty acid binding protein; MUC1, mucin1; MUC15, mucin15; PAS 6/7, periodic acid Schiff glycoprotein 6/7; XDH/XO, xanthine oxidoreductase. (Mather, I. H., in press)

XOR in milk secretion is still unclear. XOR occurs as a homodimer of 300 kDa. Each subunit contains four redox centers; a molybdenum cofactor (Mo-Co), one FAD molecule, and two $Fe_2S_2$ clusters (48). XOR is recognized as the terminal enzyme of purine metabolism, catalyzing the hydroxylation of hypoxanthine to xanthine and of xanthine to urate (48). Additionally, XOR is a potential source of reactive oxygen species (ROS), which mediate not only ischemia-reperfusion injury but also function in innate immunity (49). XOR catalyzes the oxidation of xanthine and hypoxanthine to uric acid at the molybdopterin domain and oxidation of NADH at the FAD site (48). The reduction of $NAD^+$ or molecular oxygen takes place at the FAD domain (48).

In the bovine mammary gland, most XOR is in the cytoplasm, but a small fraction is membrane bound (50). Membrane-bound XOR is released by washing with salt or nonionic detergents indicating that it is loosely associated with the membrane (50). XOR may play a crucial role in milk fat globule secretion because the expression of XOR starts to increase in mid pregnancy, sharply increases at the onset of lactation, and decreases during involution (23). McManaman et. al. have suggested that XOR is a cytoplasmic protein during pregnancy and involution, which becomes concentrated in the apical plasma membrane during lactation in association with BTN (23). This XOR/BTN complex subsequently binds to ADPH on the lipid droplet surface, thus recruiting cytoplasmic lipid droplets to the apical plasma membrane (23). However, there is no evidence that ADPH interacts with either BTN or XOR, *in*

*vivo* or *in vitro*. Interestingly, one strain of XOR-deficient mice (*Xdh*$^{+/-}$) has a lactation phenotype, in that intracellular lipid accumulates, because lipid secretion is impeded (50).

CD36 is an integral membrane protein with a molecular mass of 76 to 78 kDa (6). CD36 is highly expressed in cells that store and secrete TAGs, such as differentiated adipocytes and mammary secretory epithelial cells (51). In the mammary gland, CD36 is concentrated in the apical plasma membrane, but is also expressed on basal/lateral surfaces of secretory epithelial cells and capillary endothelial cells (6, 51, 52). The cytoplasmic segment of CD36 associates with FABP and as a complex may effect mammary gland differentiation (51). However, the possible involvement of CD36 in lipid secretion has not been studied. Phenotypic characterization of CD36-deficient mice has been reported in several tissues, but not in lactating mammary gland (53, 54).

BTN is a type 1 integral membrane protein with a molecular mass of 66,000. BTN is the most abundant protein in bovine MFGM that localizes only to the apical plasma membrane (34). Most members of the BTN gene family are type 1 integral membrane proteins (55) that may play multifunctional roles in diverse physiologies including lactation (56), selection and regulation of T-cells in the immune system (57), and modulation of autoimmune disease (58, 59). Human BTN genes consist of several subfamilies, which are BTN1A1,

BTN2A1 to 3, and BTN3A1 to 3 (60). BTN families 2 and 3 are expressed in a variety of tissues at low levels, but BTN1A1 is expressed at very high levels in the lactating mammary gland.

The exoplasmic domain of BTN comprises two Ig folds, one of the intermediate type (IgI) closest to the N terminus, and a constant type (IgC1) close to the membrane anchor (55). Recent studies have shown that the IgI fold inhibites T-cell activation (59). Also, BTN in the diet may modulate the autoimmune disease, multiple sclerosis (MS), because of structural similarity between the IgI fold of BTN and the IgV fold of myelin oligodendrocyte glycoprotein (MOG), a brain-specific autoantigen (58).

The cytoplasmic domain of BTN consists of a putative N-terminal coiled-coil domain, a B30.2 domain, and cytoplasmic tail domain (55). This intracellular region is dominated by the B30.2 domain which comprises a distorted β-sheet sandwich core structure (61, 62), that is assumed to function as a protein binding module in many proteins (61, 62). According to amino acid sequence alignments, the secondary structures of the β-strands between BTN subfamily members are similar to each other, but the loop regions are very different suggesting that the loop regions may be involved in binding to individual partner proteins (61, 62).

BTN may function in lipid droplet secretion, because ablation of BTN in

mice causes a lactation phenotype. This phenotype is very similar to that of *Xdh*$^{+/-}$ mice, in which lipid droplets accumulate in the cytoplasm, and lipid secretion is impaired. Secreted lipid droplets are much bigger and very unstable compared with those of wild type mice (56, 63).

ADPH is a member of the PAT family of proteins which binds to the outer surface of intracellular lipid droplets (6). ADPH was initially identified as adipose differentiation-related protein (ADRP), because it was thought to be only expressed in adipocytes (6, 64). However, further studies showed that ADPH is also found in many other cell types, in which synthesized lipid droplets accumulate (65). In the mammary gland, recent studies suggest that ADPH may play a role in lipid droplet secretion in association with XOR in mammary epithelial cells (23). Expression of ADPH correlates with increased formation of CLDs suggesting that there is a developmental relationship in secretory mammary epithelial cells between expression of ADPH and development of the secretory mechanism (66).

PAS 6/7 is a bovine homolog of mouse milk fat globule-EGF factor 8 protein (MFG-E8) with a molecular mass range of 43 to 58 kDa (6). MFG-E8 is present in the apical plasma membrane during lactation and is upregulated during involution, at which point it binds to phosphatidylserine on the external surface of apoptotic cells (67, 68). In *Mfge8* mutant mice, the mammary gland is inflamed and tissue remodeling is retarded during involution (67). However,

there is no known role for MFG-E8 in lipid droplet secretion.

### 1.6. Three proposed models for molecular mechanism of lipid droplet secretion

There are three proposed models for molecular mechanism of lipid droplet secretion. In one model, Mather and Keenan have suggested that BTN localizes in the apical plasma membrane and interacts with XOR (6, 43, 56). BTN and XOR are the most abundant MFGM proteins in many species, and the outer layer of the MFGM is directly derived from the apical plasma membrane (6). During secretion, BTN/XOR complexes are postulated to be required for formation of the outer envelope of the MFGM and expulsion of the lipid droplets into the lumen (6, 43, 56). Electron micrographs reveal that one face of isolated MFGM displays a membrane-like structure, but the other side of the membrane is coated with a thick layer of bound materials (37). This thick layer is composed of proteins, and appears as a fuzzy electron dense coat in isolated MFGM (39, 40). In addition, the lipid droplet remains a constant distance of 10-20 nm from the outer apical membrane bilayer in the process of lipid droplet secretion (4), thus suggesting that BTN as an integral membrane protein and XOR as a major cytosolic MFGM protein are recruited to form a layer of cytoplasmic protein, which is essential for lipid droplet secretion**.** However, this model did not specify where XOR is located, either on the lipid droplet surface, in the apical plasma membrane, or sandwiched between both places (Fig. 1.5 a).

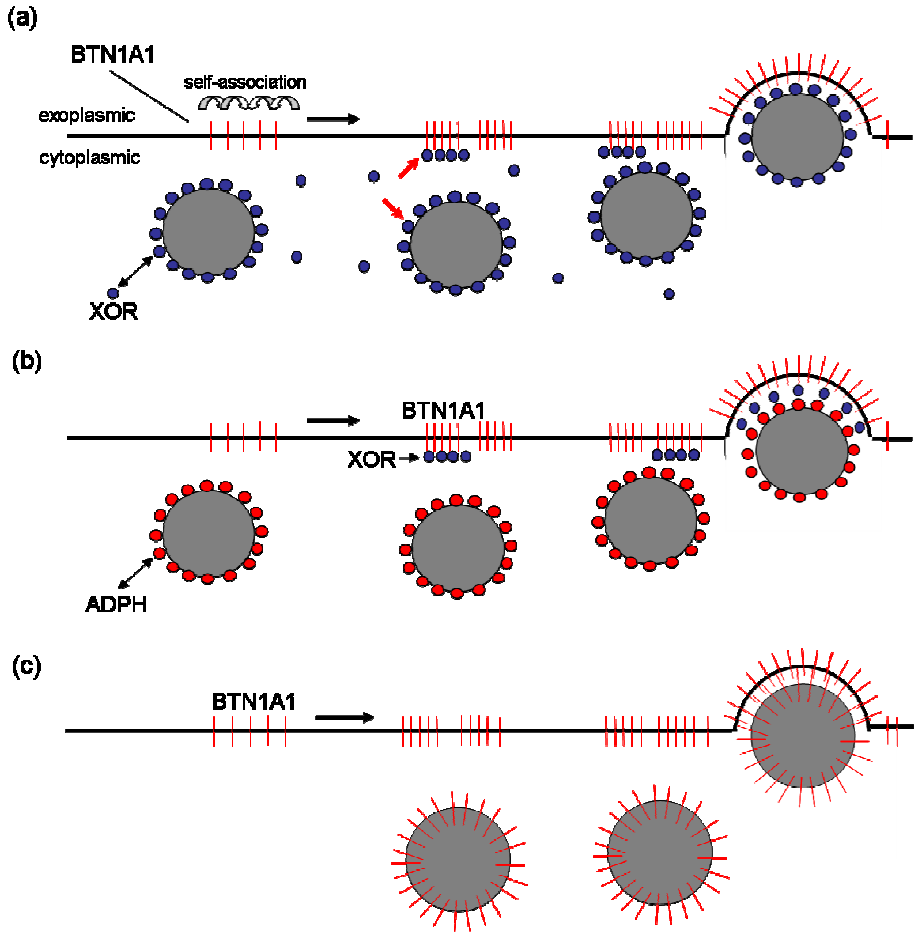


**Fig. 1.5. Three proposed models for the molecular mechanism of milk-lipid secretion.** (a) BTN in the apical membrane interacts with XOR either in the apical membrane or on the surface of the lipid droplets, and the BTN/XOR complex is required for the formation of the outer envelope of the MFGM (6, 43, 56). (b) XOR is sandwiched between BTN in the apical membrane and adipophilin (ADPH) on the surface of lipid droplet through disulfide bonds (23). (c) Milk-lipid secretion is regulated entirely by interactions between BTN molecules in both the apical membrane and the surface of lipid droplets (69).

In an alternative model, McManaman et. al. suggested that XOR is sandwiched between BTN in the apical plasma membrane and ADPH on the surface of the lipid droplet (23). The distribution of BTN, XOR, and ADPH overlap in immunofluorescence micrographs of lactating mammary tissue. However, the resolution was too low to establish their exact locations. Furthermore, they showed that disulfide bonds bridge XOR with BTN and ADPH in solubilized preparations of MFGM (Fig. 1.5 b).

In a radically different model, Robenek et. al. proposed that BTN in the MFGM is concentrated in a network of ridges, which link BTN in the outer membrane layer to BTN on the droplet surface. This hypothesis was based on freeze-fracture Immunocytochemistry, which apparently showed that BTN was more abundant on intracellular droplets than the apical membrane and that BTN was distributed in a mirror image on the droplet surface and bilayer membrane (69). Thus, in this model, milk-lipid secretion is regulated entirely by interactions between BTN molecules localized in both the apical plasma membrane and the surface of intracellular lipid droplets (56) (Fig. 1.5 c).

Even though the molecular mechanism for lipid droplet secretion has been controversial, there is convincing evidence through the use of gene-targeting knock-down techniques that both BTN and XOR play pivotal roles in lipid droplet secretion (56, 63). Ablation of the BTN gene causes severe defects in the secretion of milk-lipid, the accumulation of lipid droplets in

mammary epithelial cells (Fig. 1.6), and a discontinuous and disrupted MFGM (56) (Fig. 1.7). Furthermore, one strain of XOR-deficient mice (*Xdh*$^{+/-}$) has a similar lactation phenotype to that of *Btn1a1*$^{-/-}$ mice (Fig. 1.8) (63), which suggests that BTN may function in the lactating mammary gland by self-association and/or by binding to XOR.

To test the hypothesis that BTN specifically interacts with XOR and that the interaction has a crucial role in lipid droplet secretion and/or lipid metabolism in the mammary gland, I used biochemical and cellular approaches to identify the binding sites between two proteins. In addition, mutant mouse lines were used in attempts to identify the functional roles of BTN and XOR in lactating mammary gland. We tested the three models discussed above by:-

(1) Developing *in vivo* (cell expression) and *in vitro* (GST pull-down) protein assays to identify the binding sites between BTN and XOR.

(2) Localizing BTN and XOR in cultured cell lines, and in lactating mammary tissue from wild-type and BTN knock-out mice.

(3) Expressing the interactive domain of BTN *in vivo* using adenoviral vectors to determine whether it acts as a dominant negative inhibitor of lipid secretion in transduced cells.

(4) Attempting to 'rescue' the lactation phenotype of the BTN knockout mouse by reducing the amount milk fat and lipid droplet size by feeding conjugated linoleic acid (CLA) in the diet.

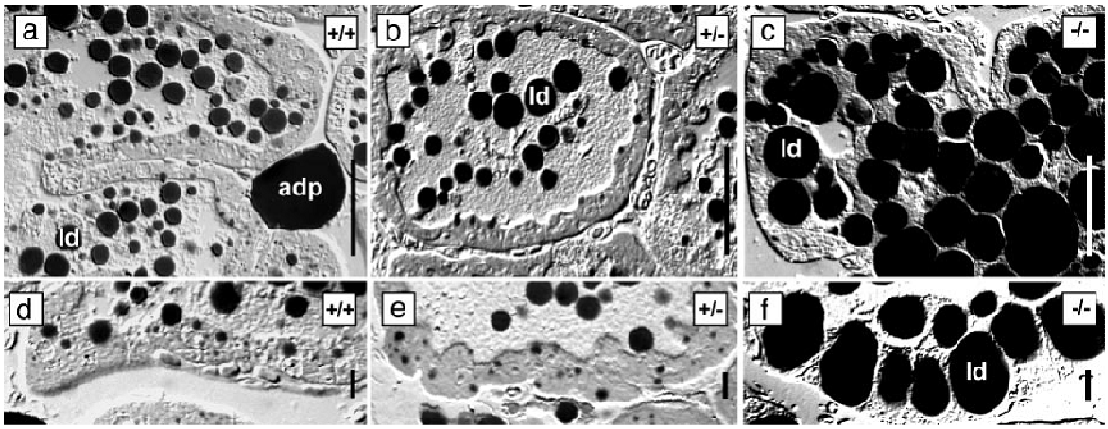


**Fig. 1.6. Light micrographs of lactating mammary tissue from Btn1a1$^{+/+}$, *Btn1a1*$^{+/-}$, and *Btn1a1*$^{-/-}$ mice.** Differential interference contrast micrographs are shown. Lipid droplets in milk and tissue (ld) and adipocytes (adp) stain black with OsO4. (Bars: 50 μm in a–c; 10 μm in d–f) (56).

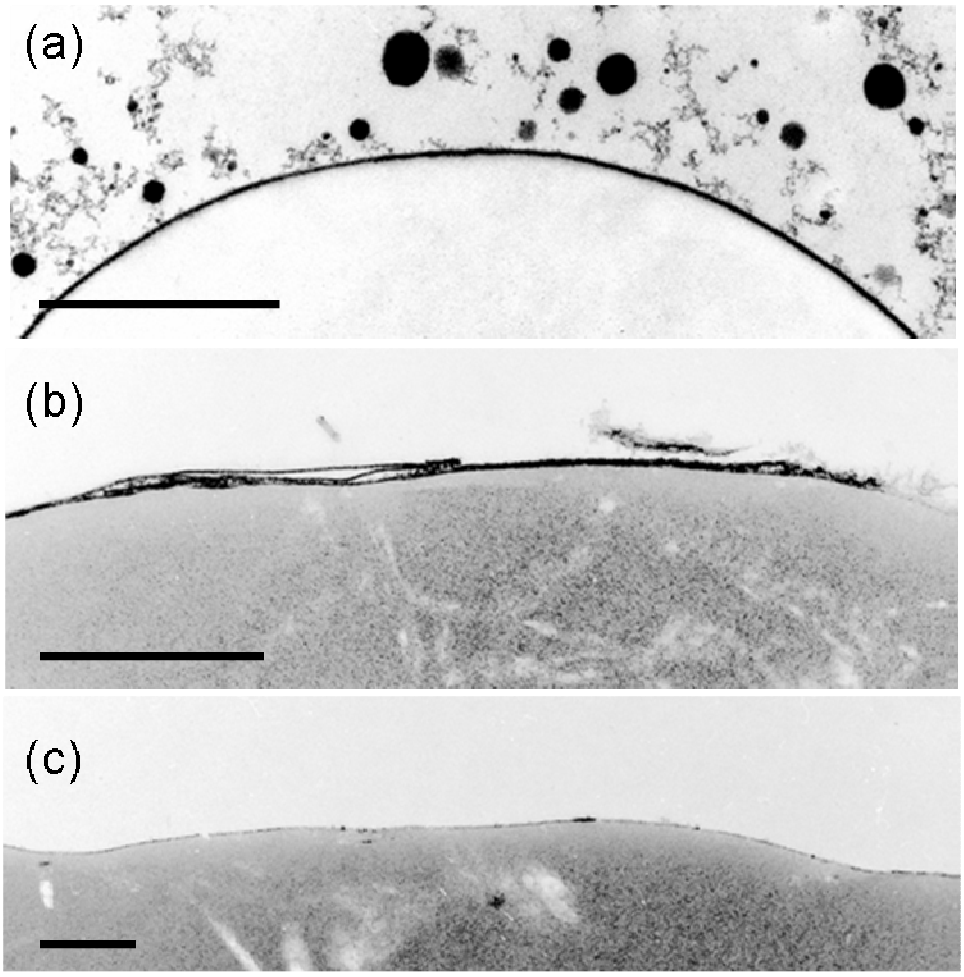


**Fig. 1.7. Electron micrographs of MFGM on lipid droplets in milk from *Btn1a1*$^{+/+}$ and *Btn1a1*$^{-/-}$ mice.** (a-c) MFGM on lipid droplets in milk. (a) micrograph of lipid droplet in wild type mice; (b, c) micrographs of lipid droplets in *Btn1a1*$^{-/-}$ mice. Bars, 1 μm (56).

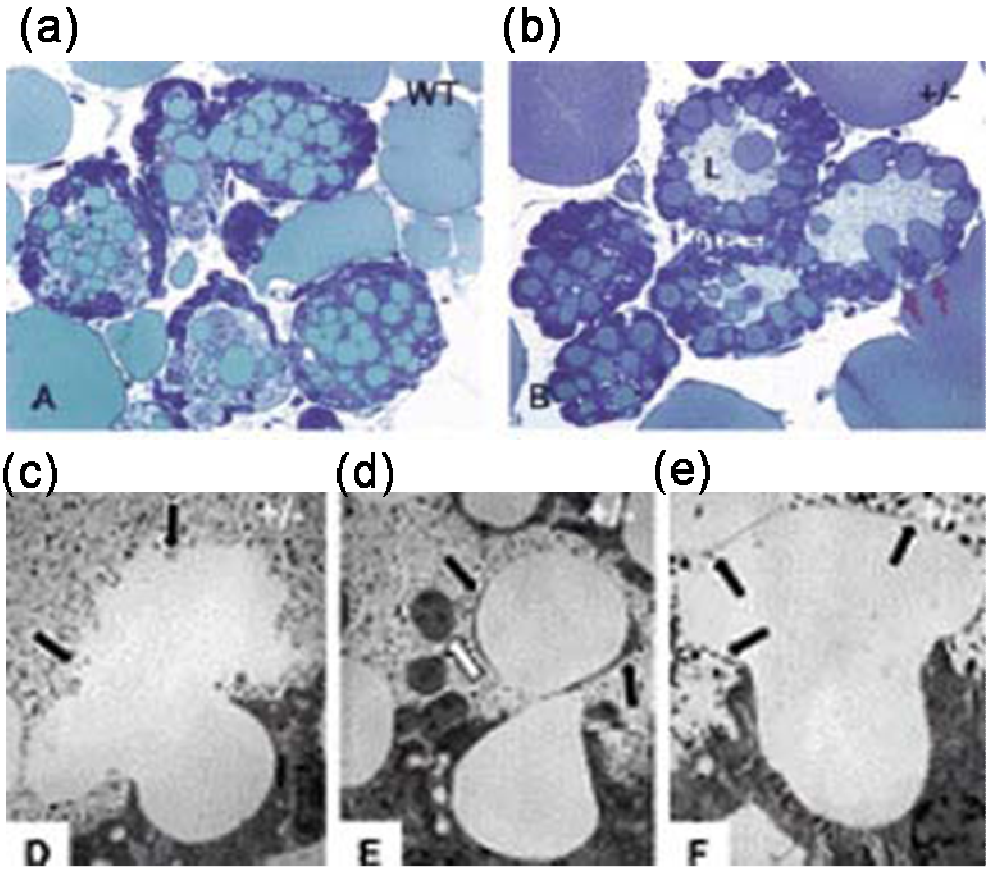


**Fig. 1.8. Histological analysis of mammary glands of wild-type and *Xdh*$^{+/-}$ mice.** (a-b) light micrographs. (a) wild-type mice, (b) *Xdh*$^{+/-}$ mice. (c-e) electron micrographs from *Xdh*$^{+/-}$ mice (63).

# Chapter 2: Materials and Methods

## 2.1. Materials

Reduced glutathione, vitamins, amino acids, pepstatin A, leupeptin, $N^{\alpha}$-*p*-tosyl-L-lysine chloromethyl ketone, $N^{\alpha}$-*p*-tosyl-L-phenylalanine chloromethyl ketone, aprotinin, digitonin, bovine serum albumin (BSA), dexamethasone, insulin from bovine pancreas, prolactin, epidermal growth factor (EGF), 3-isobutyl-1-methyxanthine (IBMX), and adjuvants were obtained from Sigma (St. Louis, MO). The ESP® yeast protein expression and purification system was from Stratagene (La Jolla, CA). Glutathione-coated beads for the purification of glutathione *S*-transferase (GST) fusion proteins, thrombin, ECL Western blot detection reagents, supplies for surface plasmon resonance (SPR), cyanogen bromide-activated Sepharose 4B, and protein A-coated Sepharose beads were from Amersham Biosciences/GE Healthcare (Pittsburgh, PA). Rabbits were purchased from Covance (Princeton, NJ). Horseradish peroxidase-conjugated goat anti-rabbit secondary antibody (blotting grade), Triton X-100, SDS, acrylamide, IQ™ SYBR® Green supermix, and bisacrylamide were from Bio-Rad (Hercules, CA). Protease inhibitor tablets were from Roche Applied Science. DNA polymerases, restriction enzymes, dNTPs, and trypsin were from Promega (Madison, WI), and phenylmethylsulfonyl fluoride and keyhole limpet hemocyanin were obtained from Calbiochem (Gibbstown, NJ). Lipofectamine 2000, rabbit anti-green fluorescent protein (GFP) antibody, goat anti-(rabbit IgG)-FITC, goat

anti-(rabbit IgG)-Alexa568, Dulbecco's modified Eagle's medium (DMEM) and Roswell Park Memorial Institute (RPMI) Medium 1640, wheat germ agglutinin Alexa fluor® 633 conjugate, Nile Red and Dulbecco's phosphate-buffered saline (PBS) were from Invitrogen (Carlsbad, CA). O.C.T compound was from Sakura Finetek U.S.A (Dublin, OH). In situ cell death detection kit, Fluorescein was from Roche (Florence, SC). All other chemicals were from Fisher. Four well LABTek chambers were from Nalge Nunc International (Rochester, NY).

## 2.2. Methods

### 2.2.1. Preparation of vectors encoding fluorescent fusion proteins of mBTN and mXOR

Total RNA was purified from lactating mouse mammary gland using TRIzol reagent (Invitrogen) and XOR and BTN cDNAs prepared by reverse transcription PCR (RT-PCR) using the SuperScript$^{TM}$ III One-Step RT-PCR kit from Invitrogen and specific primers complementary to the 5' and 3' mouse XOR and BTN open reading frames, respectively. The region of the cDNA encoding the processed form of mBTN with the N-terminal signal sequence removed was amplified with a second set of primers (Table 2.1), which introduced XhoI and XmaI restriction enzyme sites into the 5' and 3' ends, respectively, and the amplified product was cloned into the pECFP-C1 vector (Clontech Living Color vectors), which had been mutated so as to encode

**Table 2.1. Primers used for PCR**

| Vector constructed | Sequence (consecutive pairs of forward and reverse primers) |
|---|---|
| pGST-mBTNcyto | 5'-TATTACCCGGGACTTGGAAACTATACAAGG-3'<br>5'-ATATTCCCGGGTGGTGCCGCTTGGCTAGG-3' |
| pGST-mBTNcyto$\Delta_{493\text{-}524}$ | 5'-TATTACCCGGGACTTGGAAACTATACAAGG-3'<br>5'-ATATTCCCGGGGTCGTCCTGGACATTAGC-3' |
| pGST-mBTNcyto$\Delta_{480\text{-}524}$ | 5'-TATTACCCGGGACTTGGAAACTATACAAG G-3'<br>5'-ATATTCCCGGGCCCATTGGCAGTTGAAC-3' |
| pGST-mBTNcyto$\Delta_{470\text{-}524}$ | 5'-TATTACCCGGGACTTGGAAACTATACAAGG-3'<br>5'-ATATTCCCGGGCTTTTTACCACAGGACCAC-3' |
| pGST-mBTNcyto$\Delta_{269\text{-}285;\ 480\text{-}524}$ (B30.2) | 5'-TATTACCCGGGTCTAAAGAGAGACTTC-3'<br>5'-ATATTCCCGGGCCCATTGGCAGTTGAAC-3' |
| pGST-mBTNcyto$\Delta_{269\text{-}310;\ 480\text{-}524}$ | 5'-TATTACCCGGGGACACAGCCCACCCC-3'<br>5'-ATATTCCCGGGCCCATTGGCAGTTGAAC-3' |
| pGST-bBTNcyto | 5'-CTATCCCGGGAGACTATACAAGGAAAGA-3'<br>5'-CATCCCCGGGAGGCACCCCTTGGCTGGG-3' |
| pGST-bB30.2 | 5'-TATTACCCGGGTCTAAAGAGAAACTCCTG-3'<br>5'-TTAATCCCGGGCCCATCAGTGACTGGGC-3' |
| pGST-hBTNcyto | 5'-TATTACCCGGGTGGAGACTATACAACG-3'<br>5'-TTAATCCCGGGAGGTGCCCCTTGGCTGGG-3' |
| pGST-hB30.2 | 5'-TATTACCCGGGAGCTCTAAAGAGAGACTC-3'<br>5'-TTAATCCCGGGCCCATCAGCAATTGGGCAG-3' |

| | |
|---|---|
| pGST-hBTN2A1cyto | 5'-TATTACCCGGGATCAACAAACTCCAAAAGG-3' |
| | 5'-TTAATCCCGGGTAGGCTCTGGTGGGTCCC-3' |
| pGST-hBTN3A1cyto | 5'-TATTACCCGGGCAACAGCAGGAGGAAAAAAAG-3' |
| | 5'-TTAATCCCGGGCGCTGGACAAATAGTCAGG-3' |
| pGST-hRoRet B30.2 | 5'-TATTACCCGGGGAGGCTGTCTCCTTGGAAC-3' |
| | 5'-ATATTCCCGGGTTAGTCACCTGGGGGAGG-3' |
| pECFP-mBTN | 5'-TATTAGCTAGCCGCCACCATGGCAGTTCCCACCAAC-3' |
| | 5'- ATTATACCGGTGCCGAATCCAGCGTGGGCAG-3' |
| | 5'-TATTACTCGAGCCGCAGCTCCCTTCGATGTGACC-3' |
| | 5'-ATATTCCCGGGTGGTGCCGCTTGGCTAGG-3' |
| pECFP-mBTN $\Delta_{507-524}$ | 5'-TATTACTCGAGCCGCAGCTCCCTTCGATGTGACC-3' |
| | 5'-ATATTCCCGGGGTCTCCAGAAGTACAGCCTTC-3' |
| pECFP-mBTN $\Delta_{493-524}$ | 5'-TATTACTCGAGCCGCAGCTCCCTTCGATGTGACC-3' |
| | 5'-ATATTCCCGGGGTCGTCCTGGACATTAGC-3’ |
| pECFP-mBTN $\Delta_{480-524}$ | 5'-TATTACTCGAGCCGCAGCTCCCTTCGATGTGACC-3' |
| | 5'-ATATTCCCGGGCCCATTGGCAGTTGAAC-3' |
| pECFP-mBTN $\Delta_{470-524}$ | 5'-TATTACTCGAGCCGCAGCTCCCTTCGATGTGACC-3' |
| | 5'-ATATTCCCGGGCTTTTTACCACAGGACC-3' |
| pEGFP-mB30.2 | 5’-TATTACTCGAGGCTCTAAAGAGAGACTTC-3’ |
| | 5'-ATATTCCCGGGCCCATTGGCAGTTGAAC-3' |
| pmXOR-EYFP | 5'-TATTAGCTAGCATGACGAGGACAACGGTAG-3' |
| | 5'-ATATTCCCGGGGGGACCAGGCACTCCTAG-3' |

| | |
|---|---|
| FeS-EYFP | 5’-TATTAGCTAGCATGACGAGGACAACGGTAG-3’ |
| | 5’-ATATTCCCGGGCTTGGCAAAGGTCCGG-3’ |
| EYFP-FAD | 5’-TATTGCTAGCCGGAAGACGTTGCGTTTTG-3’ |
| | 5’-ATATTCCCGGGGCCCAGCTTCTGAAGCAC-3’ |
| EYFP-Mo-Co | 5’-TATTAGCTAGCGACATGGTGGGCAGGCC-3’ |
| | 5’-ATATTCCCGGGGGTGGTGAACTGATCCAC-3’ |
| EYFP-FeS/FAD | 5’-TATTAGCTAGCATGACGAGGACAACGGTAG-3’ |
| | 5’-ATATTCCCGGGGCCCAGCTTCTGAAGCAC-3’ |
| mADPH-EYFP | 5’-TTGAGGCTAGCATGGCAGCAGCAGTA-3’ |
| | 5’-TAGGCCCCGGGGCTGAGCTTTGACCT-3’ |

Primers used for qRT-PCR

| Target genes | Sequence (consecutive pairs of forward and reverse primers) |
|---|---|
| mXOR | 5’-ACACCATGAAAACCCAGAGC-3’ |
| | 5’-AAGCCTCCACCCATTCTTTT-3’ |
| reference genes | |
| slc44a3 | 5’-TGCAGAGAAAACAAGGCAAA-3’ |
| | 5’-TGAACACCAAACCAGTCCAA-3’ |
| SPG21 | 5’-GAACTGGCTTCAAGGCTAACTC-3’ |
| | 5’-GCACTCTGGTCAAACACATCC-3’ |

monomerized ECFP (enhanced cyan fluorescent protein). The signal peptide of mBTN was then inserted 5' of the ECFP gene using primers incorporating NheI and AgeI restriction enzyme sites at the 5' and 3' ends, respectively. The completed vector thus encoded the mBTN signal sequence, followed by the ECFP gene fused to the mature form of mBTN. Deletion constructs (Table 2.2) were prepared by amplifying the appropriate regions of the open reading frame of BTN using the primers listed in Table 2.1. A vector encoding mXOR with monomerized EYFP (enhanced yellow fluorescent protein) at the C terminus was constructed using primers encoding NheI and XmaI restriction enzyme sites at the 5' and 3' ends, respectively (Table 2.1 and 2.2), and the amplified product cloned into the pEYFP-N1 vector (Clontech). Vectors encoding separate domains of mouse XOR ($Fe_2S_2$, FAD, Mo-Co, and $Fe_2S_2$/FAD) and ADPH with monomerized EYFP at the C terminus were constructed using primers encoding NheI and XmaI restriction enzyme sites at the 5' and 3' ends, respectively (Table 2.1 and 2.2), and the amplified product cloned into the pEYFP-N1 vector (Clontech). All PCR products were verified by sequencing.

### 2.2.2. Cell culture

HEK 293T cells were grown in Dulbecco's modified Eagle's medium (DMEM) with glutamine, 10% FBS, 1 mM sodium pyruvate, and 1% antibiotics at 37 ℃ in a 5% $CO_2$ incubator. HC 11 cells were maintained in 10% bovine calf serum

## Table 2.2. Summary of recombinant vectors

| Vector | Protein encoded | Amino acid residues included in sequence[2] |
|---|---|---|
| **pESP1** | **GST fusion proteins with the following protein domain at the C terminus**: | |
| pGST-mBTNcyto | the cyto domain of mouse BTN1A1 | T269-P524 |
| pGST-mBTNcytoΔxxx-xxx | the cyto domain of mouse BTN1A1 with | |
| pGST-mBTNcyto$\Delta_{493-524}$ | the following residues deleted: | |
| pGST-mBTNcyto$\Delta_{480-524}$ | T493-P524 | T269-D492 |
| pGST-mBTNcyto$\Delta_{470-524}$ | P480-P524 | T269-G479 |
| pGST-mBTNcyto$\Delta_{269-310;\ 480-524}$ | P470-P524 | T269-K469 |
| | T269-P310; P480-P524 | D311-G479 |
| pGST-mBTNcyto$\Delta_{269-285;\ 480-524}$ | T269-G285; P480-P524 (mB30.2) | S286-G479 |
| pGST-bBTNcyto | the cyto domain of bovine BTN1A1 | T268-P526 |
| pGST-bB30.2 | the bovine BTN1A1 B30.2 domain | S285-G478 |
| pGST-hB30.2 | the human BTN1A1 B30.2 domain | S285-G478 |
| pGST-hBTNcyto | the cyto domain of human BTN1A1 | T268-P526 |
| pGST-hBTN2A1cyto | the cyto domain of human BTN2A1 | I269-L527 |
| pGST-hBTN3A1cyto | the cyto domain of human BTN3A1 | Q272-A513 |
| pGST-hRoRet | the B30.2 domain of hRoRet | E264-D465 |
| **Living Color Vectors** | **ECFP or EYFP fusion proteins** | |

[2] The numeric positions of amino acid residues are taken from the following sequences in the NCBI Database: mouse BTN1A1, NM 013483; mouse XOR, NM 011723; bovine BTN1A1, NM 174508; human BTN1A1, NP 001723; human BTN2A1, NM 007049; human BTN3A1, NM 007048; human RoRet, NM 006355; mouse ADPH, 11520.

| | | |
|---|---|---|
| | **with:** | |
| pECFP-mBTN | mouse BTN1A1 whole protein with ECFP at the N- terminus, after the signal sequence | M1-P524 |
| pmBTN1A1-EYFP | mouse BTN1A1 whole protein with EYFP at the C- terminus | M1-P524 |
| pECFP-mBTNΔxxx-xxx | mouse BTN1A1 with ECFP at the N-terminus, after the signal sequence and with the following residues deleted: | |
| pECFP-mBTNΔ$_{507-524}$ | K507-P524 | M1-D506 |
| pECFP-mBTNΔ$_{493-524}$ | I493-P524 | M1-D492 |
| pECFP-mBTNΔ$_{480-524}$ | P480-P524 | M1-G479 |
| pECFP-mBTNΔ$_{470-524}$ | P470-P524 | M1-K469 |
| pmXOR-EYFP | mouse XOR whole protein with EYFP at the C-terminus | M1-I1335 |
| EYFP-FeS | $Fe_2S_2$ centers of mouse XOR with EYFP at the C-terminus | M1-F165 |
| EYFP-FAD | FAD of mouse XOR with EYFP at the C-terminus | R226-R531 |
| EYFP-Mo-Co | Mo-Co of mouse XOR with EYFP at the C-terminus | S590-S1332 |
| EYFP-FeS/FAD | $Fe_2S_2$/FAD of mouse XOR with EYFP at the C-terminus | M1-R531 |
| mADPH-EYFP | mouse ADPH whole protein with EYFP at the C- terminus | |

(CS) in RPMI 1640 with 10 ng/ml insulin, 10 ng/ml epidermal growth factor and 2 mM L-glutamine. Cells were maintained at 37 °C in 95% air and 5% $CO_2$, and the medium replaced once every 2 days. Cells were split 1:6 when at or near confluency. Cells were treated with 1 μM dexamethasone, 5 μg/ml insulin, and 5 μg/ml prolactin after 2 days of growth in EGF-containing medium (10 ng/ml) to induce the expression of XOR. 3T3-L1 cells were cultured in DMEM containing 10% CS in 5% $CO_2$ at 37 ℃. Two days after complete confluency (day 0), differentiation was induced by changing the medium to DMEM containing 10% CS plus 0.0115 g/ml 3-isobutyl-1-methyxanthine (IBMX), 5 μg/ml insulin and 1 μM dexamethasone. After 48 h (day 2), the medium was replaced with DMEM containing 10% CS plus 5 μg/ml insulin. On day 4, the medium was replaced with DMEM containing only 10% CS, and cells fed with 10% CS/DMEM every two days. Full differentiation was achieved by day 8.

### 2.2.3. Cell Expression Assay for Protein Binding

HEK 293T cells were grown to 80–90% confluency in 20 x 10 x 10 mm LABTek culture chambers and co-transfected, using Lipofectamine 2000 (Invitrogen), with pmXOR-EYFP and a pECFP-mBTN vector (0.15 μg, each), encoding either full-length ECFP-mBTN or deletion constructs (Table 2.1). Cultures were incubated overnight, and the cells then washed three times

with KHM buffer (20 mM HEPES, pH 6.5, 110 mM potassium acetate, and 2 mM $MgCl_2$). Micrographs of selected cells were recorded using a Leica DMIRE2 fluorescence light microscope employing excitation wavelengths of 456 nm for ECFP and 500 nm for EYFP and separately visualizing the fluorophores between 426 and 450 nm and 488 and 512 nm, respectively. KHM buffer containing 20 μM digitonin was then added to permeabilize the plasma membrane. Soluble fluorescent fusion protein was allowed to diffuse out of the cells, and a second set of micrographs was recorded after there was no further change in the fluorescence signal (3–5 min). Transfection efficiencies were in the 50–70% range for each experiment, and ~90% of the doubly transfected cells in any one microscope field displayed the fluorescence patterns described.

### 2.2.4. Cell fractionation

Cells were suspended in 3 mM imidazole buffer, pH 7.4, containing 250 mM sucrose, 0.5mM EDTA, and proteinase inhibitors, and mechanically disrupted by passage through a 27-gauge needle (10 times). The post-nuclear supernatants were fractionated into membrane and cytosol fractions by centrifugation at 100,000 $g_{av}$ for 1 h and analyzed by Western blotting. Fusion proteins on the blots were detected with cross-reactive antibody to GFP (Invitrogen) diluted 1 to 2,500 fold, followed with a 1 to 10,000 fold dilution of goat anti-(rabbit IgG) horseradish peroxidase conjugate.

### 2.2.5. Immunoprecipitation

For immunoprecipitation from HEK 293T cells, cultures were grown in 10 cm dishes and transfected with a total of 12 g of DNA using Lipofectamine 2000. Control and transfected cells were harvested in Dulbecco's PBS (Invitrogen) with proteinase inhibitors and mechanically disrupted by passage through a 27-gauge needle a total of 10 times. The nuclei were removed by centrifugation at 1,000 $g_{av}$ for 10 min at 4 ℃, and the protein concentration of the postnuclear supernatants was adjusted to 2.4 mg/ml. RIPA buffer (2X) was then added so that the final concentrations of the constituents were protein 1.2 mg/ml, 50 mM Tris-HCl, pH 7.4, 40 mM NaCl, 1.0% (v/v) Nonidet P-40, 0.5% (w/v) sodium deoxycholate, and 0.1% (w/v) SDS. The mixtures were incubated at 4 ℃ with end-over-end stirring for 10 min, the detergent-soluble extracts were recovered by centrifugation at 16,000 x $g_{av}$ for 5 min and then precleared by incubation with protein A-coated beads at 4 ℃ for 1 h (20 μl of beads per 1.2 ml of RIPA buffer extract). To ensure optimal precipitation of potential XOR-BTN complexes, protein A-Sepharose beads (GE Healthcare) were titrated with rabbit polyclonal antibody to mXOR to determine the minimum amount of antibody required to precipitate all of the XOR from the RIPA buffer extracts. Immunoprecipitates were collected on the beads by incubating 20 μl of optimally coated XOR-antibody/protein A beads with 1.0 ml of each RIPA buffer extract, overnight, at 4 ℃ with gentle agitation. The beads were then washed three times with ice-cold PBS with proteinase inhibitors, and the bound protein was dissolved in SDS-PAGE

buffer at 95 ℃ for 3 min and analyzed by SDS-PAGE and Western blotting. For immunoprecipitations from lactating mammary tissue, total membrane fractions were collected from the postnuclear supernatants of tissue homogenates. After washing once with TBS containing proteinase inhibitors, the microsomal membranes were extracted with RIPA buffer, and the immunoprecipitations were conducted on the clarified RIPA buffer extracts, essentially as described above for HEK 293T cells. The immunoprecipitations were repeated with total membrane fractions from three wild-type (*Btn1a1*$^{+/+}$) and three *Btn1a1*$^{-/-}$ C57/Bl6 mice, all at day 10 of lactation.

### 2.2.6. Expression and Purification of Recombinant Proteins

Recombinant proteins were expressed in Schizosaccharomyces pombe, because the genome does not contain the XOR gene. Potential interactions between BTN and endogenous XOR were thus avoided. cDNAs were inserted 3' to the GST gene in the pESP-1 vector supplied with the ESP-Yeast Protein Expression and Purification System (Stratagene) (Table 2.2 for details, definitions, nomenclature, and abbreviations for the vectors used). Deletion constructs were prepared using PCR (Table 2.1 for primer pairs). SP-Q01 S. pombe cells were transformed with the completed vectors and grown in 1L cultures, as recommended by the manufacturer. In initial experiments, cells were resuspended in a mixture of 140 mM NaCl, 2.7 mM KCl, 10 mM $Na_2HPO_4$, and 1.8 mM $KH_2PO_4$ (PBS1) and lysed by vortexing with glass beads for 5–7 min in the presence of proteinase inhibitors [1 mM

phenylmethylsulfonyl fluoride, 1 μl/ml aprotinin (8.2 IU/ml), 1 μM pepstatin A, 100 μM leupeptin)] and 0.5% (v/v) Triton X-100. In later experiments, improved yields of protein (6–10 mg of protein/l) were obtained by resuspending the cells in a modified lysis buffer (150mM NaCl, 0.5mM EDTA, 50mM Tris-HCl, pH 7.4, Roche Applied Science protease inhibitors, 1mM phenylmethylsulfonyl fluoride, and 1 μl/ml aprotinin (8.2 IU/ml) and breaking the cells with a French press. Lysates were clarified by centrifugation at 17,000 x $g_{av}$ for 30 min, followed by 100,000 x $g_{av}$ for 1 h in a Beckman model XL-90 ultracentrifuge. Recombinant proteins were purified by chromatography on glutathione resins following standard procedures.

### 2.2.7. Preparation of Thrombin-cleaved Proteins

GST was removed from the recombinant proteins by digestion with thrombin (GE Healthcare). Batches of purified fusion protein (approx. 5mg) were rebound to glutathione-Sepharose beads and incubated overnight with gentle agitation at 22 ℃ in 5.0 ml of 20 mM Tris-HCl buffer, pH 8.4, containing 150 mM NaCl, 2.5 mM $CaCl_2$, and thrombin (10 NIH enzyme units/mg of fusion protein). The recombinant protein was recovered from the supernatant, and the thrombin was removed by gel filtration on Superdex 200.

### 2.2.8. *In Vitro* Glutathione Bead Binding Assay for Protein-Protein Interactions

GST fusion proteins at final concentrations of 0.01 – 2 μM were bound to

0.2 ml (packed volume) of glutathione-coated beads in 0.5–1.0 ml of 50mM Tris-HCl buffer, pH 7.4, for 3 h at 4 ℃, and the beads were then washed three times with 1.0 ml aliquots of PBS. For the binding assays, the beads were divided into 20 μl portions and incubated overnight with XOR purified from bovine milk (bXO) (0.1–2 μM, monomeric $M_r$) in a total volume of 1.0 ml at 4 ℃, with end-over-end stirring, in 1.5 ml Eppendorf tubes. The beads were then briefly washed three times with 1.0 ml aliquots of ice-cold PBS and heated to 95 ℃ in SDS-PAGE sample buffer. Aliquots of the centrifuged supernatants were analyzed by SDS-PAGE, together with known amounts of fusion protein and bXOR as standards (0.5 – 8 μg). Gels were stained with Coomassie Blue and destained in 10% (v/v) acetic acid, and amounts of fusion protein and bXOR in the samples were determined using Quantity One 1-D Analysis software (Bio-Rad). Binding was assayed either with constant amounts of fusion protein on the beads and increasing amounts of bXOR or with increasing amounts of fusion protein on the beads and saturating amounts of bXOR. Association and dissociation constants ($K_A$ and $K_D$) were determined from the binding data by non-linear regression curve fit (hyperbola) using Prism version 5.0 software (Graphpad Software Inc.).

### 2.2.9. FPLC Gel Filtration

Proteins were separated by FPLC in a Superdex 200 HR prepacked column (1 X 30 cm) equilibrated with TBS, pH 7.4. For Mr estimations, the column was calibrated using the following protein standards; thyroglobulin

(669,000), ferritin (440,000), aldolase (158,000), bovine serum albumin (67,000 and dimer), ovalbumin (43,000), chymotrypsinogen A (25,000), and ribonuclease A (13,700).

### 2.2.10. Surface Plasmon Resonance (SPR)

The binding of bXOR to GST fusion proteins in real time was evaluated by SPR using a Biacore 3000 Biosensor (GE Healthcare, Biacore, Uppsala, Sweden). Carboxymethyldextran sensor chips (CM5) in flow cells 1 and 2 were coated with 14000 –15000 resonance units (RU) of monoclonal anti-GST antibody by standard amine coupling techniques according to the manufacturer's instructions (Biacore). GST fusion proteins were captured on the chips at a level of 50 RU by injecting an aliquot of GST alone (0.5 μg/ml) into flow cell 1, and GST fusion proteins (1.0 μg/ml) into flow cell 2, respectively, in HBS-EP buffer (10mM HEPES, 150mM NaCl, 3mM EDTA, and 0.005% (v/v) surfactant p20, pH 7.4, filtered through a 0.2 μm filter and degassed before use). The kinetics of binding of bXOR to the immobilized GST fusion proteins were evaluated at a flow rate of 30 μl/min at 25 ℃ to minimize mass transport effects. bXOR at concentrations from 0 to 500 nM, in 60 ul aliquots, was injected into flow cells 1 and 2, and the association and dissociation rates were recorded for up to 6 min. To assess the effect of pH on binding kinetics, bXOR was diluted in HBS-EP buffer adjusted to pH 6.0, 6.5, 7.0, 7.4, or 8.0 with HCl or NaOH, and the association and dissociation analyses were performed as described above. The effect of salt on binding

was similarly determined by using HBS-EP buffer containing variable amounts of NaCl. Chip surfaces were regenerated by removing GST proteins with 50 μl injections of 10mM glycine-HCl buffer, pH 2.2. Sensorgrams were analyzed with BIAevaluation version 3.2 software (Biacore). Signals from the reference channel (GST) were subtracted from the channel containing GST fusion proteins to correct for refractive index changes, injection noise, and nonspecific binding to the reference surface. The signal obtained with a blank injection of HBS-EP buffer alone was then subtracted from the resulting data. Data were globally fitted to the Langmuir model for 1:1 binding and analyzed for significance by Student's t test.

### 2.2.11. Tissue extraction

Mice were killed on day 10 of lactation by asphyxiation in $CO_2$, and all of the mammary glands were excised and weighed. Three volumes of Tris-buffered saline (TBS; 10 mM Tris-HCl, 140 mM NaCl, pH 7.2) containing proteinase inhibitors [0.1 mM phenylmethylsulfonyl fluoride, 0.1 mM $N^{\alpha}$-p-tosyl-L-lysine chloromethyl ketone, 0.1 mM $N^{\alpha}$-p-tosyl-L-phenylalanine chloromethyl ketone, 1.0 ml/100 ml (8.2 IU/ml) aprotinin, and 1 mM ε-aminocaproic acid] were added per g of tissue. The tissue was minced finely and homogenized on ice using a Polytron homogenizer by giving five pulses of 10 s each at a speed setting of six. Homogenates were centrifuged at 1,000 x $g_{av}$ for 10 min at 4 ℃ to obtain sediments, operationa lly called the nuclear pellet. The postnuclear supernatants were further centrifuged at

100,000 x gav at 4 ℃ for 1 h, and the resulting po stmicrosomal supernatants and sediment membrane fractions were retained for analysis.

### 2.2.12. XOR Assays

XOR was assayed aerobically in 100 mM sodium phosphate buffer, pH 7.2, containing 10% (v/v) dimethyl sulfoxide and 150 μM xanthine at 37 ℃. The conversion of xanthine into uric acid was followed at 293 nm using a PerkinElmer Life Sciences Lambda 25 spectrophotometer. Enzyme activity (IU) was calculated using a molar extinction coefficient for uric acid under the assay conditions of 12.5 X $10^3$ $M^{-1}$ $cm^{-1}$. Protein was assayed by the bicinchoninic acid (BCA) method, using bovine serum albumin as a standard.

### 2.2.13. Immunofluorescence microscopy

Lactating mice were killed by asphyxiation in $CO_2$, and all of the mammary glands were excised. Mammary tissues were fixed in 4% paraformaldehyde, and embedded in OCT (Optimal Cutting Temperature) compound and frozen in isopentane surrounded with liquid nitrogen. The frozen tissue was sectioned into 16 μm sections. Thin sections of mammary tissue were permealized with 0.2 % Triton X-100 for 15 min. The permealized tissues were treated with blocking solution (2 % BSA in PBS/0.2% Triton X-100) for 1 h, and then incubated with primary antibody diluted 1 to 100-fold in the blocking solution for 2 h. The sections were washed with PBS 5 times, and then incubated with secondary antibody diluted 1 to 500-fold in blocking

solution for 1 h. Sections were finally washed with PBS five times and examined using a Leica TCS SP5-X Laser scanning confocal microscope. Micrographs were recorded using excitation wavelengths of 488 nm and visualizing the fluorophores between 510-525 nm for EGFP. To separately visualize ECFP and EYFP, excitation wavelengths of 458 and 512 nm, were used, respectively, and the fluorophores were visualized at emission wavelengths between 470 and 480 nm, and 525 and 540 nm.

### 2.2.14. Preparation of anti-peptide antibodies to mouse BTN and XOR

Anti-peptide antibodies to mouse BTN and XOR were prepared as either described in Kreis et. al. with modification (70) or by a commercial company (Epitomics Burlingame, CA). The peptide sequences used were as follows:- the C-terminus of mouse BTN (SGD KDTLHSKLIPFSPSQAAP), a region of mouse BTN B30.2 domain (CRENVVKKGFDPMTPDNGF), and the C-terminus of mouse XOR (QFTTLCATGTPENCKSWSVRI).

### 2.2.15. Fluorescence recovery after photobleaching (FRAP) and Fluorescence loss in photobleaching (FLIP)

Milk-lipid droplets containing expressed mBTN-EGFP were placed on coverslips, and kept at 37℃. Imaging was performed with a Leica TCS SP5-X Laser scanning confocal microscopy by using the 488 nm line of an Argon laser. A small circular area (2 μm diameter) on the surface of the droplet was photobleached at 488nm using maximum laser power. Three prebleach

images at 1 sec intervals were acquired before photobleaching. Fluorescence recovery was monitored at low laser intensity for 160 sec. FRAP experiments were performed on at least 25 milk-lipid droplets from 3 mice, and data were averaged to generate a single FRAP curve.

For FLIP analysis, milk-lipid droplets containing expressed mXOR-ECFP were placed on coverslips, and kept at 37℃. Imaging was performed with a Leica TCS SP5-X Laser scanning confocal microscopy by using the 458 nm line of an Argon laser excitation/emission with x 50 laser power. Milk-lipid droplets containing cytoplasmic inclusions and mXOR-ECFP were selected for analysis, and repetitively photobleached in a small rectangular area (2 μm diameter) at maximum laser power. Three prebleach images were acquired before photobleaching. Photobleaching was continued for 50 – 100 sec. FLIP experiments were performed on at least 6 milk-lipid droplets from 4 mice.

### 2.2.16. Quantitative Real Time Polymerase Chain Reaction (qRT-PCR)

cDNA was prepared to test selected genes: mouse XOR, slc5a8, Tnfrsf12a, Apaf1, FAS, MFG-E8, ADPH, ATP1B1, slc44a3, and SPG21. Each cDNA was synthesized using a SuperScript™ III One-Step RT-PCR kit from Invitrogen. For qRT-PCR analysis, 4 μl of diluted cDNA were combined with 15 μl of a mixture composed of 10 μl 1x SYBR Green master mix (IQ™ SYBR® Green Supermix), 0.8 μl each of 10 μM forward and reverse primers, and 4.4 μl DNase/RNase free water in a 96 well iCycler iQ Real-time PCR

Detection system (Bio-Rad). Each sample was run in triplicate and a 4-point relative standard curve (4-fold dilution) plus the non-template control were used. The reactions were performed in the following conditions: 2 min at 50 ℃, 10 min at 95℃, 40 cycles of 15 sec at 95℃, and 1 min at 60℃. The presence of a single PCR product was verified by the dissociation protocol using incremental temperatures to 95℃ for 15 sec p lus 65℃ for 15 sec. Data were analyzed with 7900 HT Sequence Detection Systems Software (version 2.2.3, Applied Biosystems).

### 2.2. 17. Transduction of mouse mammary glands *in vivo*

Mice were anesthetized by the intraperitoneal injection of avertin at a dosage of 125 to 250 mg/kg body weight. Glands were washed with 70% ethanol and distilled water. Glass micropipettes for infusion were prepared by pulling the glass tip over a Bunsen flame into a fine tip of 60 to 75 μm and the ends fire-polished to remove sharp edges. A stock of adenoviral vector (1.0 x $10^7$pfu/ml) was made by diluting the original adenoviral vector stock with storage buffer (10 mM Tris-HCl, pH 7.5, 10 mM histidine, 75 mM NaCl, 1 mM $MgCl_2$, 100 μM EDTA, 0.5% v/v EtOH, 50% v/v glycerol). Final doses (1.0 x $10^7$ pfu) for number 4 mammary glands, as described by Russell. *et al*, (71) were made by diluting the 1.0 x $10^7$ pfu/μl stock with 90 μl of sterile filtered Ringer's solution (156 mM NaCl, 8.1 mM $Na_2HPO_4$, 1.2 mM $K_2HPO_4$, 2.7 mM $KH_2PO_4$, 0.9 mM $CaCl_2$, 0.5 mM $MgCl_2$). This dilution was made immediately before the infusion to ensure the stability of the vectors. The solution was

loaded into a 50 μl glass micropipette, the tip was gently inserted into the nipple canal, and the solution was slowly injected into the luminal tissue spaces. Micropipettes were washed three times each with Ringer's solution, 70% ethanol and filtered Ringer's solution between each vector infusion. Each gland was infused two times with 50 μl aliquots of vector, for a total of 100 μl per gland.

### 2.2.18. Animal care

C57BL and CD1® mice were maintained on Formulab Diet 5008 (PMI Nutrition International, Richmond, IN), and water was available ad libitum. The knock-out BTN strain was created as described by Ogg et. al. (56), and the Xdh-deficient strain was obtained from T. Finkel (NIH) (24). CD1® mice were purchased from Charles River Inc (Wilmington, MA). and were used for infusion of adenoviral vectors. The first full day after parturition was counted as day 1 of lactation, and litters were adjusted to six pups for each experiment.

### 2.2.19. Conjugated linoleic acid (CLA) study

Two groups of lactating mice (Btn1a1$^{+/+}$ and *Btn1a1*$^{-/-}$) were fed either a control diet containing oleic acid (20g/kg), or a CLA diet, in which 6.67 g/kg oleic acid was replaced with 6.67g/kg CLA from day 6 to day 10 of lactation. Litter size was adjusted to 6 pups for each mouse. Milk samples were collected on day 10 of lactation and milk lipid percentage (*vol/vol*) was estimated by crematocrit (72).

### 2.2.20. Apoptosis

Tissue sections from Btn1a1$^{+/+}$, *Btn1a1*$^{-/-}$, mice at day 10 of lactation and Btn1a1$^{+/+}$ mice at day 2 of involution were analyzed by the TUNEL assay to identify apoptotic cells. Tissue sections were fixed in 4% paraformaldehyde, and prepared as described in the manufacture's manual (In situ Cell Death Detection Kit, Fluorescein; Roche). Mammary tissue at day 10 of lactation was fixed as described in Section 2.2.13 and cut into 10 μm frozen sections. Sections were incubated with specific antibody to mouse cleaved caspase-3, followed by goat anti-(rabbit IgG)-Alexa568 as secondary detecting agent.

### 2.2.21. Purification of XOR

XOR was purified from bovine milk by the method of Sullivan *et al.* (73), omitting Triton X-100 from the electrofocusing step.

# Chapter 3: Determination of the physical interaction between BTN and XOR

## 3.1. Rationale

BTN and XOR are abundant proteins in the milk of most species (6, 21, 23, 34). BTN is a major integral protein found in the MFGM, which localizes to the apical plasma membrane (34, 37, 55). XOR is expressed in most cell types and at very high levels in the secretory epithelial cells of the lactating mammary gland (6, 74, 75). Ablation of the BTN gene causes severe defects in the secretion of milk-lipid and lipid droplets accumulate in the cytoplasm, which suggests that BTN is essential for the regulated secretion or metabolism of lipid droplets during lactation (56). In addition, one strain of XOR-deficient mice (*Xdh*$^{+/-}$) has a similar phenotype to *Btn1a1*$^{-/-}$ mice (63). Therefore, BTN may function in lipid droplet secretion and/or lipid metabolism in the mammary gland by specifically binding to XOR. To determine whether the two proteins interact, and if so, to identify the binding sites, we developed *in vivo* cell expression and *in vitro* GST pull-down protein binding assays.

## 3.2. *In vivo* cell expression assay using HEK 293T cells

In order to determine the domain in BTN which binds to XOR, an *in vivo* cell expression assay was devised, in which fluorescent fusion proteins of mouse BTN (mBTN) and mouse XOR (mXOR) were expressed in HEK 293T cells, and transfected cells were treated with digitonin (Fig. 3.1). Digitonin

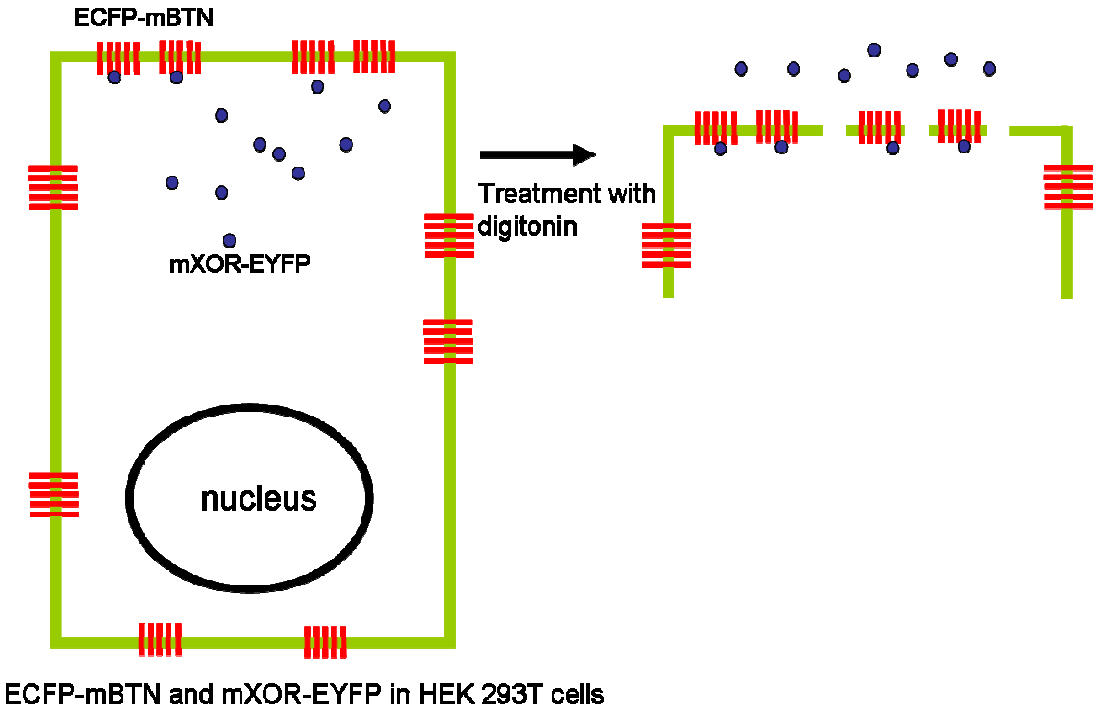


**Fig. 3.1. Experimental scheme to analyze the localization of BTN and XOR.** Cells were co-tansfected with a plasmid encoding ECFP-mBTN and mXOR-EYFP, and treated with digitonin to remove unbound cytoplasmic protein. Most of the cytoplasmic mXOR-EYFP was washed out of the cells after treatment with digitonin, but mXOR-EYFP bound to ECFP-mBTN remained in the plasma membrane. The distribution of expressed ECFP-mBTN and mXOR-EYFP was determined by fluorescence or confocal microscopy.

generates pores in membranes by binding to cholesterol, which is a major sterol in the plasma membrane. Thus, after digitonin treatment, most soluble cytoplasmic proteins are washed out, but proteins trapped or bound to organelles remain in the cells (Fig. 3.1).

Vectors were prepared encoding mBTN (mBTN signal sequence, followed by ECFP fused to the mature form of mBTN) (pECFP-mBTN), and mXOR fused at the C-terminus to EYFP (pmXOR-EYFP) (Fig. 3.2). In HEK 293T cells transfected with pECFP-mBTN, ECFP-mBTN was expressed and localized to the plasma membrane as expected, but was also expressed in intracellular sites (Fig. 3.3 a-c). The intracellular site was close to or associated with the trans-Golgi network, because mBTN-EYFP co-localized with the Golgi apparatus marker, galactosyltransferase-ECFP (Fig 3.3 a-c). In contrast, mXOR-EYFP was expressed throughout the cytoplasm (Fig. 3.3 d). That both ECFP-mBTN and mXOR-EYFP were expressed as full-length proteins was confirmed by Western blot (Fig. 3.3 e). Furthermore, as expected, ECFP-mBTN was in the membrane fractions (Fig. 3.3 e, lane 2), and mXOR-EYFP was in the soluble cytoplasmic fractions (Fig. 3.3 e, lane 6). Both expressed proteins were of the expected size (95 kDa for ECFP-mBTN, and 175 kDa for mXOR-EYFP) with little evidence of degradation. That mXOR-EYFP was expressed in the cytoplasm was confirmed by treatment of the cells with digitonin to permeabilize the cells and wash out soluble, cytoplasmic proteins. As expected for a membrane protein, ECFP-mBTN remained in the plasma membrane and in intra-cellular organelles after

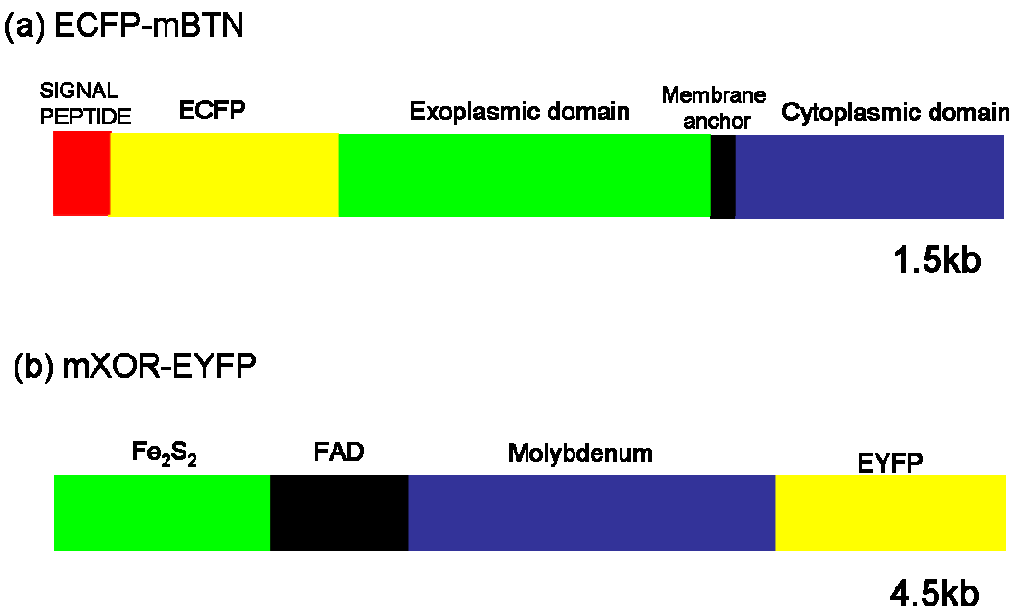


**Fig. 3.2. Constructs used for cell expression protein-binding assay.** (a) A vector was prepared encoding fluorescent mBTN by ligating cDNAs in the following order; cDNA encoding mBTN signal sequence was ligated to the 5' end of ECFP, and the 3'-end of ECFP was ligated to the mature form of mBTN (pECFP-mBTN). (b) A vector encoding fluorescent mXOR was prepared by ligating cDNA encoding mXOR to the 5' end of EYFP (pmXOR-EYFP).

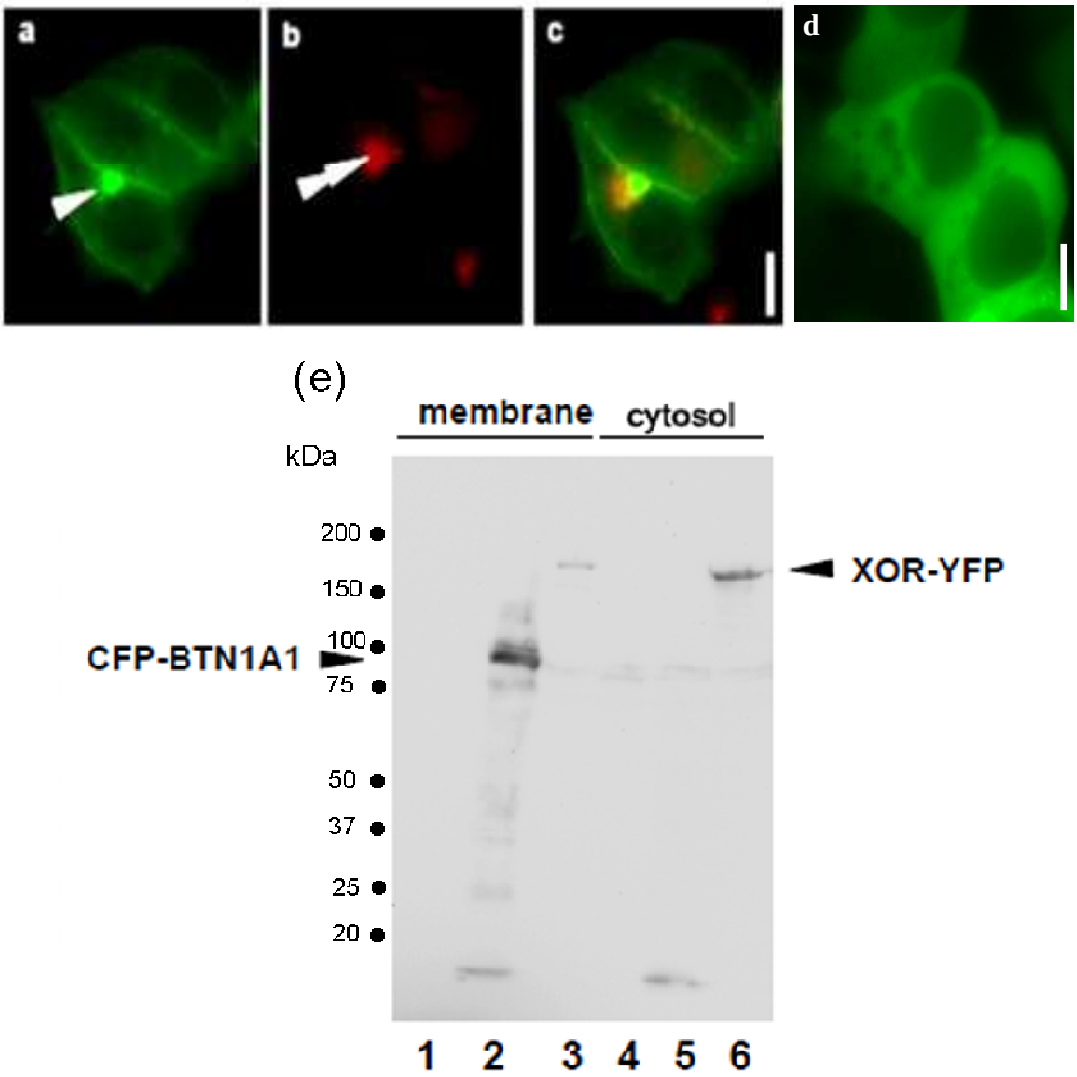


**Fig. 3.3. Expression of mBTN-EYFP and mXOR-EYFP in HEK 293T cells.** (a-c) Localization of a fraction of mBTN-EYFP in the plasma membrane and intracellular membranes close to the Golgi apparatus, and (d) localization of mXOR-EYFP in the cytoplasm. Cells were co-transfected with (a) pmBTN-EYFP and (b) p-galactosyl- transferase-ECFP. (c), merged image. Cells were transfected with (d) pmXOR-EYFP. (e) Cell fractions were analyzed by Western blot (50 μg protein/lane) using antibody to GFP. Lanes 1-3, membrane fractions; lanes 4-6, cytosol fractions. Lanes 1 and 4, untransfected control cells; Lanes 2 and 5, cells transfected with pECFP-mBTN; lanes 3 and 6, cells transfected with pmXOR-EYFP. Bars, 10 μm.

treatment with digitonin (Fig. 3.4 a-b). However, all of the mXOR-EYFP in the cells was removed by digitonin treatment (Fig. 3.4 c-d). To identify potential interactions between the two proteins, HEK 293T cells were transfected with pECFP-mBTN and pmXOR-EYFP together, and the cells were treated with digitonin. Even after treatment with digitonin, some of the expressed mXOR-EYFP co-localized with ECFP-mBTN at the plasma membrane and Golgi region (Fig. 3.5).

### 3.3. Co-immunoprecipitation in HEK 293T cells

To determine whether the two proteins are physically bound to each other *in vivo*, total detergent extracts of transfected HEK 293T cells were immunoprecipitated with antibody to mXOR. Expressed mXOR-EYFP was specifically precipitated with antibody to mXOR (Fig. 3.6, lane 2-4), and as a control, expressed GFP was not co-precipitated with expressed mXOR-EYFP (Fig. 3.6, lane 3, 5). Using a specific antibody to the C-terminus of mBTN (56), mBTN was detected on blots of immunoprecipitates from cells transfected with plasmids encoding both ECFP-mBTN and mXOR-EYFP (Fig. 3.6, lane 4), thus confirming that mBTN and mXOR interact *in vivo*. Untransfected cells served as a control (Fig. 3.6, lane 1).

### 3.4. *In vivo* cell expression assay with mutated forms of mBTN

To determine which region of the cytoplasmic domain of mBTN is required for the interaction with mXOR, plasmids encoding mutated forms of ECFP-mBTN

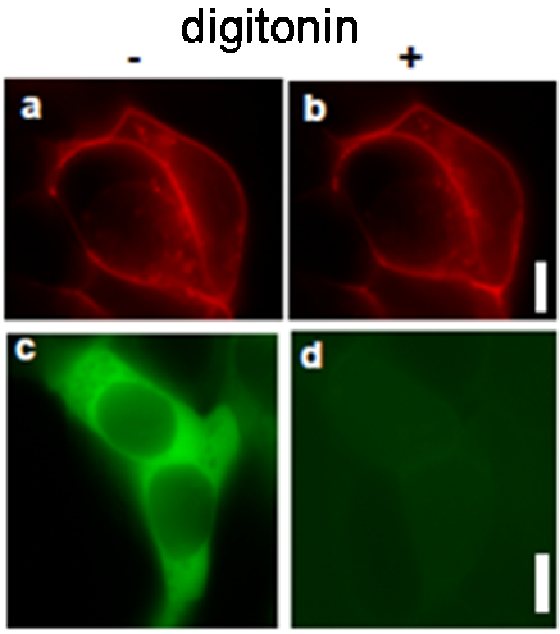


**Fig. 3.4. *In vivo* cell expression assay: expression of ECFP-mBTN and mXOR-EYFP in HEK 293T cells.** (a-d) Cells were transfected with either pECFP-mBTN (*a* and b) or pmXOR-EYFP (c and d) before (-) (a and c), and after (+) (b and d), treatment with digitonin. Bar, 10 μm.

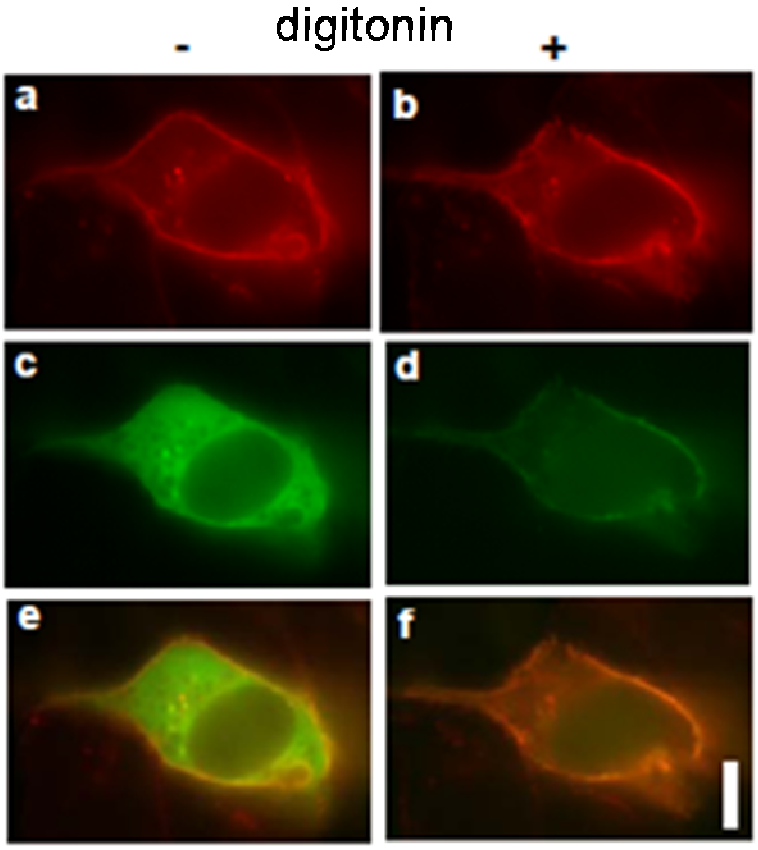


**Fig. 3.5. Co-localization of ECFP-mBTN and mXOR-EYFP in HEK 293T cells.** (a-f) Cells were co-transfected with pECFP-mBTN and pmXOR-EYFP. (a, c, and e), before (-); (b, d, and f), after (+) treatment with digitonin. Shown is the fluorescence signal for ECFP-mBTN (a and b), mXOR-EYFP (c and d), and merged image (e and f). Bar, 10 μm

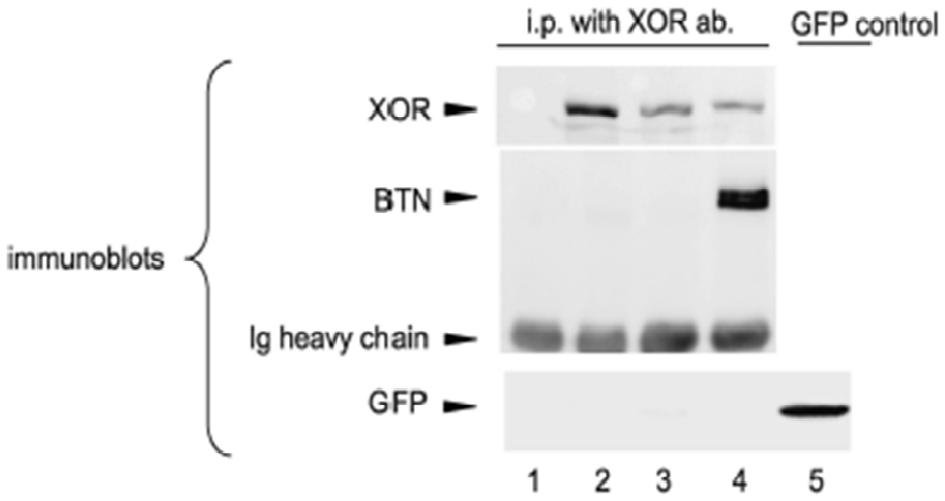


**Fig. 3.6. Immunoprecipitation of ECFP-mBTN and mXOR-EYFP complexes in HEK 293T cells.** Cells were co-transfected with pECFP-mBTN and pmXOR-EYFP in HEK 293T cells. Proteins were immunoprecipitated (i.p.) from RIPA buffer extracts with antibody to mXOR, separated by SDS-PAGE (6% polyacrylamide gel), and first blotted with antibody to mBTN (middle blot). The blot was then stripped and reprobed with antibody to mXOR (top blot). Aliquots of the same immunoprecipitates were also separated by SDS-PAGE on a 10% polyacrylamide gel to resolve GFP (bottom blot). Immunoprecipitates from non-transfected cells (lane 1), cells transfected with pmXOR-EYFP (lane 2), pmXOR-EYFP and a vector encoding GFP (lane 3), and pmXOR-EYFP and pECFP-mBTN (lane 4). The RIPA buffer extract used for the immunoprecipitation of mXOR-EYFP and GFP was separated in lane 5 to validate the antibody to GFP (GFP control).

were co-transfected and expressed with pmXOR-EYFP in HEK 293T cells. The cytoplasmic domain of BTN comprises three domains; a coiled coil domain (stem region), the B30.2 domain, and cytoplasmic tail domain (Fig. 3.7). ECFP-fused cytoplasmic domain-less BTN (ECFP-mBTN$_{\Delta 269\text{-}524}$) did not co-localize with mXOR-EYFP in the plasma membrane, and all expressed protein was washed out of the cell following digitonin treatment. (Fig. 3.8, panel 1). Serial deletion of the C-terminal region of ECFP-mBTNcyto showed that the entire tail domain (480-524) is unnecessary for binding to mXOR-EYFP (Fig. 3.8, panel 2). However, removal of the first C-terminal ten amino acid residues (470-479) in the B30.2 domain resulted in abnormal localization of ECFP-mBTN in intracellular vesicles and abrogated binding to mXOR-EYFP (Fig. 3.8, panel 3). These results indicate that the B30.2 domain of BTN is a potential binding domain with XOR.

### 3.5. Glutathione/GST pull-down assays between the cytoplasmic domain of BTN and purified bovine XOR

The interaction between the cytoplasmic domain of BTN and XOR was confirmed by glutathione-S-transferase (GST) pull down assays. The N-terminal region of the cytoplasmic domain of BTN was conjugated to the C-terminus of GST and the GST fusion proteins bound to glutathione/agarose beads. XOR purified from bovine milk (bXOR) was used as a potential binding partner. Binding of bXOR to the whole cytoplasmic domain of mouse BTN (GST-mBTNcyto) was saturable with apparent $K_D$s in the 50 nM range (Fig.

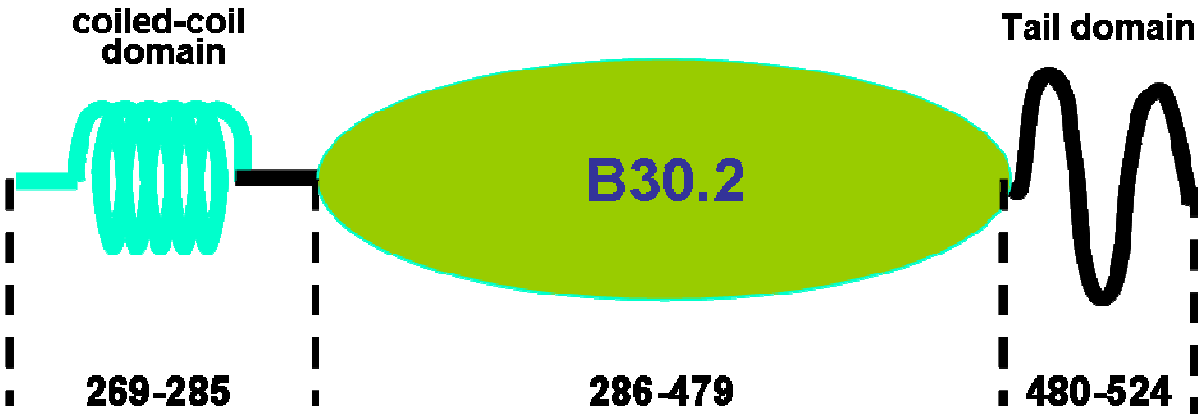


**Fig. 3.7. Domain structure of the cytoplasmic domain of mouse BTN.** The cytoplasmic domain of BTN comprises three domains; a coiled coil domain (stem region), the B30.2 domain, and cytoplasmic tail domain

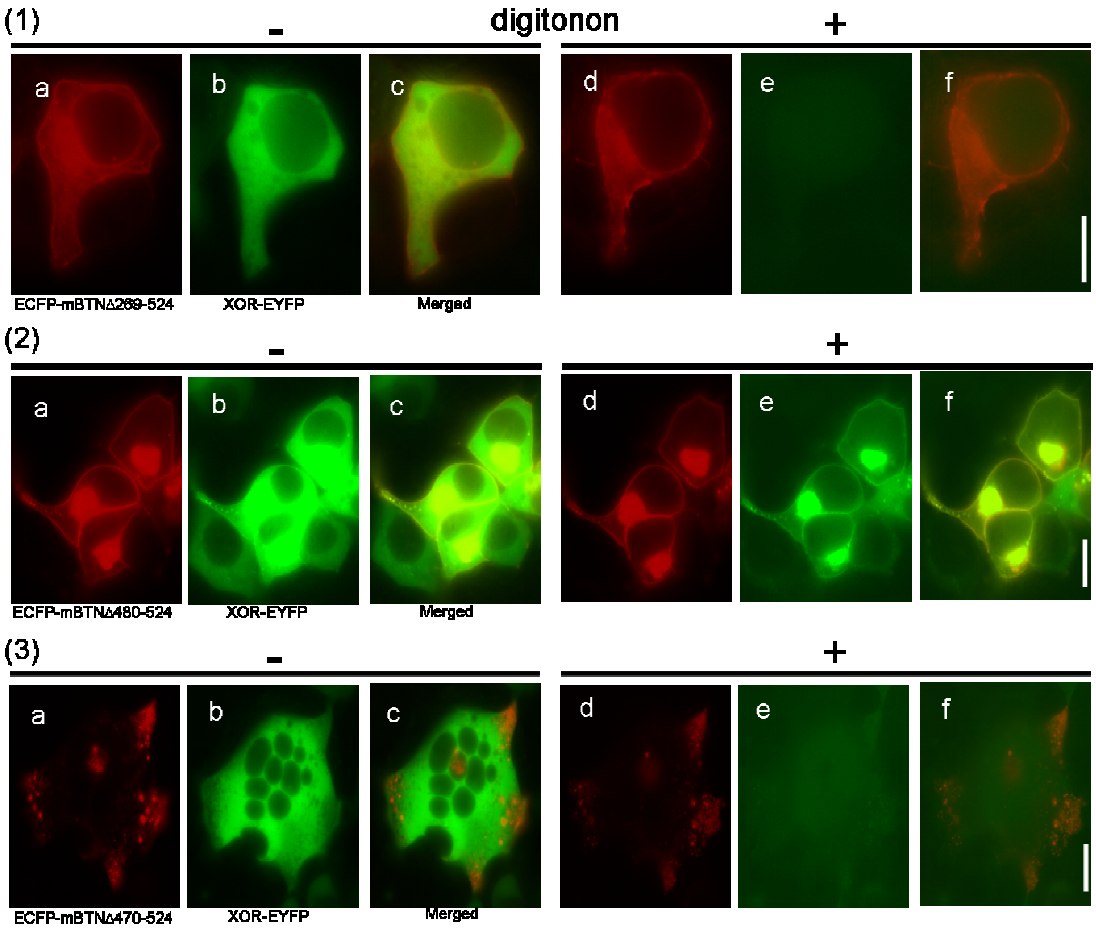


**Fig. 3.8. *In vivo* cell expression assay with mutated forms of mBTN.** (1-3) Co-expression of full-length mXOR and mutated forms of mBTN in HEK 293T cells. In each panel, (a-c) before digitonin, (d-f) after digitonin. (1) ECFP-mBTN$_{\Delta 269\text{-}524}$ (a and d) and XOR-EYFP (b and e); (2) ECFP-BTN$_{\Delta 480\text{-}524}$ (a and d) and XOR-EYFP (b and e); (3) ECFP-mBTN$_{\Delta 470\text{-}524}$ (a and d) and XOR-EYFP (b and e). In each panel, (c and f, merged images). Bars, 10 μm.

3.9). Consistent with results from the cell expression protein binding assay, deletion of the tail domain of mBTNcyto (Δ480-524) had no effect on the binding of bXOR at saturating concentrations of bXOR (Fig. 3.10 a, lane 4; compare with controls in lanes 1, 2). In addition, the stem region (269-285) did not have a role in binding to bXOR (Fig. 3.10 a, lane 7). However, deletion of 10 amino acids (Δ470-479) from the C-terminal region of the B30.2 domain and deletion of 25 amino acids (2 putative α-helix domains) (Δ286-310) from the N-terminal region abrogated the interaction (Fig. 3.10 a, lanes 5, 6). Most significantly, the B30.2 domain alone was sufficient for binding to bXOR (Fig. 3.10 a, lane 7). Bead binding and cell expression protein binding assays for interaction between mouse or bovine XOR and wild type or mutated forms of mBTNcyto are summarized in Fig. 3.11.

### 3.6. SPR to determine the affinity and kinetics of binding between XOR and BTN

The binding of bXOR to GST-fused BTN in real time was evaluated by SPR using a Biacore 3000 Biosensor. The binding constant ($K_D$) was calculated by measuring the association and dissociation rates ($K_D = k_d / k_a$). Ligand (GST-fusion proteins) was immobilized on a glutathione-coated SPR chip in a microflow cell, and then saturating amounts of analyte (bXOR) was injected over the ligand layer. As the analyte bound ligand, an increase in SPR signal (expressed in response units, RU) was observed. After a desired association time (saturation), a solution without the analyte (the buffer only) was injected,

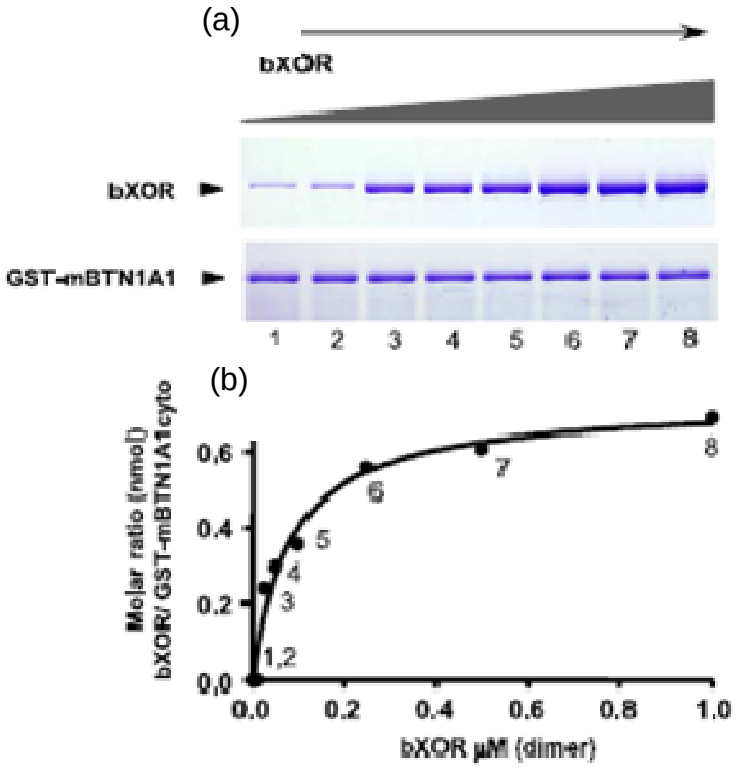


**Fig. 3.9. Glutathione/GST pull-down assays between the cytoplasmic domain of mBTN and purified bovine XOR.** Glutathione/agarose beads were loaded with GST-BTN fusion proteins and saturated with bXOR. After washing with PBS, the beads were boiled in SDS-PAGE buffer and the eluted proteins separated by SDS-PAGE. (a) Binding between GST-mBTNcyto (0.1 nmol) and increasing amounts of bXOR (0 –1.0 µM dimer), to determine the $K_D$ and stoichiometry at maximal binding. (b) Densitometric data derived from the gels shown in (a). (collaboration with Jinling Xu)

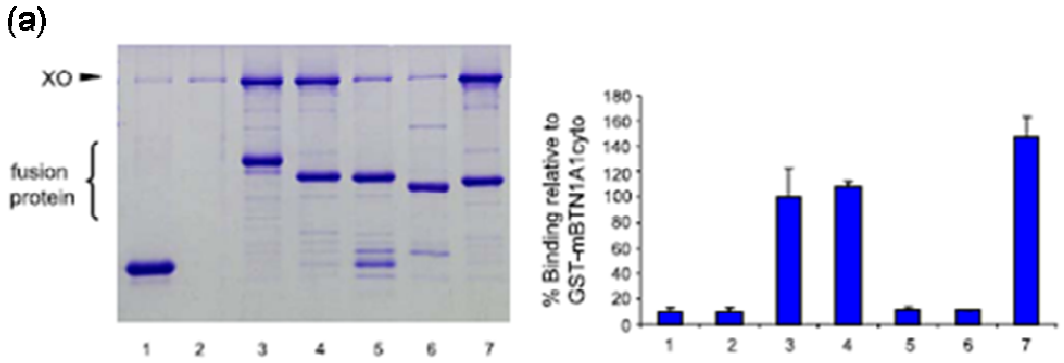


**Fig. 3.10. Glutathione/GST pull-down assays between wild-type and mutant forms of GST-mBTNcyto, and purified bovine XOR.** (a) Analysis of binding between saturating amounts of bXOR and mutant forms of GST-mBTNcyto. Lane 1, GST; lane 2, no protein; lane 3, GST-mBTNcyto; lane 4, GST-mBTNcyto$_{\Delta 480–524}$; lane 5, GST-mBTNcyto$_{\Delta 470–524}$; lane 6, GST-mBTNcyto$_{\Delta 269–310;480–524}$; lane 7, GST-mBTNcyto$_{\Delta 269–285;480–524}$ (mB30.2) (n=3). Densitometric analysis of the results from three experiments (mean ± S.D.) are shown in the right panel. Band densities are normalized (100%) to GST-mBTNcyto (lane 3).

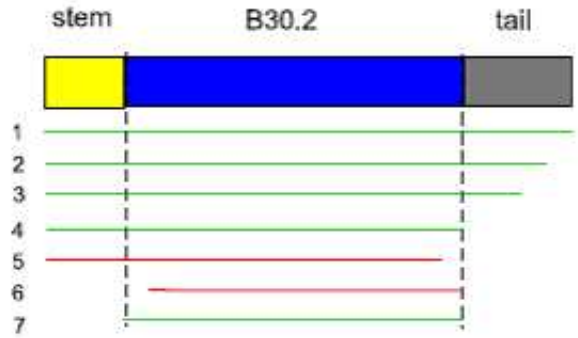


| Construct | Deletion | Btn/XOR Binding? in transfected cells | in vitro |
|---|---|---|---|
| 1 | wild type | +[1] | + |
| 2 | Δ507-524 | + | nd[2] |
| 3 | Δ493-524 | + | + |
| 4 | Δ480-524 | + | + |
| 5 | Δ470-524 | - | – |
| 6 | Δ269-310; 480-524 | nd | – |
| 7 | Δ269-285; 480-524 | nd | + |

[1] +, binding; -, no binding
[2] nd, not done

**Fig. 3.11. Summary of bead binding and cell expression assays for interaction between mBTNcyto and XOR.** Regions of mBTNcyto that bound to XOR are indicated by green lines, and regions that did not bind are shown by red lines. For the cell expression protein binding assay, the vectors used were pmXOR-EYFP in combination with pECFP-mBTN (1), pECFP-mBTN$\Delta_{507–524}$ (2), pECFP-mBTN$\Delta_{493–524}$ (3), pECFP-mBTN$\Delta_{480–524}$ (4), and pECFP-mBTN$\Delta_{470–524}$ (5). For the *in vitro* bead binding assay, the vectors used were pGST-mBTNcyto (1), pGST-mBTNcyto$\Delta_{493–524}$ (3), pGST-mBTNcyto$\Delta_{480–524}$ (4), pGST-mBTNcyto $\Delta_{470–524}$ (5), pGST-mBTNcyto $\Delta_{269–310}$;$\Delta_{480–524}$ (6), and pGST-mBTNcyto$\Delta_{269–285}$;$\Delta_{480–524}$ (mB30.2) (7).

and the protein complex dissociated. As the analyte dissociated from the ligand, a decrease in SPR signal (expressed in response units, RU) was observed. From these association ($k_a$) and dissociation rates ($k_d$), the equilibrium dissociation constant (binding constant, $K_D$) was calculated (Fig. 3.12 a). GST-fusion proteins encoding either full-length bovine or mouse BTNcyto domains (GST-bBTNcyto and GST-mBTNcyto) were used as ligands and bXOR as analyte. Dissociation constants ($K_D$) for GST-BTNcyto from either species at 25 ℃ were not significantly different; the average for cow and mouse was 112 and 113 nM, respectively (Fig. 3.12 b). Dissociation constants for bXOR and GST-bB30.2 were statistically similar (101 nM) to the $K_D$s for GST-BTNcyto from either species (Fig. 3.12 b), thus confirming that the B30.2 domain is necessary and sufficient for maximal interaction between the two proteins. Either SPR or the bead binding assay showed that binding was pH-dependent, because no binding was detected below pH 6.0 (Fig. 3.13 a), and binding affinities increased 5–7-fold when the NaCl concentration was lowered from 150 to 20 mM (Fig. 3.13 b)

### 3.7. *In vitro* bead binding assay to determine the interaction between bXOR and BTNs from different species

The amino acid sequence of B30.2 domain between BTN families is highly conserved particularly in the β-sheet regions, but the loop regions are relatively variable between families (Fig 3.14). To investigate binding specificity within and across species, the whole cytoplasmic domain of bovine

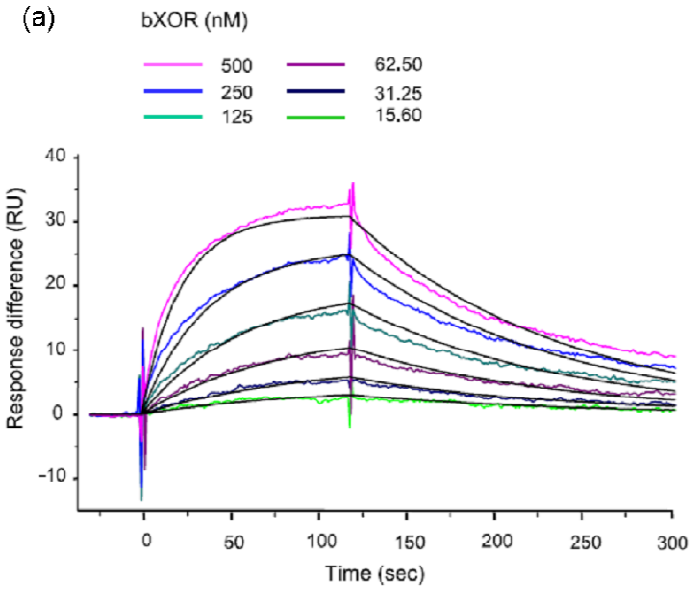


(b)

| parameter | Binding between bXOR and | | |
|---|---|---|---|
| | GST-mBTNcyto | GST-bBTNcyto | GST-bB30.2 |
| Dissociation constants (p H7.4), $K_D$ (nM) | | | |
| By bead binding assay | 47 ± 35 (3) | 50 ± 27 (3) | 26 ± 14 (3) |
| By SPR | 113 ± 6.4 (2) | 112 ± 7.1 (2) | 101 ± 31 (10) |

**Fig. 3.12. Determination of equilibrium and kinetic rate constants for interaction between BTN proteins and bXOR by SPR.** (a) Representative example of the biosensor analysis of binding of bXOR to GST-bBTNcyto. (b) Summary of binding characteristics for interaction between BTN fusion proteins and bXOR. $K_D$ values within each assay are not significantly different ($p > 0.05$; MIXED procedure, version 9.1, SAS Institute (Cary, NC)). The number of determinations is shown in parentheses. (Dr. Yinghua Zhang in University of Maryland Medical School, Baltimore conducted the SPR spectroscopy on a fee-for-service basis).

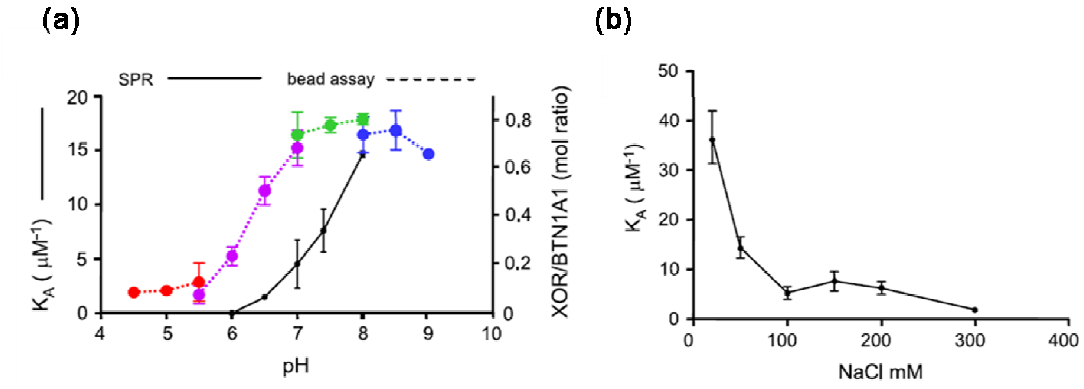


**Fig. 3.13. Effect of pH and salt on binding of bXOR to GST-bB30.2.** (a) Effect of pH on binding of bXOR to GST-bB30.2. Solid line, SPR analysis ($K_A$ $\mu M^{-1}$). Dotted lines, bead binding assay, using the following buffers: $KH_2PO_4$-KOH, pH 4.5–5.5 (red); MES, pH 5.5–7.0 (purple); HEPES, pH 7.0–8.0 (green); and Tricine, pH 8.0 –9.0 (blue). (b) Effect of NaCl on the binding of bXOR to GST-bB30.2 ($K_A$ $\mu M^{-1}$). The effect of salt on binding was similarly determined by using HBS-EP buffer (pH 7.4) containing variable amounts of NaCl. (Collaboration with Dr. Yinghua Zhang in University of Maryland Medical School, Baltimore on a see-for-service basis).

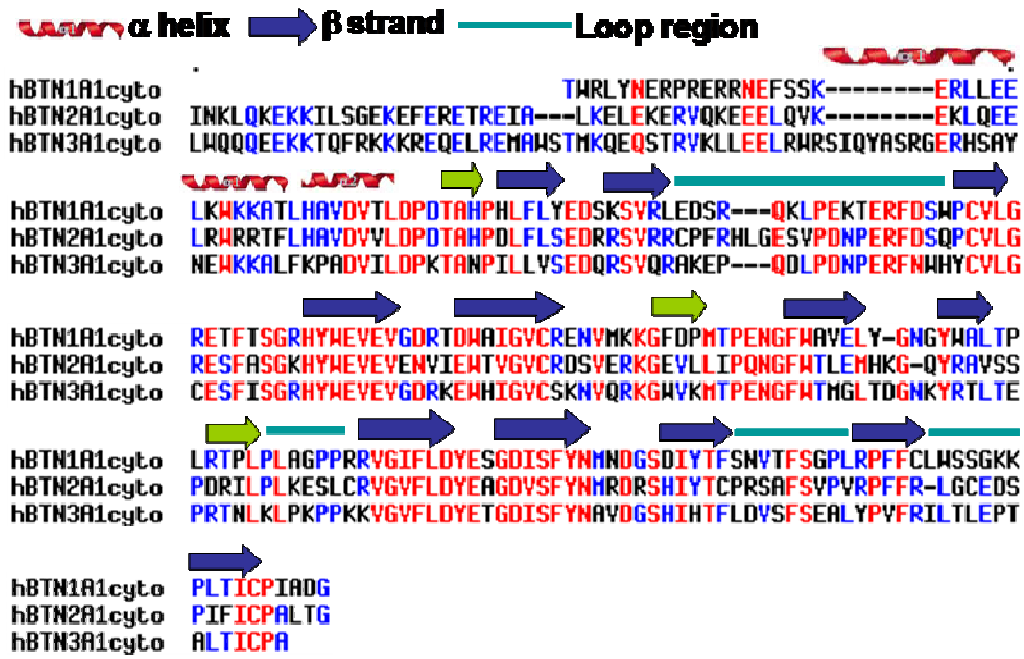


**Fig. 3.14. Amino acid alignment between human BTN1A1, BTN2A1, and BTN3A1.** The amino acid sequence of the B30.2 domain between BTN families is highly conserved in the β-sheet strand regions (arrows), but loop regions are relatively variable between families (the region between arrows or lines).

and human BTN1A1, the B30.2 domain of human BTN1A1, and the entire cytoplasmic domain of human BTN2A1 and BTN3A1 were prepared. Additionally, GST fused to the predicted B30.2 domain of human RoRet (TRIM 56) was prepared to test potential interaction with a B30.2 domain outside of the BTN protein family. bXOR bound to the whole cytoplasmic domain of bovine and human BTN1A1 (Fig. 3.15, lane 1, 2) and the B30.2 domain of human BTN1A1 (Fig. 3.15, lane 3). However, there was no interaction with human BTN2A1, BTN3A1, and the B30.2 domain of human RoRet (Fig. 3.15, lane 4-6). An assay with no fusion protein served as a control (Fig. 3.15, lane 7). These data suggest that BTN1A1 specifically interacts with XOR, and since BTN1A1 is highly expressed during lactation, the interaction between BTN1A1 and XOR may be essential for milk secretion during lactation in the mammary gland.

### 3.8. Gel filtration of protein complexes to determine the oligomeric state of BTN and the apparent Mr values of the purified proteins, separately, and together as BTN-XOR complexes

The apparent Mr values of the purified GST-fusion proteins, thrombin-cleaved purified proteins and BTNcyto-XOR complexes were determined by gel filtration on Superdex 200 (FPLC). GST-bBTNcyto was eluted with apparent *M*r values of 190,000 and 215,000, respectively which indicated that these proteins form tetramers (Fig. 3.16 a, example for GST-bBTNcyto, dotted blue line, summarized in Table 3.1). Because GST itself forms a dimer,

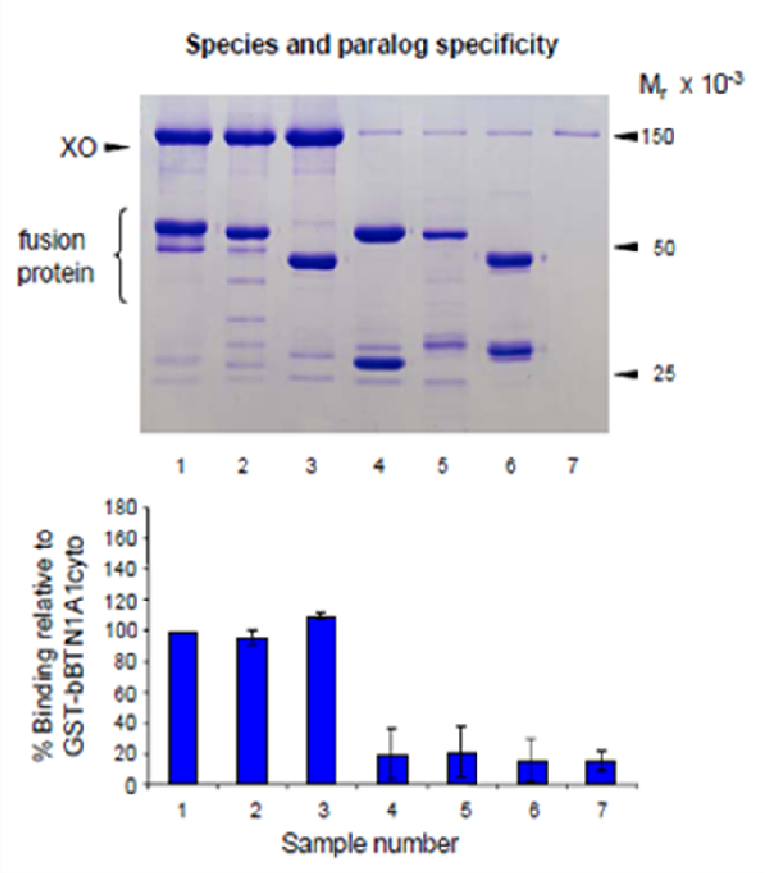


**Fig. 3.15. *In vitro* bead binding assay to determine the interaction between bXOR and BTNs from different species.** Specificity of binding between bXOR and different orthologs and paralogs of BTN. Lane 1, GST-bBTNcyto; lane 2, GST-hBTN1A1cyto; lane 3, GST-hBTN1A1-B30.2; lane 4, GST-hBTN2A1cyto; lane 5, GST-hBTN3A1cyto; lane 6, GST-hRoRet(TRIM56)-B30.2; lane 7, no protein. Densitometric analysis of the results from three experiments (mean ± S.D.) are shown in the bar graph. Band densities were normalized (100%) to GST-bBTNcyto (lane 1).

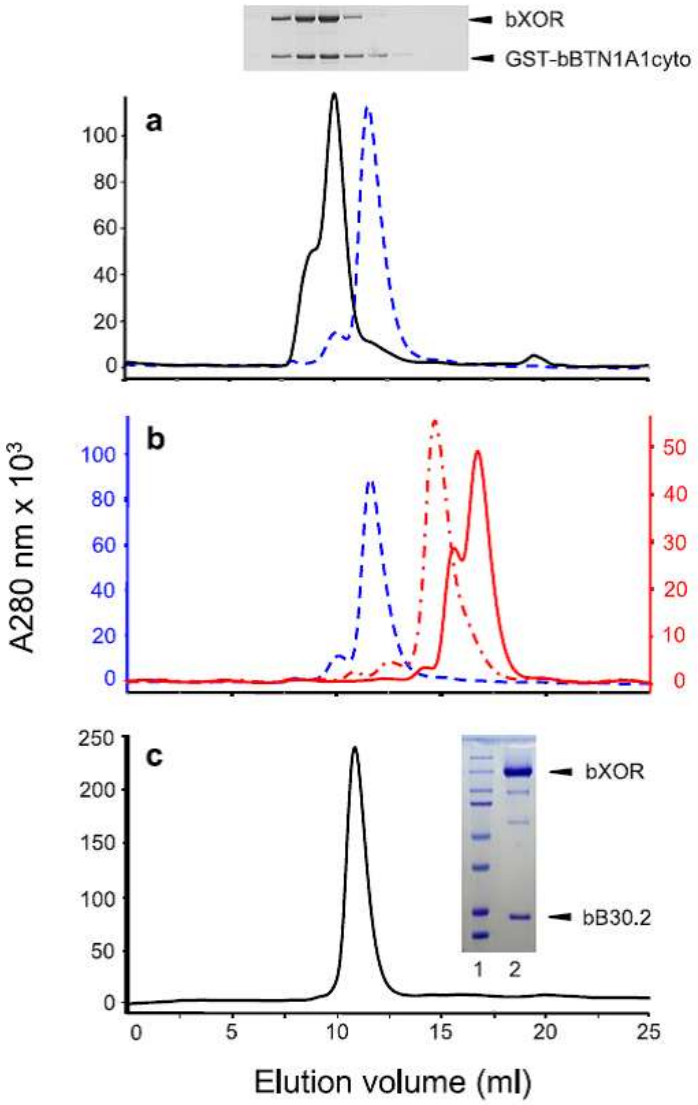


**Fig. 3.16. Gel filtration of protein complexes.** (a-c) Samples were separated by FPLC on a 1 x 30 cm column of Superdex 200 in TBS, pH 7.4, and protein was detected at A280 nm. (a) GST-bBTNcyto (10 nmol) (dotted blue line) and GST-bBTN-bXOR complex (10 nmol) (black line). The SDS-PAGE gel shows analysis of peak fractions. (b) GST-bBTNcyto (8 nmol) (dotted blue line), bBTNcyto (8 nmol) (dotted red line), and bB30.2 (8 nmol) (solid red line). (c) GST-bB30.2-bXOR complex; SDS-PAGE gel shows analysis of peak fraction (lane 2) in comparison with protein standards (from top to bottom, 250, 150, 100, 75, 50, 37, 25, and 20 kDa; lane *1*).

**Table 3.1. Protein *Mr* values estimated by gel filtration on Superdex 200.**

| Protein | $M_r \times 10^{-3}$ | |
|---|---|---|
| | Mouse | Cow |
| GST-BTN1A1cyto; $M_r$ expected for monomer | 189 ± 19 (5); 55.92 | 216 ± 4.2 (3); 56.51 |
| BTN1A1cyto; $M_r$ expected for monomer | ND | 48 ± 3.1 (3); 30.51 |
| B30.2; $M_r$ expected for monomer | ND | [30.8], 19.5 (1); 23.44 |
| GST-BTN1A1cyto-bXOR complex | [764 ± 33] (5)<br>496 ± 29 | [807 ± 10] (3)<br>528 ± 8 |
| B30.2-bXOR complex | ND | 344 ± 13 (3) |

Underlined values indicate the most abundant species. Values in parentheses indicate the number of determinations, and values in square brackets indicate the approximate molecular weight of proteins within a prominent shoulder associated with a major peak. ND, not done.

GST was removed from GST-bBTNcyto by digestion with thrombin to determine whether bBTNcyto intrinsically oligomerizes. The entire cytoplasmic domain of bBTNcyto was eluted with a molecular mass of 48,000, which is 80% of the mass expected for a dimer (61,020) (Fig. 3.16 b and Table 3.1). However, the purified bovine B30.2 domain (bB30.2) was eluted with a molecular mass of 19,500, close to that expected for a monomer (23,437) (Fig. 3.16 b and Table 3.1). These data indicate that the fusion proteins form tetramers through separate dimeric interactions between the GST domains and dimeric interactions between the cytoplasmic domains of BTN. Furthermore, interactions between BTN molecules appear to be due to interactions within either the stem or tail regions, since the B30.2 domain was eluted as a monomer. The complex between the B30.2 domain and XOR, eluted with an apparent *M*r value of 344,000, which indicates that two monomers of B30.2 domain are bound to one dimer of XOR. This confirms that the B30.2 domian itself is sufficient to bind to XOR (Fig. 3.16 c and Table 3.1).

### 3. 9. Identification of the domains in XOR that bind to the B30.2 domain of BTN

XOR is a homodimer of 300kDa. Each subunit contains four redox centers; a molybdo-pterin cofactor (Mo-Co), one FAD molecule, and two $Fe_2S_2$ centers (FeS). In order to determine the domains of XOR that bind to BTN, an *in vivo* cell expression protein binding assay, similar to the one

discussed in section 3.1, was used. Fluorescent fusion proteins of mouse BTN (ECFP-mBTN) and the separate domains of mouse XOR (FeS-EYFP, FAD-EYFP, and Mo-Co-EYFP) were expressed in HEK 293T cells and the cells were treated with digitonin. ECFP-mBTN and FeS-EYFP co-localized in the plasma membrane and Golgi apparatus even after treatment with digitonin (Fig. 3.17 c, f, and i). In contrast, neither expressed FAD-EYFP nor Mo-Co-EYFP co-localized with ECFP-mBTN after treatment with digitonin (Fig. 3.18). However, expressed FAD-EYFP still remained in cell organelles even after treatment with digitonin suggesting that the fusion protein was mis-folded and was non-specifically bound to membrane structures (Fig. 3.18 b, e). Therefore, as an additional test, a construct containing both FeS and FAD domains (pFeS/FAD-EYFP) was prepared.

Co-expression of ECFP-mBTN and FeS/FAD-EYFP showed that FeS/FAD-EYFP bound to ECFP-mBTN, before and after treatment with digitonin (Fig. 3.19). These data suggest that the domain of XOR which binds to the cytoplasmic domain of BTN is located within the $Fe_2S_2$ centers, and possibly the FAD domain, but not the molybdo-pterin domain.

### 3. 10. Confirmation, by immunoprecipitation, that the FeS domain of XOR binds to BTN

To confirm that BTN physically interacts with the FeS domain of XOR, total detergent extracts of HEK 293T cells, transfected with ECFP-mBTN and EYFP fusion proteins of separate domains of XOR, were immunoprecipitated

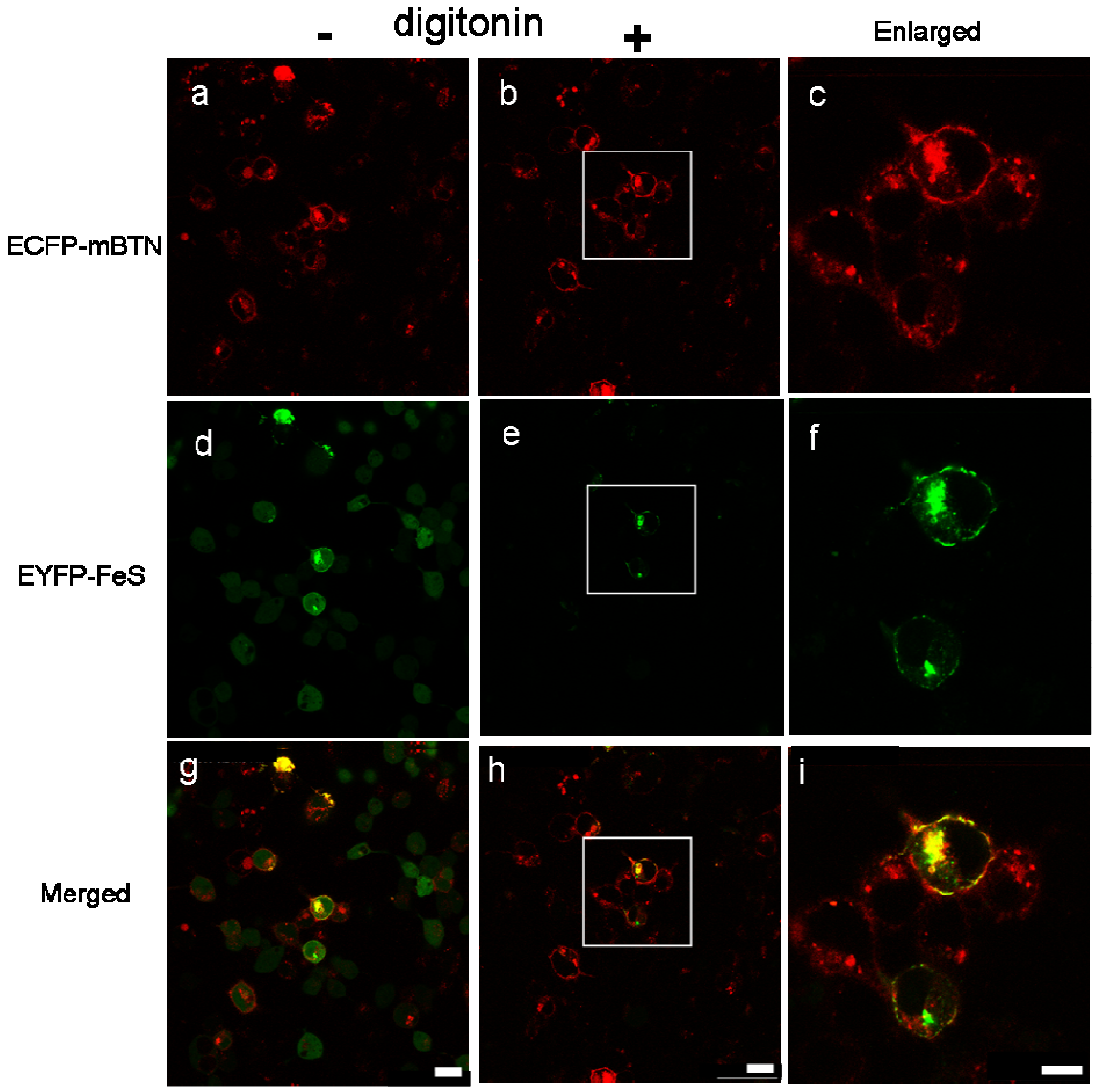


**Fig. 3.17. Co-expression of ECFP-mBTN and FeS-EYFP in HEK 293T cells.** (a, b, c) ECFP-mBTN, and (d, e, f) FeS-EYFP were co-expressed in HEK 293 cells, and the cells treated with digitonin. (a, d, g) before treatment with digitonin (-), and (b, e, h) after treatment with digitonin (+). Enlarged images (boxes) (c, f, i). Bars, 10 μm.

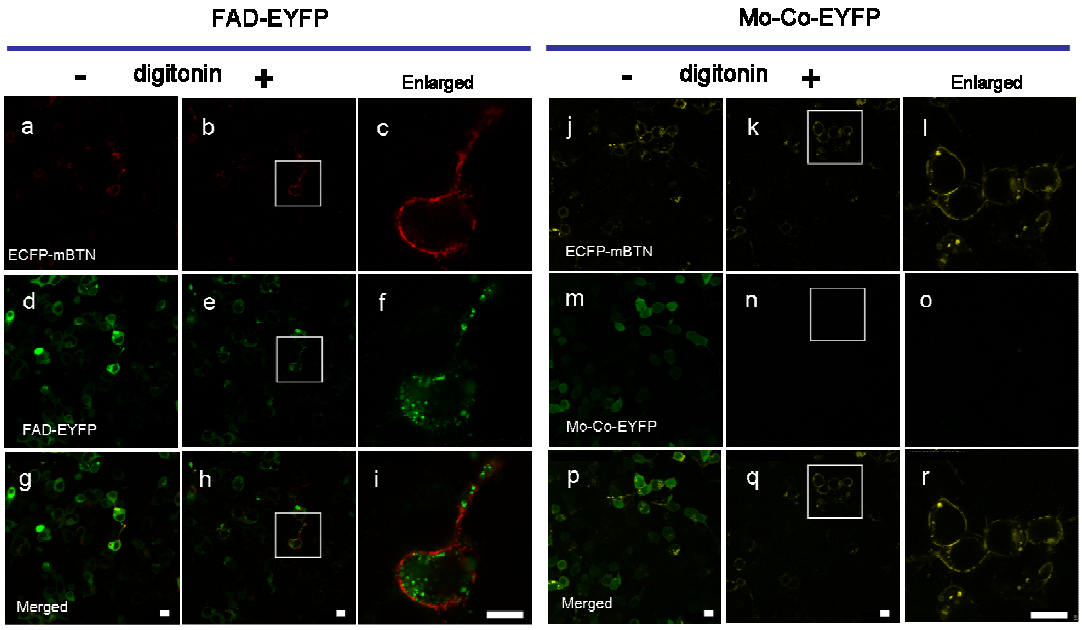


**Fig. 3.18. Co-expression of ECFP-mBTN and either FAD-EYFP or Mo-Co-EYFP in HEK 293T cells.** (a-i) ECFP-mBTN (a, b, and c) and FAD-EYFP (d, e, and f) were co-expressed in HEK 293T cells, and the cells were treated with digitonin. (a, d, and g) before treatment with digitonin, and (b, e, and h) after treatment with digitonin. Enlarged images (box) (c, f, and i). (j-r) ECFP-mBTN (j, k, and l) and Mo-Co-EYFP (m, n, and o) were co-expressed in HEK 293T cells, and the cells treated with digitonin. (j, m, and p) before treatment with digitonin, and (k, n, and q) after treatment with digitonin. Enlarged images (box) (l, o, and r). Bars, 10 μm.

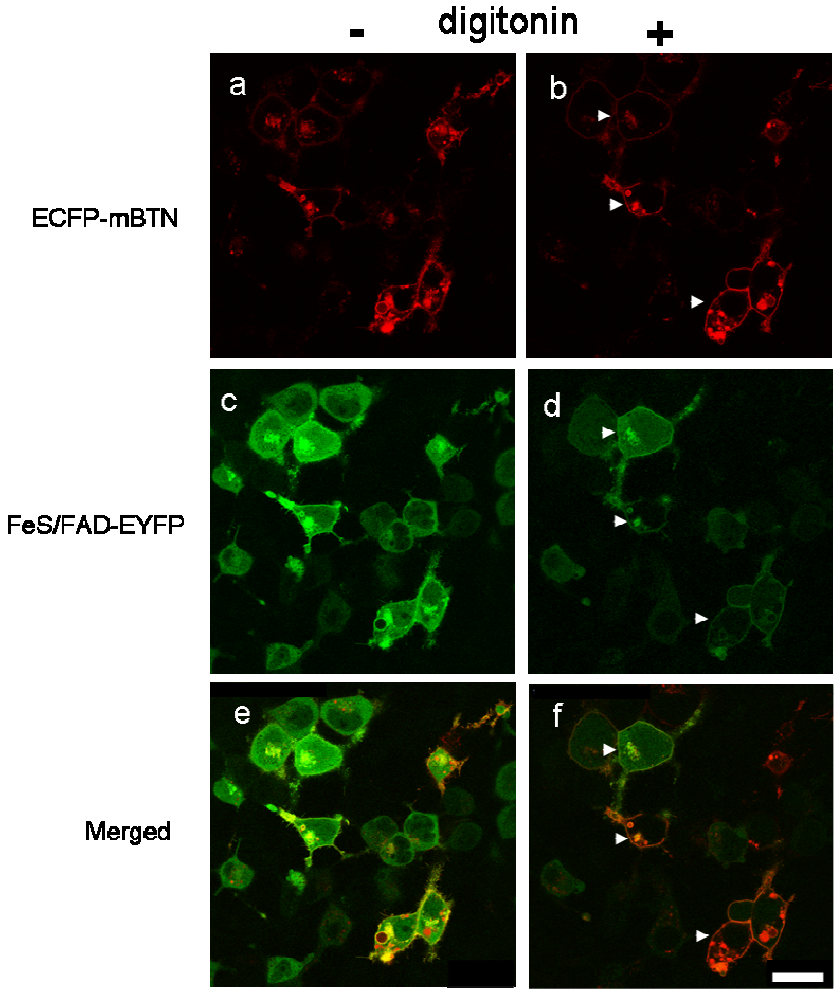


**Fig. 3.19. Co-expression of ECFP-mBTN and FeS/FAD-EYFP in HEK 293 cells.** ECFP-mBTN (a, b) and FeS/FAD-EYFP (c, d) were co-expressed in HEK 293T cells, and the cells treated with digitonin. (a, c, and e) before treatment with digitonin, and (b, d, and f) after treatment with digitonin; merged images (e, f). Bar, 25 μm.

with antibody to mBTN. Co-expressed ECFP-mBTN and FeS-EYFP were immunoprecipitated together with antibody to mBTN, and detected by Western blot using an antibody to GFP (Fig. 3.20, lane 1). Interestingly, expressed FAD-EYFP (65 kDa) also immunoprecipitated with ECFP-mBTN, which suggests that the FAD domain in XOR might share BTN binding sites (Fig. 3.20 lane 2). In agreement with this, expressed FeS/FAD-EYFP (85 kDa) was immunoprecipitated with ECFP-mBTN. (Fig. 3.20, lane 4). However, pull down of total detergent extract of HEK 293T cells, expressing ECFP-mBTN and Mo-Co-EYFP, with antibody to mBTN did not lead to precipitation of expressed Mo-Co-EYFP (105 kDa), confirming that the molybdenum domain does not bind to BTN (Fig. 3.20, lane 3). Cell expression protein binding assays and immunoprecipitation assays for interaction between mBTN and the separate domains of XOR are summarized in Table. 3.2.

In summary, these data indicate that the $Fe_2S_2$ domain binds to BTN, and that the FAD domain might also share binding sites.

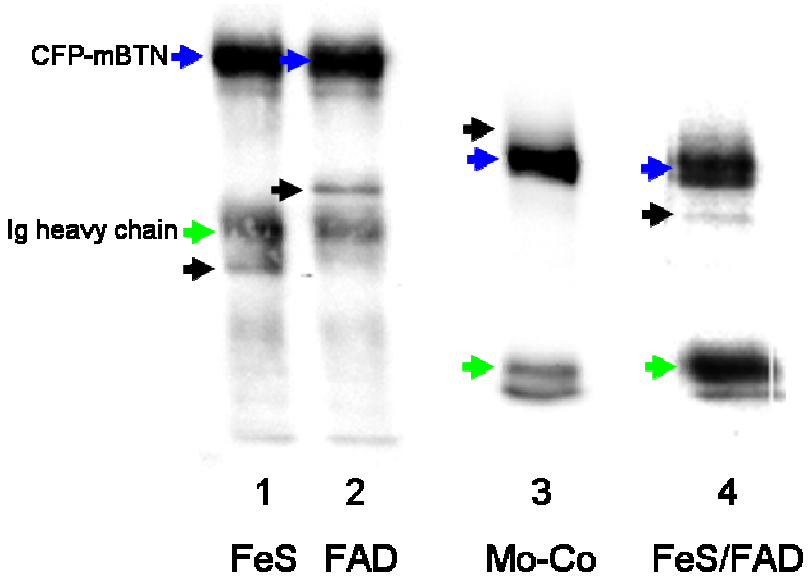


**Fig. 3.20. Immunoprecipitation of ECFP-mBTN and EYFP fusion proteins of separate domains of XOR from HEK 293T cell extracts.** Proteins were immunoprecipitated from RIPA buffer extracts with antibody to mBTN, separated by SDS-PAGE (8% polyacrylamide gel), and blotted with antibody to GFP. Immunoprecipitates from HEK 293T cells transfected with pECFP-mBTN together with pFeS-EYFP (45 kDa) (lane 1), pFAD-EYFP (65 kDa) (lane 2), pMo-Co-EYFP (105 kDa) (lane 3), and pFeS/FAD-EYFP (85 kDa) (lane 4). Green arrow, Ig heavy chain; blue arrow, ECFP-mBTN; black arrow, expected size of each fluorescent fused domain of XOR.

**Table 3.2. Summary of cell expression assays and immunoprecipitation for interaction between mBTN and separate domains of XOR.**

| | Binding of BTN1A1/Separate domain of XOR? | |
|---|---|---|
| | Cell expression assay | immunoprecipitation |
| BTN1A1/$Fe_2S_2$ | + | + |
| BTN1A1/FAD | - | + |
| BTN1A1/Mo-Co | - | - |

+, binding; -, no binding

# Chapter 4: Localization of BTN and XOR in mammary epithelial cells

## 4.1. Rationale

The intracellular distribution of BTN and XOR in the lactating mammary gland (6, 23, 43, 56, 69), and how localization of the two proteins is related to milk-lipid secretion are controversial (6, 23, 43, 56, 69). As discussed in the introduction, there are three models for the molecular mechanism of milk-lipid secretion. In one model, Mather and Keenan suggested that BTN localizes in the plasma membrane, and interacts with XOR (6, 43, 56). These putative BTN and XOR complexes are postulated to bind to other molecules on the lipid droplet surface, thus, precipitating formation of the outer envelope of the MFGM and expulsion of the lipid droplets into the lumen (6, 43, 56). However, this model does not specify where XOR is located, either on the lipid droplet surface, the apical plasma membrane, or sandwiched between both places. In an alternative model, McManaman et. al. suggested that XOR is sandwiched between BTN in the apical plasma membrane and ADPH on the surface of the lipid droplets in a complex stabilized by disulfide bonds (23). In a radically different model, Robenek et. al. proposed that milk-lipid secretion is regulated entirely by interactions between BTN molecules localized in both the apical plasma membrane and the surface of intracellular lipid droplets (69). Therefore, to determine the location of BTN and XOR in mammary cells, we expressed fluorescent forms of mBTN and mXOR, as fusion proteins in

cultured cells, and in lactating mammary glands using recombinant adenoviral vectors and expression plasmids. In addition, sections of lactating mammary gland were examined by immunofluorescence microscopy using specific antibodies to determine the location of endogenous BTN and XOR in a wild-type and knock-out mouse strains.

### 4.2. Distribution of expressed BTN and XOR in cell lines containing lipid droplets

To determine the location of exogenously expressed BTN and XOR in cells, four cell lines were used: HEK 293T cells, 3T3-L1 cells (a fibroblast-like cell line which can be converted into adipocytes), MAC-T cells (a transformed bovine mammary epithelial cell line), and HC 11 cells (a mouse mammary epithelial cell line). Although HEK 293T cells do not have an intrinsic ability to accumulate lipid, the addition of oleic acid to the medium induces the formation of some small lipid droplets. 3T3-L1, MAC-T, and HC 11 cells produce large numbers of lipid droplets under appropriate conditions. All four cell lines were used to test the predictions of either Mather and Keenan (6, 43, 56) or Robenek et. al. (69), to see if either BTN or XOR bind to the surface of intracellular lipid droplets.

HEK 293T cells were transiently transfected with pECFP-mBTN and a plasmid encoding ADPH fused at the C-terminus to EYFP (pmADPH-EYFP). As discussed in the introduction, ADPH is a member of the PAT family of proteins, which associate with the surface of lipid droplets in many cell types

(76). Thus, as expected, mADPH-EYFP was localized to the lipid droplets and the cytoplasm in HEK 293T cells treated with 50 μg/ml oleic acid (Fig. 4.1 d). However, ECFP-mBTN localized to the plasma membrane, and was not detected on the surface of the lipid droplets, even after the cells were treated with digitonin to wash out all unbound cytosolic protein, including soluble mADPH-EYFP (Fig. 4.1 a, b, and c). In an alternative procedure, fluorescence loss In photobleaching (FLIP) analysis was used. A specific region of the cytoplasm was continuously bleached, until all of the fluorescent signal associated with unbound, mobile mADPH-EYFP had been lost (green rectangle in Fig. 4.2 d-g). After photobleaching, there was no overlap between the immobile mADPH-EYFP on the lipid droplet surfaces and ECFP-mBTN (Fig. 4.2). Therefore, BTN does not have an intrinsic ability to bind to neutral lipid droplets in HEK 293T cells.

However, HEK 293T cells, a human embryonic kidney cell line, may not be the most appropriate model system, because the cells may lack essential BTN binding factors, specific to mammary cells or associated with endogenous lipid droplets. Therefore, these experiments were repeated with the lipogenic cell line, 3T3-L1, and mammary cells (MAC-T and HC 11). Similar results were obtained with 3T3-L1 cells transduced with a recombinant adenoviral vector encoding mouse BTN fused to EYFP (Adv-mBTN-EYFP) (an adenoviral vector was used because 3T3-L1 cells are refractory to transduction of plasmid DNA) (77). Cells were transduced during conversion to adipocytes (69). Two days after transduction, the cells were

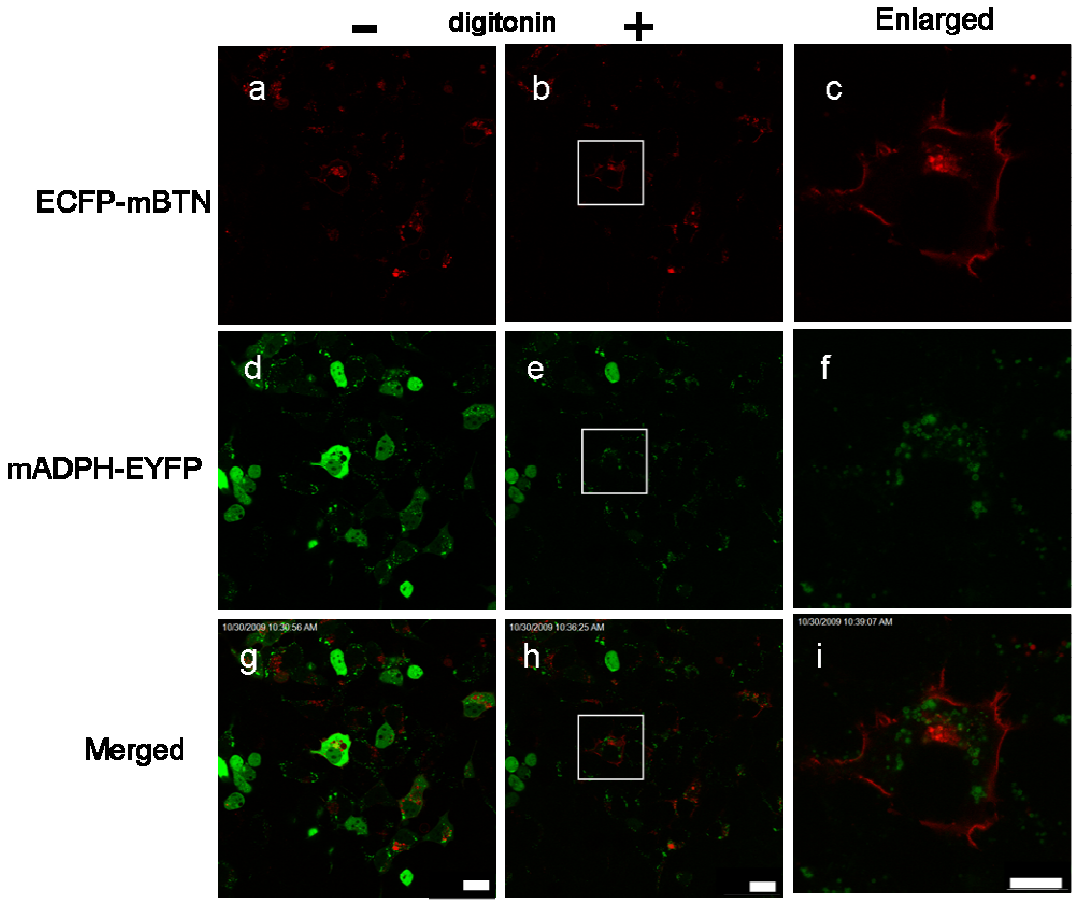


**Fig. 4.1. Detection of ECFP-mBTN and mADPH-EYFP in HEK 293T cells.** (a-i) HEK 293T cells were co-transfected with (a, b, c) pECFP-mBTN and (d, e, f) pmADPH-EYFP using lipofectamine 2000. (a, d, g) Before (-), and (b, e, h) after (+) treatment with digitonin. Enlarged images of the boxed area (c, f, i). Bars, 10 μm.

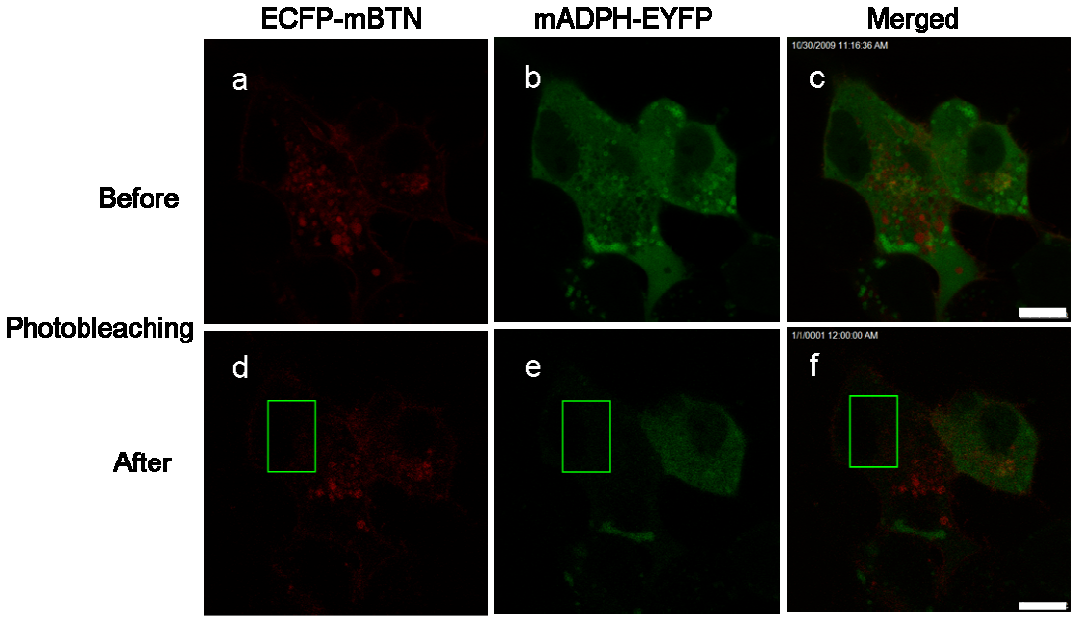


**Fig. 4.2. Detection of ECFP-mBTN and mADPH-EYFP in HEK 293T cells by following fluorescent loss in photobleaching (FLIP) analysis.** Cells were co-transfected with pECFP-mBTN (a, d) and pmADPH-EYFP (b, e); Merged images (c, f). (a, b, c) before photobleaching; (d, e, g) after photobleaching. Photobleached region is shown by green rectangle (d-f). Bar, 10 μm.

stained with nile red and the location of mBTN-ECFP was determined by confocal microscopy. mBTN-EYFP localized to the plasma membrane, but not to cytoplasmic lipid droplets (Fig. 4.3 a-c).

The MAC-T cell line produces a very small amount of BTN and XOR, in the presence of lactogenic hormones [intensity (arbitrary unit) of 7000/2000 vs. 100/200 (BTN/XOR) for mouse mammary cells vs MAC-T cells using microarray analysis] (personal communication Dr. Kadegowda), and synthesizes lipid droplets after treatment with oleic and palmitic acid. To determine the location of expressed BTN in MAC-T cells, the cells were transiently co-transfected with pECFP-mBTN and pmADPH-EYFP, and treated with oleic acid to stimulate accumulation of lipid droplets. mADPH-EYFP was specifically localized to lipid droplets (Fig. 4.3 e), and ECFP-mBTN localized to the plasma membrane (Fig. 4.3 d). ECFP-mBTN was not detected on the surface of intracellular lipid droplets (Fig. 4.3 f).

Even though MAC-T is a bovine mammary epithelial cell line, the cells do not produce much BTN or XOR, even in the presence of lactogenic hormones. However, HC 11 cells, a mouse mammary epithelial cell line, endogenously produce XOR in the presence of dexamethasone ($10^{-6}$ M) (73). Therefore, to determine whether the presence of endogenous XOR affects localization of BTN, HC 11 cells were transduced with Adv-mBTN-EGFP. The cells transduced with Adv-mBTN-EGFP showed that mBTN-EGFP localized to the plasma membrane (Fig. 4.4 a) and was not present on intracellular lipid droplets suggesting that the location of BTN is not affected by endogenous

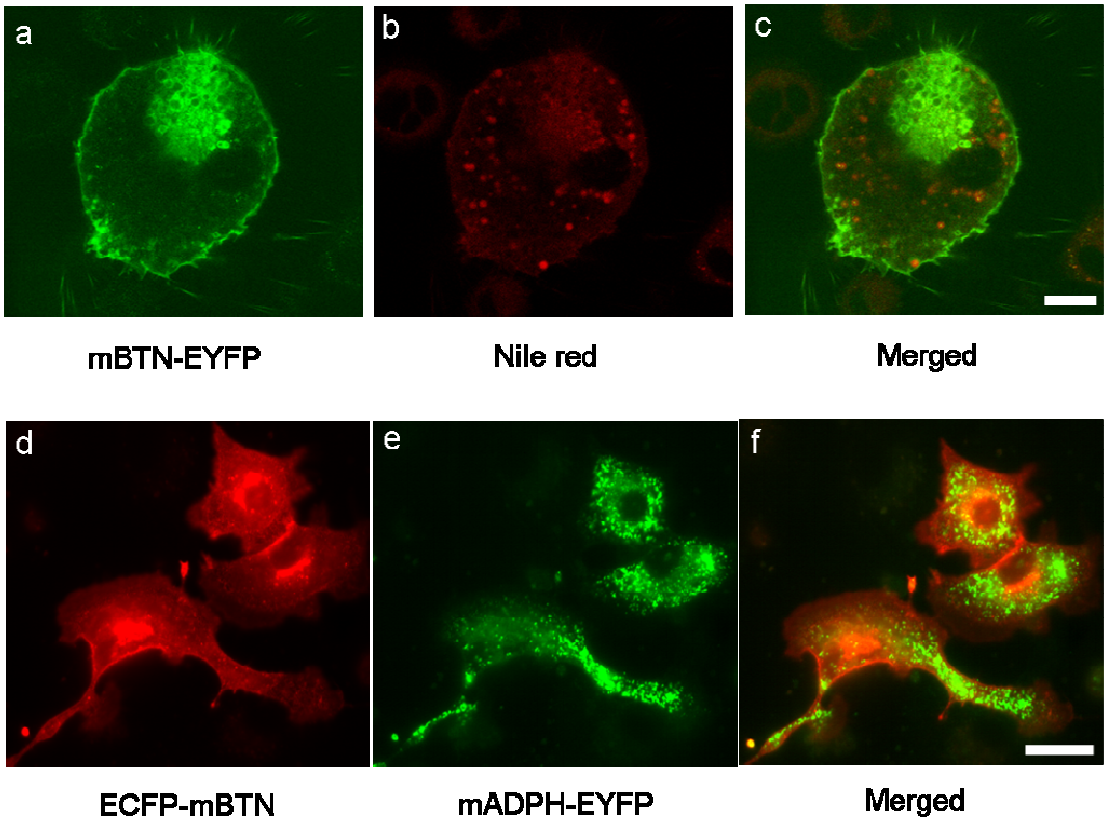


**Fig. 4.3. Detection of BTN in 3T3-L1 and MAC-T cells.** (a-c). 3T3-L1 cells were transduced with Adv-mBTN-EYFP during differentiation into adipocytes, and treated with nile red to stain the lipid droplets. (a) mBTN-EYFP, (b) Nile red, (c) merged image. (d-f) MAC-T cells were co-transfected with pECFP-mBTN and pmADPH-EYFP using lipofectamine 2000 (Invitrogen). (d) ECFP-mBTN, (e) mADPH-EYFP, (f) merged image. Bars, 10 μm.

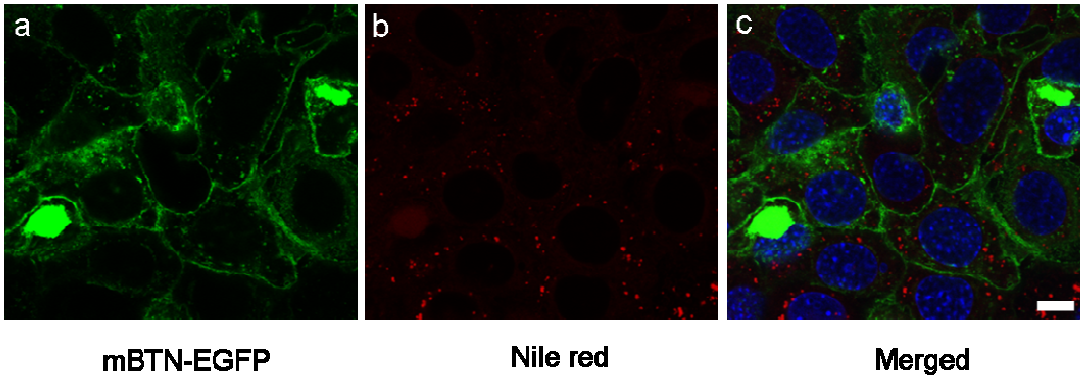


**Fig. 4.4. Detection of BTN in HC 11 cells.** HC 11 cells were treated with dexamethasone ($10^{-6}$ M) to induce XOR expression. After induction, the cells were transduced with Adv-mBTN-EGFP, and treated with nile red to stain lipid droplets. (a) mBTN-EGFP, (b) nile red, (c) merged image. Blue; DAPI staining (nuclei). Bar, 10 μm.

XOR (Fig. 4.4). Thus, under the conditions tested, BTN did not associate with intracellular lipid droplets in either 3T3-L1, MAC-T, or HC 11 cells (Figs. 4.3, 4.4). As discussed later, these results are in conflict with Robenek et. al (69).

Mather and Keenan suggested that BTN interacts with XOR either at the cell surface or on the surface of intracellular lipid droplets (6, 43, 56). To test these possibilities, the location of XOR was examined by expressing mXOR-ECFP in 3T3-L1 and MAC-T cells. 3T3-L1 cells were also used to test the potential interaction of XOR with intracellular lipid droplets. The cells were transduced with Adv-mXOR-ECFP during conversion to adipocytes. mXOR-ECFP localized to the cytoplasm, but most of it was removed by treatment with digitonin, indicating that XOR does not bind tightly to intracellular lipid droplets (Fig. 4.5 a-f). In MAC-T cells, expressed mXOR-ECFP was mainly detected in the cytoplasm, and most of it was washed out of the cytoplasm after treatment with digitonin (Fig. 4.5 g, j). However, mADPH-EYFP was still bound to intracellular lipid droplets after treatment with digitonin (Fig. 4.5 h, k).

In summary, the above results showed that BTN is located in the plasma membrane and XOR is expressed in the cytoplasm in cultured cells (HEK 293T, 3T3-L1, MAC-T, and HC11). Neither protein appears to interact with lipid droplets. Thus, these data do not agree with the predictions of either Mather and Keenan (6, 43, 56), or Robenek et. al. (69). However, binding of XOR or BTN to lipid droplets may require mammary-specific factors, which are not expressed in established cell lines. Therefore, the distribution of BTN and XOR was determined in lactating mammary glands in vivo by two

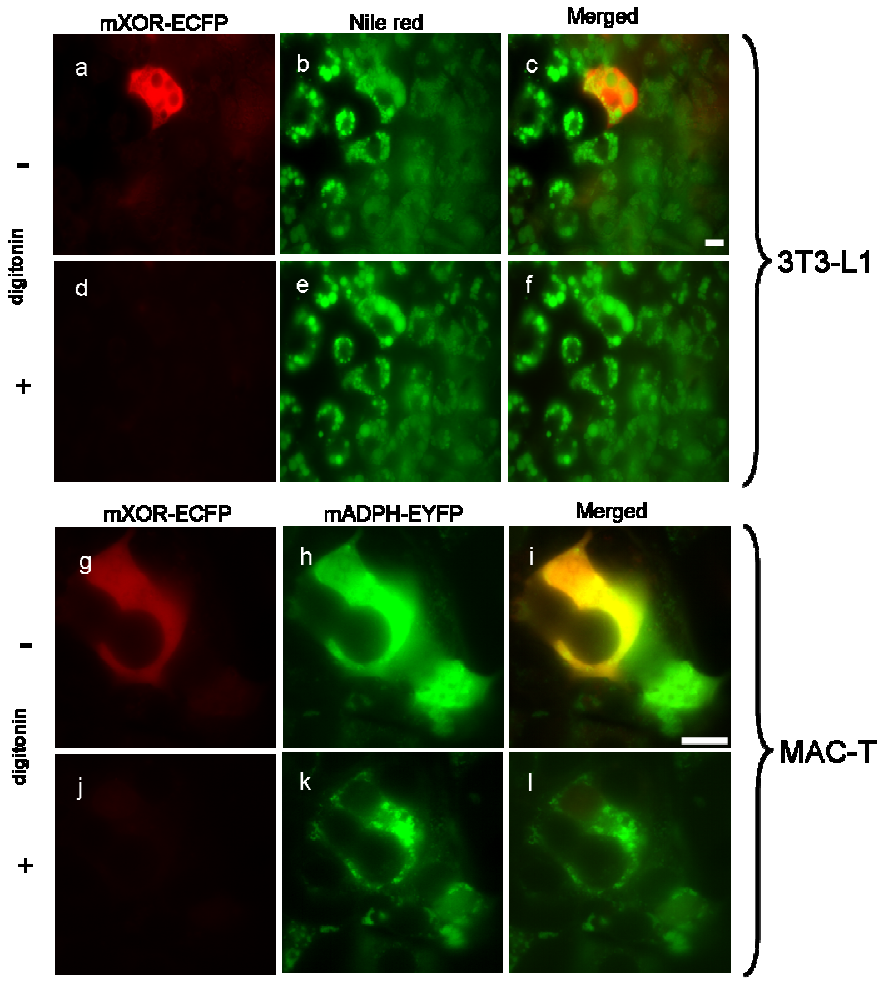


**Fig. 4.5. Detection of XOR in 3T3-L1 and MAC-T cells.** (a-f) 3T3-L1 cells were transduced with Adv-mXOR-ECFP during differentiation, and treated with nile red to stain the lipid droplets. (a, d) mXOR-ECF, (b, e) nile red, (c, f) merged images. (a-c) Before (-), and (d-f), after (+) treatment with digitonin. (g-l) MAC-T cells were co-transfected with pmXOR-ECFP and pmADPH-EYFP using lipofectamine 2000 (Invitrogen) and treated with digitonin. (g, j) mXOR-ECFP, (h, k) mADPH-EYFP, (i, l) merged images. (g-i) Before (-), and (j-l) after (+) treatment with digitonin. Bar, 10 μm.

independent methods.

### 4.3. Localization of BTN and XOR in lactating mouse mammary glands

The mammary gland is a unique model system to study secretory mechanisms because it is a skin gland, which is accessible for manipulation by the infusion of agents such as expression vectors and antibodies via the streak canal of the nipple. To localize BTN in the lactating mammary gland, Adv-mBTN-EYFP was introduced at day 17 of pregnancy into the mammary glands of Btn1a1$^{+/+}$ mice through the streak canal of the nipple and the tissues were collected on the 2nd day of lactation. mBTN-EYFP localized to the apical plasma membrane as well as secreted milk-lipid in the lumen (Fig. 4.6 a, d). In contrast, expressed mXOR-CFP was detected in the cytoplasm (Fig. 4.6 e), and did not co-localize with intracellular lipid droplets. These results are in agreement with the above data from cultured cells in which BTN is targeted to membranes, and XOR is present in the cytoplasm.

In order to determine the distributions of endogenous BTN and XOR, sections of lactating mammary tissue were stained with specific antibodies to either proteins and examined by confocal microscopy. BTN was specifically detected in the apical plasma membrane of Btn1a1$^{+/+}$ mice, and, as expected, no signal was detected in tissue from *Btn1a1*$^{-/-}$ mice (Fig. 4.7 a, e). Furthermore, BTN was present in the secreted, but not in intracellular lipid droplets (Fig 4.7 a, d). Endogenous XOR was detected in the cytoplasm, but was enriched in the apical plasma membrane in Btn1a1$^{+/+}$ mice (Fig. 4.8 a, e).

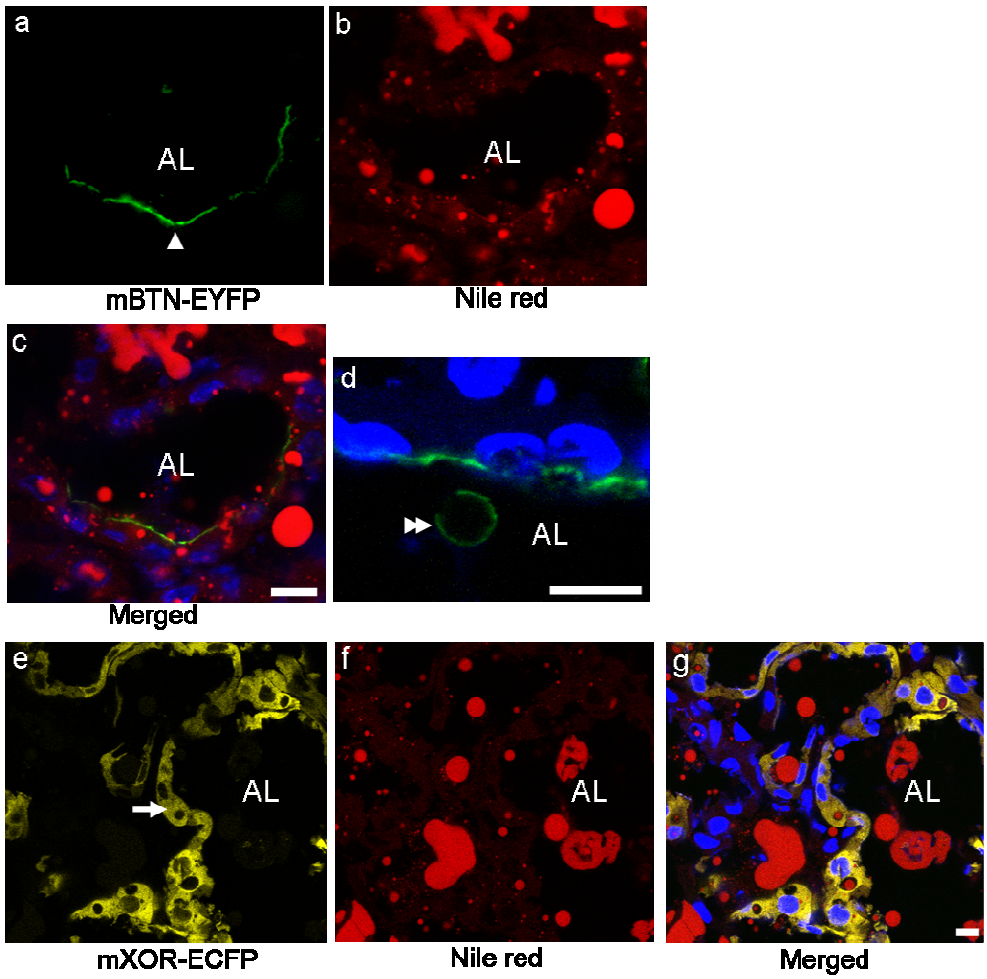


**Fig. 4.6. Detection of recombinant mBTN-YFP and mXOR-CFP in lactating mouse mammary gland.** The #4 mammary glands of day 17-pregnant mice were transduced with either (a-d) Adv-mBTN-EYFP or (e-g) Adv-mXOR-ECFP, and transduced tissues were collected on day 2 of lactation. Tissue was fixed in 4% (w/v) paraformaldehyde, embedded in OCT (Optimal Cutting Temperature) compound, and frozen in isopentane surrounded by liquid nitrogen. The frozen tissue was sectioned (10 μm), and examined by confocal microscopy: (a-d) mBTN-EYFP, (a) mBTN-EYFP (white single arrowhead), green; (b) nile red, red; (c) merged image; (d) white double arrowhead, secreted milk-fat droplet. (e-g) mXOR-ECFP: (e) mXOR-ECFP (white arrow), yellow; (f) nile red, red; and (g) merged image. AL, alveolar lumen. Bars, 10 μm.

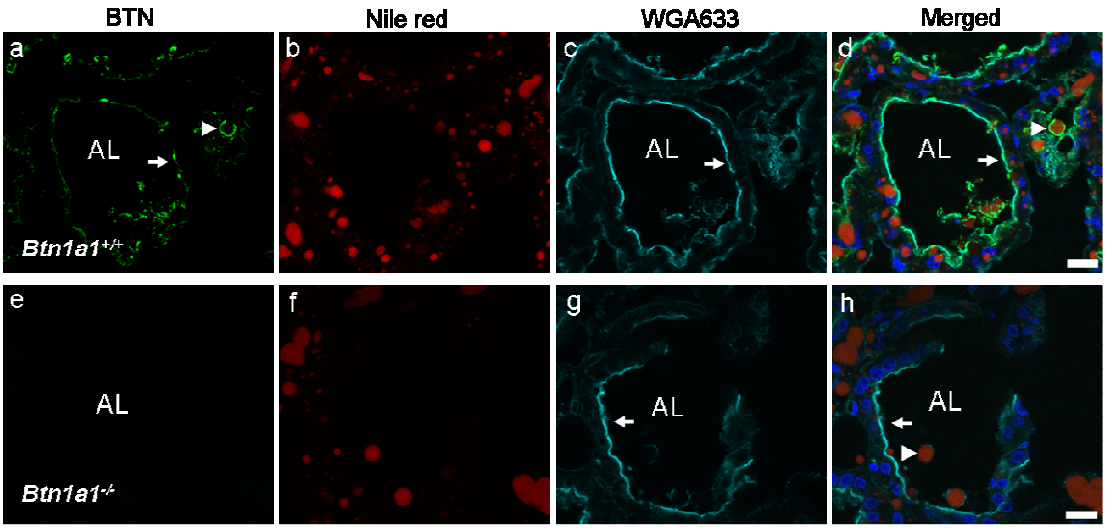


**Fig. 4.7. Detection of endogenous BTN in Btn1a1$^{+/+}$ and *Btn1a1*$^{-/-}$ mice in lactating mouse mammary gland.** Mammary tissue at day 2 of lactation was fixed as described in the legend to Fig. 4.6 and cut into 16 μm frozen sections. (a-d) Btn1a1$^{+/+}$, (e-h) *Btn1a1*$^{-/-}$ mice. Sections were incubated with specific antibody to mouse BTN (56), followed by goat anti-(rabbit IgG)-FITC as secondary detecting agent. (a, e) BTN, (b, f) nile red stain for lipid droplets, (c, g) WGA-Alexa 633 stain for apical plasma membrane, (d, h) merged image. AL, alveolar lumen; white arrows, apical plasma membrane; white arrowheads, secreted lipid droplets. Bars, 20 μm.

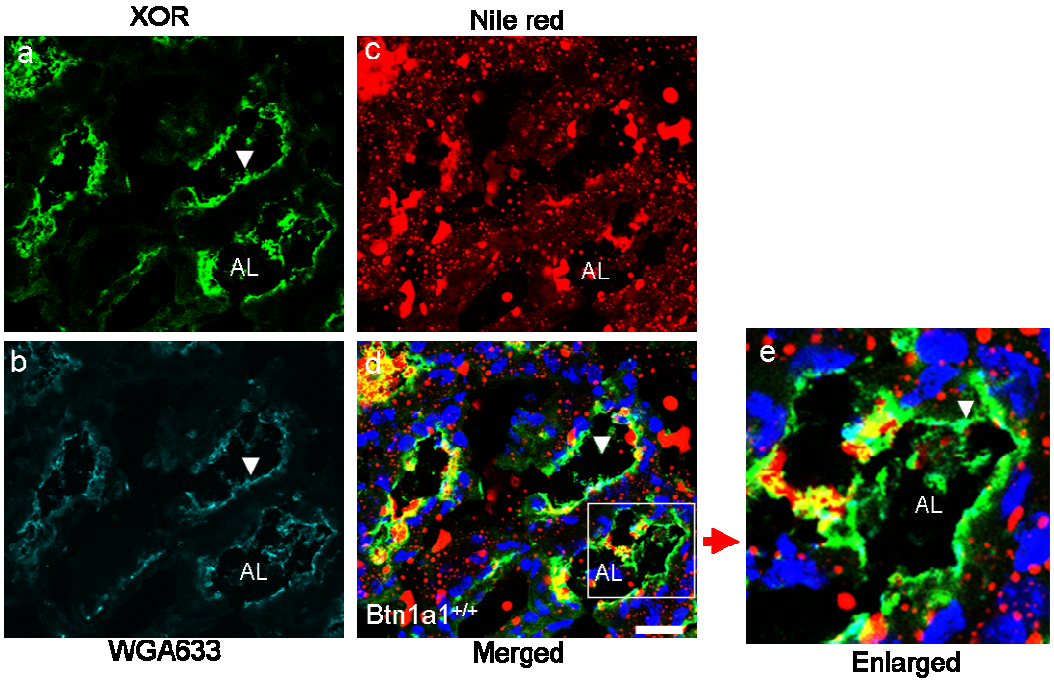


**Fig. 4.8. Detection of endogenous XOR in Btn1a1$^{+/+}$ mice by immunofluorescence microscopy.** Lactating mammary gland from Btn1a1$^{+/+}$ mice was fixed in 4% paraformaldehyde, and prepared as decribed in the legend to Fig. 4.7. Sections were incubated with a specific antibody to mXOR (56), followed by goat anti-(rabbit IgG)-FITC as secondary detecting agent. (a) XOR, (b) WGA-Alexa 633 stain for apical plasma membrane, (c) nile red stain for lipid droplets, (d) merged image, and (e) enlarged image of the boxed area in (d). White arrowheads, apical plama membrane; AL, aveolar lumen. Bar, 20 μm. (n=3).

However, in *Btn1a1*$^{-/-}$ mice, XOR is present throughout the cytoplasm and is not enriched in the apical plasma membrane (Fig. 4.9 a, e), presumably because its binding partner, BTN, is absent in the knock-out strain. These data strongly suggest that BTN recruits XOR to the apical plasma membrane.

To confirm these possibilities, tissue sections from Btn1a1$^{+/+}$ and *Btn1a1*$^{-/-}$ mice were treated with digitonin to wash out of all of the unbound cytosolic XOR, and the residual XOR was detected by confocal microscopy. XOR still co-localized with WGA 633 (wheat germ agglutinin Alexa-633), a marker for the apical plasma membrane, after treatment of Btn1a1$^{+/+}$ tissue with digitonin (Fig 4.10 a). However, all of the XOR was washed out of the *Btn1a1*$^{-/-}$ tissue (Fig 4.10 d), confirming that XOR interacts with BTN in the apical plasma membrane, and that loss of BTN allows XOR to move freely in the cytoplasm. Furthermore, z-stack analysis showed that secreting lipid droplets from mammary epithelial cells are surrounded by XOR indicating that the BTN/XOR complex in the apical plasma membrane surrounds the milk-lipid droplet during secretion (Fig. 4.11).

To confirm that XOR associates with the outer bilayer of the MFGM, rather than the lipid droplet surface, milk-fat droplets containing mXOR-ECFP in cytoplasmic inclusions were analyzed by FLIP. Btn1a1$^{+/+}$ and *Btn1a1*$^{-/-}$ mice were transduced with Adv-mXOR-ECFP and milk was collected on day 2 of lactation. Milk-fat droplets containing cytoplasmic inclusions were selected for analysis. Repetitive bleaching of one portion of the cytoplasmic inclusion (rectangle in Fig. 4.12) results in removal of all of the signal

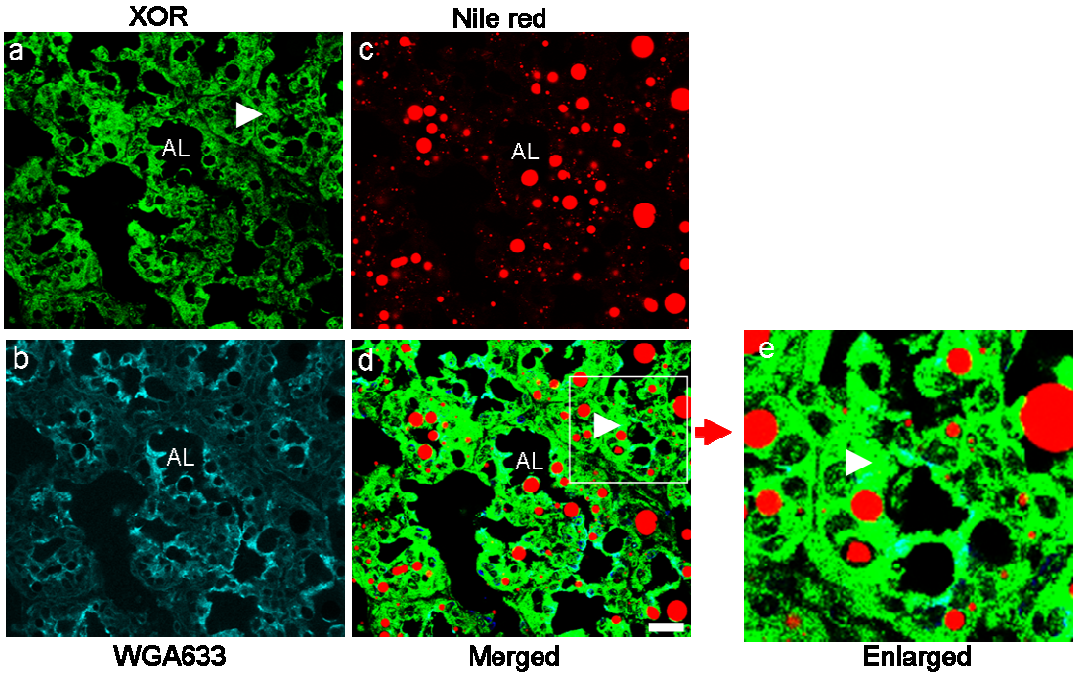


**Fig. 4.9. Detection of endogenous XOR in *Btn1a1*$^{-/-}$ mice by immunofluorescence microscopy.** Lactating mammary gland from *Btn1a1*$^{-/-}$ mice was stained with antibody to XOR as described in the legend to Fig. 4.8. (a) XOR, (b) WGA-Alexa 633 stain for apical plasma membrane, (c) nile red stain for lipid droplets, (d) merged image, and (e) enlarged image of the boxed area in (d). White arrowhead, cytoplasm; AL, aveolar lumen. Bar, 20 μm. (n=3).

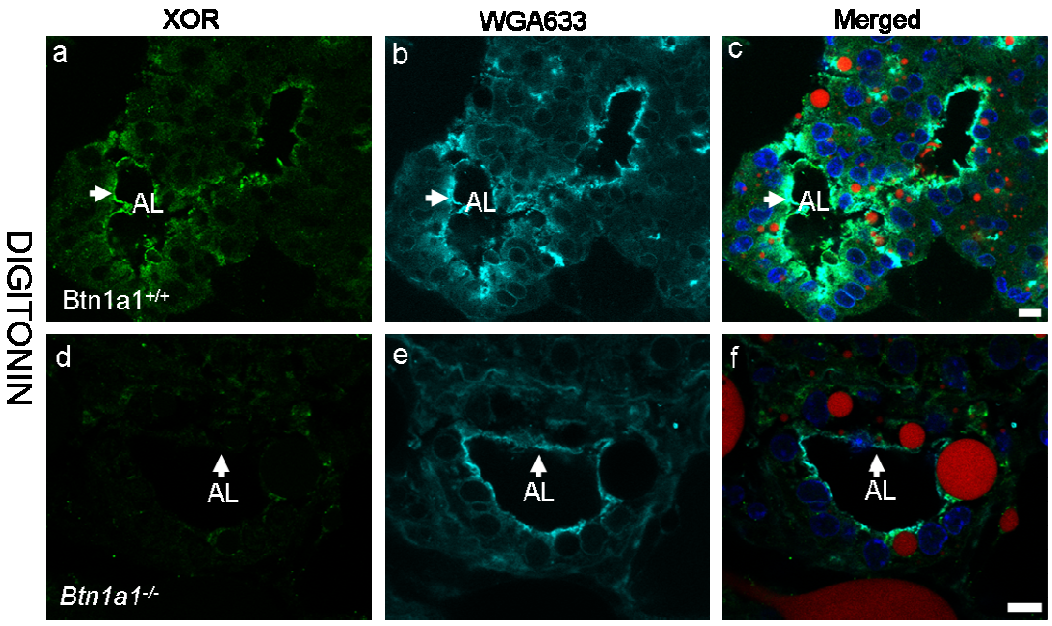


**Fig. 4.10. Detection of endogenous XOR in Btn1a1$^{+/+}$ and *Btn1a1*$^{-/-}$ mice by immunofluorescence microscopy after treatment of the sections with digitonin.** Sections of lactating mammary gland from Btn1a1$^{+/+}$ and *Btn1a1*$^{-/-}$ mice were treated with digitonin to wash out cytoplasmic unbound proteins and stained with antibody to XOR as described in the legend to Fig. 4.8. (a, d) XOR; (b, e) WGA-Alexa 633 stain for apical plasma membrane; (c, f) merged image. White arrowhead, apical plasma membrane; AL, aveolar lumen. Bars, 10 μm. (n=3).

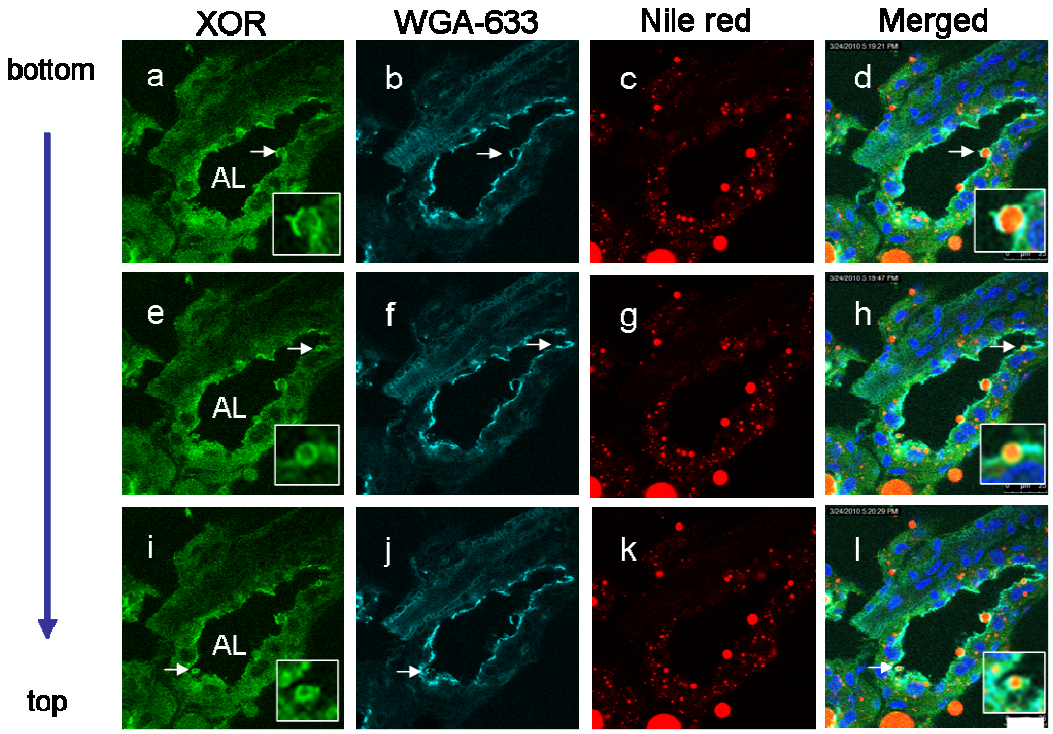


**Fig. 4.11. Localization of endogenous XOR by confocal microscopy (Z-stack).** Lactating mammary tissue from a Btn1a1$^{+/+}$ mouse was stained with antibody to XOR as described in the legend to Fig. 4.8. and examined by confocal microscopy (z-stack analysis). (a, e, i), XOR; (b, f, j), WGA-Alexa 633 stain for apical plasma membrane; (c, g, k), nile red stain for lipid droplets, (d, h, l), merged image. White arrows, secreting lipid droplets. Bar, 25 μm. (n=3)

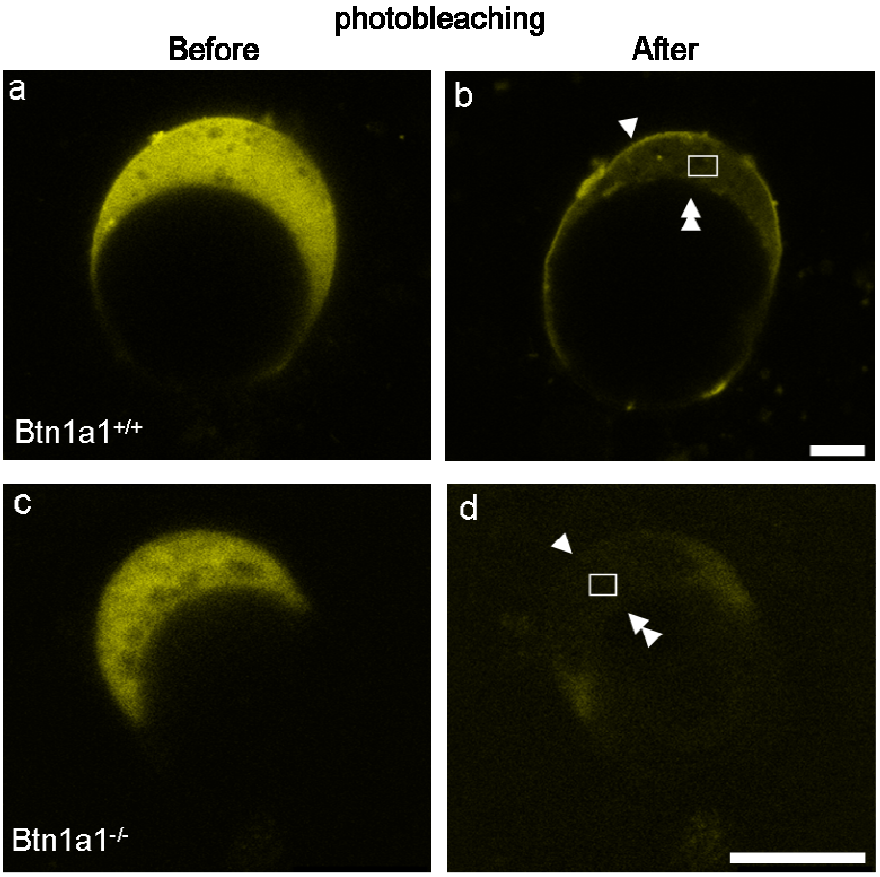


**Fig. 4.12. Fluorescence loss in photobleaching (FLIP) analysis of the mobility of mXOR-ECFP in milk-lipid droplets from Btn1a1$^{+/+}$ and *Btn1a1*$^{-/-}$ mice.** Day 17-pregnant mice were transduced with Adv-mXOR-ECFP, and milk-fat droplets were collected on day 2 of lactation. Milk-fat droplets containing cytoplasmic crescents and mXOR-ECFP were used for FLIP analysis. (a, c) before; (b, d) after bleaching (white rectangle, bleached regions). Lipid droplets from (a, b) Btn1a1$^{+/+}$, and (c, d) *Btn1a1*$^{-/-}$ mice. Single white arrowhead, the outer MFGM bilayer; double white arrowhead, the lipid droplet surface. Representative of one droplet from six separate experiments. (4 mice) Bars, 5 μm.

associated with the mobile fraction of mXOR-ECFP. Interestingly, a fraction of the expressed mXOR-ECFP was still detected in the outer membrane of the MFGM after bleaching of Btn1a1$^{+/+}$ droplets (Fig. 4.12 a, b), whereas all the signal was lost in the *Btn1a1*$^{-/-}$ droplets (Fig. 4.12 c, d). Furthermore, no fluorescent mXOR-ECFP was detected on the droplet surface after FLIP. This is consistent with the above data (Fig. 4.8 - 4.10) showing that XOR interacts with BTN in the apical plasma membrane, and is not present on the lipid droplet surface.

To confirm co-localization of BTN and XOR in the apical plasma membrane, both Adv-mBTN-EYFP and Adv-mXOR-ECFP were introduced at day 17 of pregnancy into the mammary glands of Btn1a1$^{+/+}$ mice through the streak canal of the nipple. The expression of mBTN-EYFP and mXOR-ECFP was examined at day 2 of lactation. Expressed mBTN-EYFP localized in the apical plasma membrane (Fig. 4.13 a), and mXOR-ECFP was expressed in the cytoplasm (Fig. 4.13 b). However, expressed mXOR-ECFP was enriched in the apical plasma membrane compared to the cytoplasm, and co-localized with mBTN-EYFP (Fig. 4.13 b, d).

## 4.4. Immunoprecipitation of BTN and XOR from extracts of lactating mammary gland

All the above the data describe the distribution of BTN and XOR *in vitro* and *in vivo*, but they do not establish whether the two proteins are bound together in cells. To establish *in vivo* interaction between the two proteins,

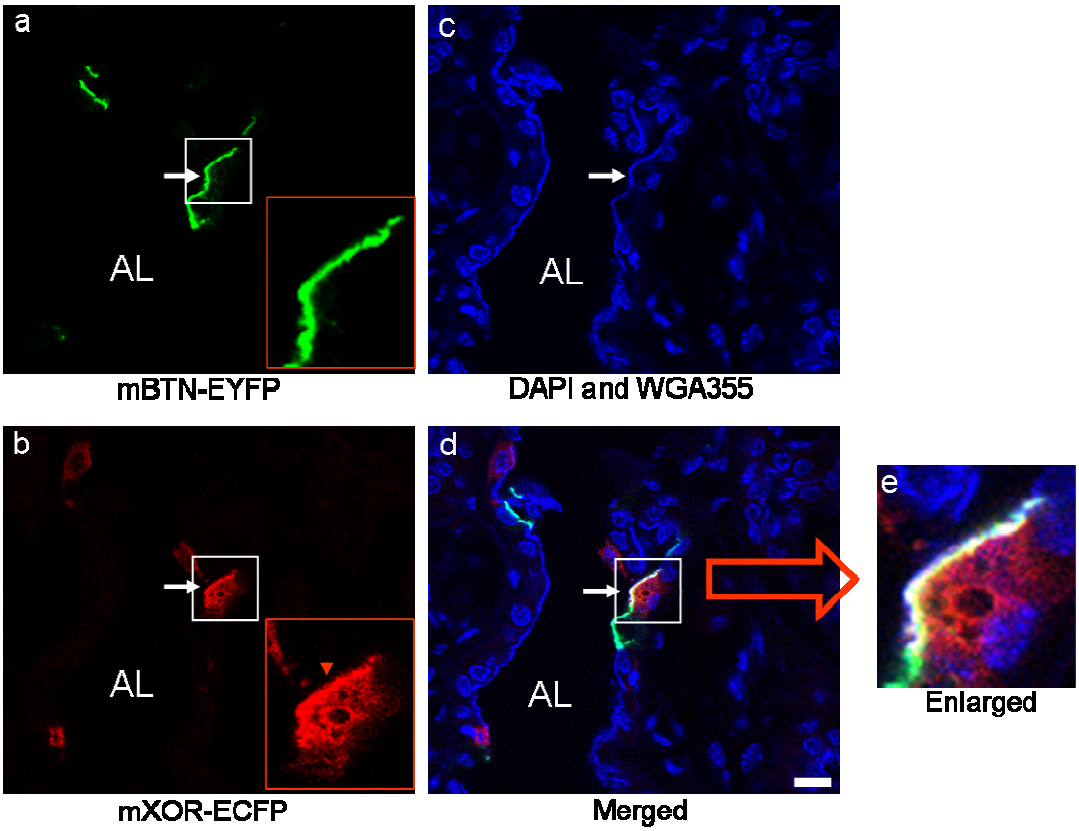


**Fig. 4.13. Co-localization of expressed mBTN-YFP and mXOR-CFP in lactating mammary gland.** (a-e) Lactating mammary gland was co-transduced with adenoviral vectors, Adv-mBTN-YFP and Adv-mXOR-ECFP, and the expressed proteins localized in the tissue by confocal microscopy. (a) BTN-EYFP (green); (b) XOR-ECFP (red); (c) DAPI stain for nuclei and, WGA-Alexa 355 stain for the apical plasma membrane; (d) merged image; (e) enlarged image of the boxed area in (d). White arrows, apical plasma membrane. Bar, 10 μm.

detergent extracts of membrane fractions, prepared from the lactating mammary tissue of both Btn1a1$^{+/+}$ and *Btn1a1*$^{-/-}$ mice, were immunoprecipitated with antibody against mXOR. A band of protein that reacted with antibody to BTN was detected in the immunoprecipitates from wild-type mice (Fig. 4.14, lane 1), whereas there was no reaction with immunoprecipitates from *Btn1a1*$^{-/-}$ mice (Fig. 4.14, lane 2). About 37.5 ± 6.2% of BTN (mean and S.D. of three determinations) was bound to XOR, as determined by densitometric analysis of the detergent extracts before and after incubation with the antibody-coated protein A beads (Fig. 4.14, lanes 3 and 5). Interestingly, XOR was also recovered in the immunoprecipitates from knock-out mice, indicating that XOR binds to membranes in the absence of BTN.

### 4.5. Mobility characteristics of BTN in secreted lipid droplets determined by Fluorescence Recovery After Photobleaching (FRAP) analysis

To measure the mobility of proteins in the bilayer of the MFGM, milk-fat droplets containing expressed mBTN-EGFP were used for FRAP analysis. Brief bleaching of one portion on the surface of the MFGM by laser light results in removal of most of the signal, and allows measurement of the mobility of unbleached molecules as they diffuse into the bleached area (Fig. 4.15 a). The distribution of mBTN-EGFP on secreted milk-fat droplets was heterogeneous: in some droplets, mBTN-EGFP was “continuous” and evenly surrounded the entire surface (Fig. 4.15 b), and in others, mBTN-EGFP was

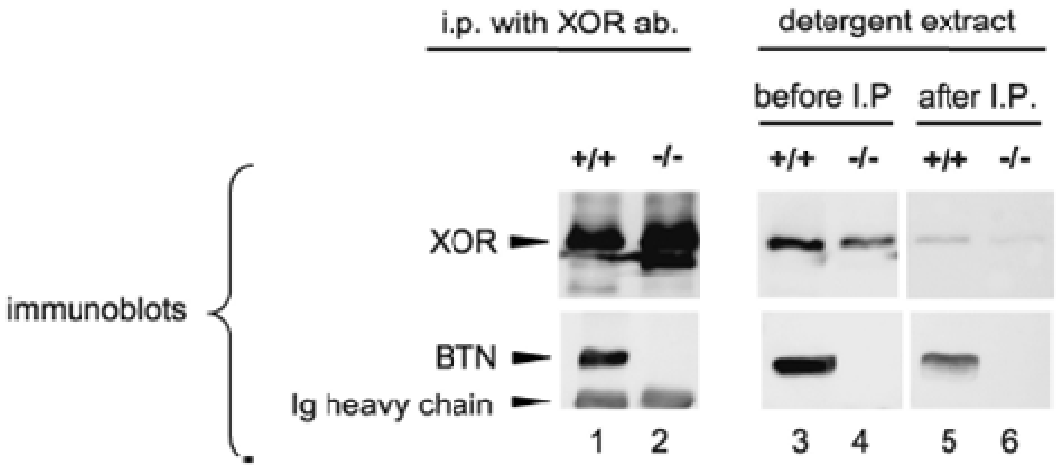


**Fig. 4.14. Immunoprecipitation of BTN-XOR complexes from the lactating mammary gland.** Proteins were immunoprecipitated from RIPA buffer extracts with antibody to mXOR, separated by SDS-PAGE (6% gel), and first blotted with antibody to mBTN (bottom blot). The blot was then stripped and reprobed with antibody to mXOR (top blot). Shown are immunoprecipitates from a wild-type mouse (lane 1) and a *Btn1a1*$^{-/-}$ mouse (lane 2). The corresponding RIPA buffer extracts, before and after incubation with the antibody-coated protein A beads, are shown for the wild-type mouse in lanes 3 and 5 and for the *Btn1a1*$^{-/-}$ mouse in lanes 4 and 6, respectively. (n=3)

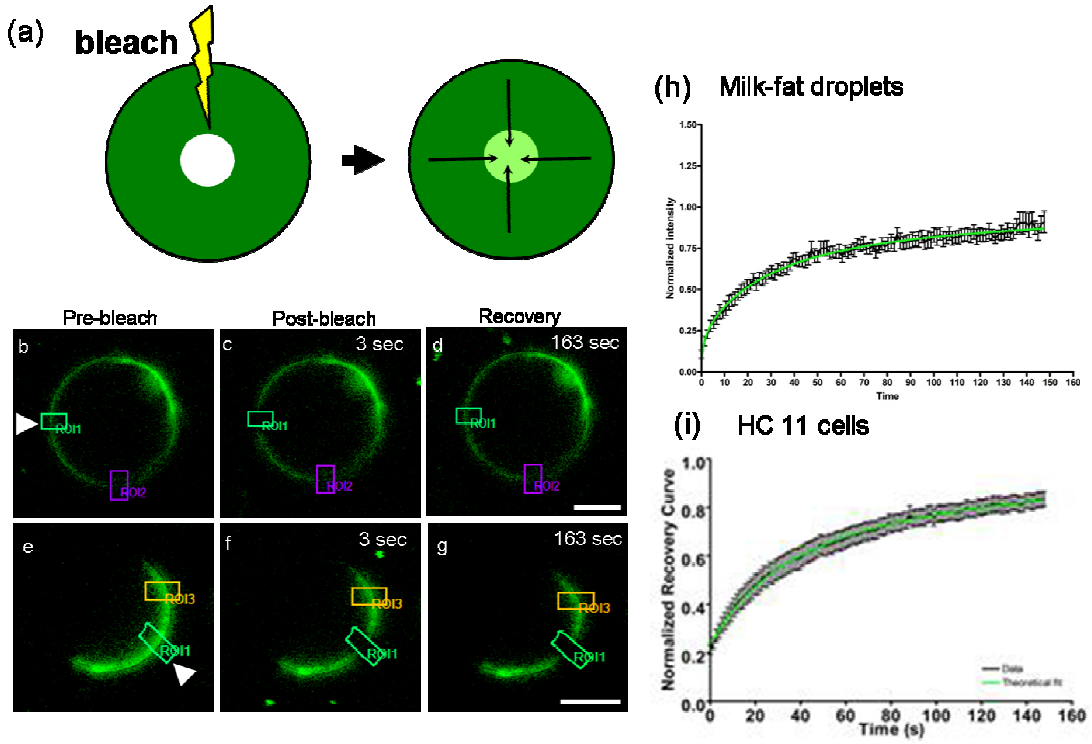


**Fig. 4.15. Fluorescence recovery after photobleaching (FRAP) analysis of the mobility of mBTN-EGFP in milk-lipid droplets from Btn1a1$^{+/+}$ mice and the plasma membrane of HC 11 cells.** Day 17-pregnant mice were transduced with Adv-mBTN-EGFP, and milk-fat droplets were collected on day 2 of lactation. Milk-fat droplets containing mBTN-EGFP were used for FRAP analysis. (a) Experimental scheme for FRAP analysis. Brief bleaching of one portion of the surface of the MFGM results in removal of most of the fluorescent signal, and allows measurement of the mobility of unbleached molecules, as they diffuse into the bleached region. (b-g) FRAP analysis from milk fat droplets containing mBTN-EGFP. (b-d) "continuous" and (e-g) "condensed" areas. (b, e), pre-bleach; (c, f), post-bleach; (d, g) recovery. Bars, 5 μm. (h, i) The summary of the analysis of recovery rates after photobleaching from (h) "continuous" milk-fat droplets (n=25) (3 mice), and (i) HC 11 cells (n=11). Bars, 5 μm. (Collaboration with Dr. Brian Daniels, NIH)

in “condensed” areas and concentrated in limited regions (Fig. 4.15 e). In “continuous” areas, mBTN-EGFP was freely mobile in the bilayer with diffusion coefficients of 0.01 $\mu m^2/s$ and recovery rates of 100% (Fig. 4.15 b-d, h and Table 5.1), and was more mobile than that in the plasma membrane of HC 11 cells (Fig. 4.15 i and Table 5.1). However, mBTN-EGFP was less mobile in “condensed” areas (Fig. e-g and Table 5.1), which suggests that there are structural changes to the MFGM after secretion as suggested from the electron micrographs of Wooding et. al. (78). Thus, BTN is freely mobile in the bilayer membrane of MFGM in some areas (“continuous”) of secreted lipid droplets but less mobile in “condensed” regions.

**Table 4.1. Measurement of mobility of mBTN-EGFP in milk-fat droplets and HC 11 cells.**

| Sample | Recovery (R, %) | Diffusion coefficient ($\mu m^2/s$) |
|---|---|---|
| Milk fat droplets | | |
| "continuous" (n=33) | 101 +/- 4[a] | 0.012 +/- 0.002[c] |
| "condensed" (n=12) | 19 +/- 7[b] | 0.005 +/- 0.002[d] |
| HC 11 cells (n=11) | 108 +/- 7[a] | 0.006 +/- 0.002[d] |

Data in columns with different superscript letters are significantly different ($P<0.05$). a and b $P<0.001$; c and d $P<0.05$.

In collaboration with Dr. Brian Daniels, NICHD, NIH.

# Chapter 5: Functional significance of BTN/XOR interactions in the lactating mammary gland

## 5.1. Rationale

As discussed in Chapter 3 and 4, we characterized the physical interaction between BTN and XOR (79), and showed that they interact in the apical plasma membrane. However, these data do not establish any functional roles for BTN/XOR complexes in the lactating mammary gland. Therefore, to address the function of BTN and XOR in lactation, we determined whether expression of XOR correlated with the amount of BTN in cultured cells, or in Btn1a1$^{+/+}$, *Btn1a1*$^{+/-}$, and *Btn1a1*$^{-/-}$ mice, and attempted to block binding of endogenous XOR to BTN *in vivo*, to see if milk-lipid secretion was inhibited.

## 5.2. Co-relationship between BTN and XOR in HC 11 cells

To determine potential relationships between the expression of BTN and XOR, HC 11 cells were transduced with Adv-mBTN-EGFP, and the total amount and distribution of endogenous XOR determined in cell fractions. As discussed above, HC 11 cells endogenously express XOR after treatment with dexamethasone (73). Surprisingly, the total level of XOR was decreased by up to 50% in cells transduced with Adv-mBTN-EGFP, compared with cells transduced with Adv-EGFP, or non-transduced controls (Fig. 5.1 a, b). As expected, expression of BTN leads to a redistribution of XOR from the

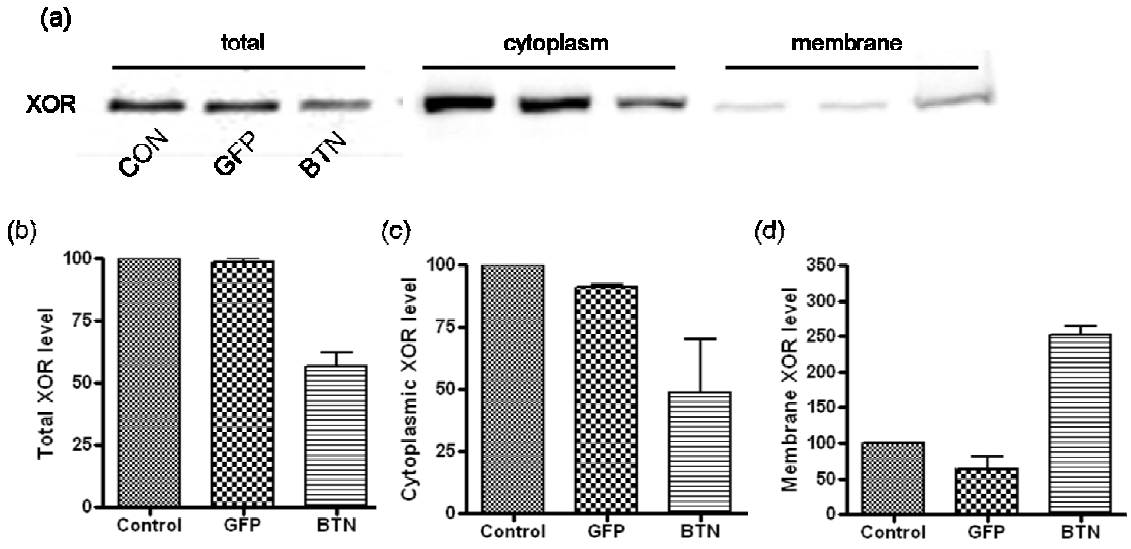


**Fig. 5.1. Expression of BTN decreases the total amount of endogenous XOR in HC 11 cells and promotes binding of XOR to cellular membranes.** HC 11 cells, grown in the presence of $10^{-6}$ M dexamethasone, were transduced with a vector encoding BTN-GFP (Adv-mBTN-GFP) (test), or GFP (Adv-GFP) (transduced control). Untransduced cells served as a second control. (a) Total extracts, cytoplasmic and membrane fractions from HC 11 cells were analyzed for XOR by Western blot. (b-d) Bar graph showing densitometric analysis of the blots shown above. Densities were normalized (100%) from untransduced cells. (b) total extracts, (c) cytoplasmic fractions, and (d) membrane fractions (n=5).

cytoplasm to membranes; cytoplasmic XOR was decreased by 50%, whereas membrane-bound XOR increased 2.5 fold compared with non-transduced cells. (Fig. 5.1 c, d). These data suggest that BTN regulates the amount of XOR in cells and influences its intracellular location.

To confirm that over-expressed mBTN-EGFP binds to endogenous XOR in the plasma membrane and intracellular organelles, the distribution of the two proteins was determined in transduced HC 11 cells. mBTN-EGFP was specifically detected in the plasma membrane or intracellular organelles, and, as predicted, XOR relocated to mBTN-EGFP-containing intra-cellular organelles and the plasma membrane compared with non-transduced controls (Fig 5.2 a-d).

To confirm the data, HC 11 cells over-expressing mBTN-ECFP were treated with digitonin to remove any soluble unbound XOR, stained with specific antibody to mXOR, and examined by confocal microscopy. Very little XOR was detected in the non-transduced cells (Fig. 5.2 e), but endogenous XOR was still bound to mBTN-ECFP in the plasma membrane and intra-cellular organelles even after treatment with digitonin (Fig 5.2 f-h). Collectively, these data indicate that BTN both binds to XOR in cellular membranes and regulates the total amount of XOR in cells, at either the post-transcriptional, or post-translational level.

### 5.3. Intracellular XOR mRNA and protein accumulate in *Btn1a1*$^{-/-}$ mice

To examine the relationship between BTN and XOR in lactating

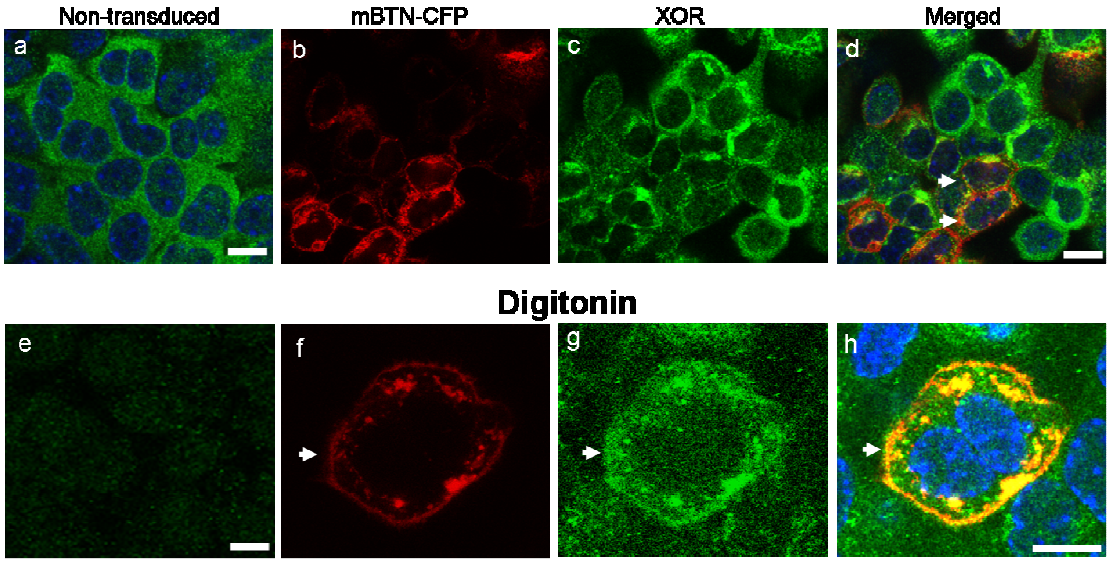


**Fig. 5.2. Expression of BTN recruits cytoplasmic XOR to the plasma membrane and intra-cellular organelles in HC 11 cells.** XOR was localized by immunofluorescence microscopy in either, (a) untransduced control cells or (b-d) cells transduced with Adv-mBTN-ECFP. (e-h) either untransduced control cells or those transduced with Adv-mBTN-ECFP, were treated with digitonin. (b, f) mBTN-ECFP, (c, g) XOR, and (d, h), merged images. White arrows, plasma membrane. Bars, 10 μm.

mammary tissue, the total amount of XOR in extracts from wild-type and mutant mouse lines was estimated by either Western blot or enzyme assay. The amount of XOR protein in *Btn1a1*$^{-/-}$ mice was 3 fold higher than in Btn1a1$^{+/+}$ mice, and 2 fold higher than in *Btn1a1*$^{+/-}$ mice using Western blot to analyze for XOR (Fig. 5.3 a). Analysis of XOR activity in six genotypes (Btn1a1$^{+/+}$, *Btn1a1*$^{+/-}$, *Btn1a1*$^{-/-}$, *Xdh*$^{+/-}$, *Btn1a1*$^{+/-}$/*Xdh*$^{+/-}$, and *Btn1a1*$^{-/-}$/*Xdh*$^{+/-}$) showed that there is an inverse linear relationship between the amount of BTN and XOR in cells (Fig. 5.3 b). Thus, activity of XOR in the total extracts and the cytoplasmic fractions is increased by 3 fold and 6 fold respectively, in *Btn1a1*$^{+/-}$ and *Btn1a1*$^{-/-}$ mice, and is expressed at predictable levels in heterozygous animals (Fig. 5.3 c, d). Interestingly, enzyme activity increased by 2 and 2.5 fold respectively, in microsomal fractions from *Btn1a1*$^{+/-}$ and *Btn1a1*$^{-/-}$ mice, presumably because accumulated XOR passively absorbed to the membrane fraction (Fig. 5.3 e).

The level of total XOR protein correlated with the amount of XOR mRNA. The amount of mRNA increased by 1.5 fold and 2 fold in *Btn1a1*$^{-/-}$ mice, compared with Btn1a1$^{+/+}$ mice, as estimated by microarray and qRT-PCR, respectively, suggesting that BTN negatively regulates the amount of XOR in cells (mRNA and protein) as well as serving as a membrane anchor that binds directly to XOR (Fig. 5.4).

### 5.4. Over-expression of the B30.2 domain acts as a dominant negative inhibitor in transduced mammary cells *in vivo*.

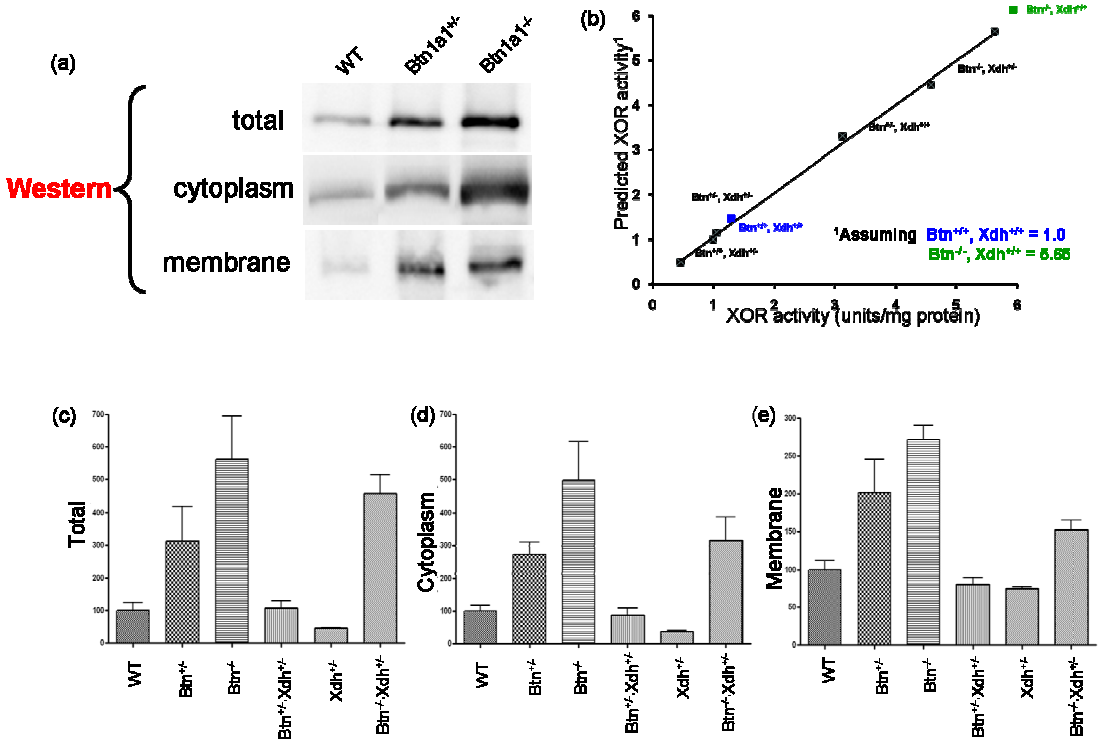


**Fig. 5.3. Amount of intracellular XOR mRNA and protein are inversely correlated with the expression of BTN.** (a) Total extracts, cytoplasmic, and membrane fractions of tissue samples from Btn1a1$^{+/+}$, *Btn1a1*$^{+/-}$, and *Btn1a1*$^{-/-}$ mice were analyzed for XOR protein by Western blot. (b) Diagram showing the amount of XOR is inversely proportional to the amount of BTN. X-axis, measured XOR activity; Y-axis, predicted XOR activity. (c-e) Analysis of XOR activity in mammary extract from six different genotypes; (c) total tissue extracts, (d) cytoplasmic fractions, and (e) membrane fractions. (n=3)

| method | Fold increase XOR mRNA |
|---|---|
| microarray | 1.5 |
| qRT-PCR | 2.0 |

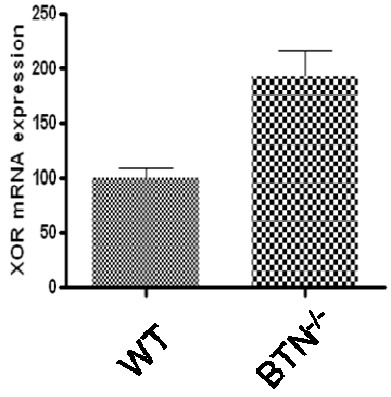


**Fig. 5.4. The amount of XOR mRNA correlated with the level of total XOR protein.** Determination of XOR mRNA levels. microarray analysis (left) and qRT-PCR (right) (n=5).

To examine the functional relationship between BTN and XOR in lactating mammary epithelial cells, we over-expressed the B30.2 domain of BTN as a soluble protein to see if it would prevent binding of XOR to endogenous membrane-bound BTN, thus acting as a dominant negative inhibitor (Fig 5.5 a). To test this, we designed a recombinant adenoviral vector separately encoding GFP and the soluble mB30.2 domain (Adv-mB30.2+EGFP), and infused it into mammary glands on day 18 of pregnancy (Fig 5.5 b). Adenoviral vectors separately encoding GFP and mB30.2$\Delta_{10}$ domain (Adv-mB30.2$\Delta_{10}$+EGFP), and EGFP (Adv-EGFP) were used as controls (Fig 5.5 b). If soluble B30.2 inhibits binding of XOR to BTN, then lipid secretion should be inhibited and large lipid droplets should accumulate in the cytoplasm, as in *Btn1a1*$^{-/-}$ mice. As predicted, mammary epithelial cells over-expressing the cytosolic B30.2 domain (marked with GFP as reporter) accumulated large lipid droplets, which is similar to the phenotype of *Btn1a1*$^{-/-}$ mice (Fig. 5.6 e-g). However, lipid droplets in cells, expressing either mB30.2$\Delta_{10}$ or GFP were no larger than droplets in untransduced cells (Fig. 5.6 h-m). The size of intracellular lipid droplets (diameter and volume) was measured and compared with those in Btn1a1$^{+/+}$ and *Btn1a1*$^{-/-}$ mice. The size of intra-cellular lipid droplets in the cells expressing the B30.2 domain approached those in *Btn1a1*$^{-/-}$ mice (Fig. 5.6 n). Whereas, lipid droplets in cells expressing mB30.2$\Delta_{10}$ and EGFP alone were the same size as those in Btn1a1$^{+/+}$ mice (Fig. 5.6 n). These data strongly suggest that the B30.2 domain, when over-expressed as a soluble protein, inhibits the interaction between XOR and

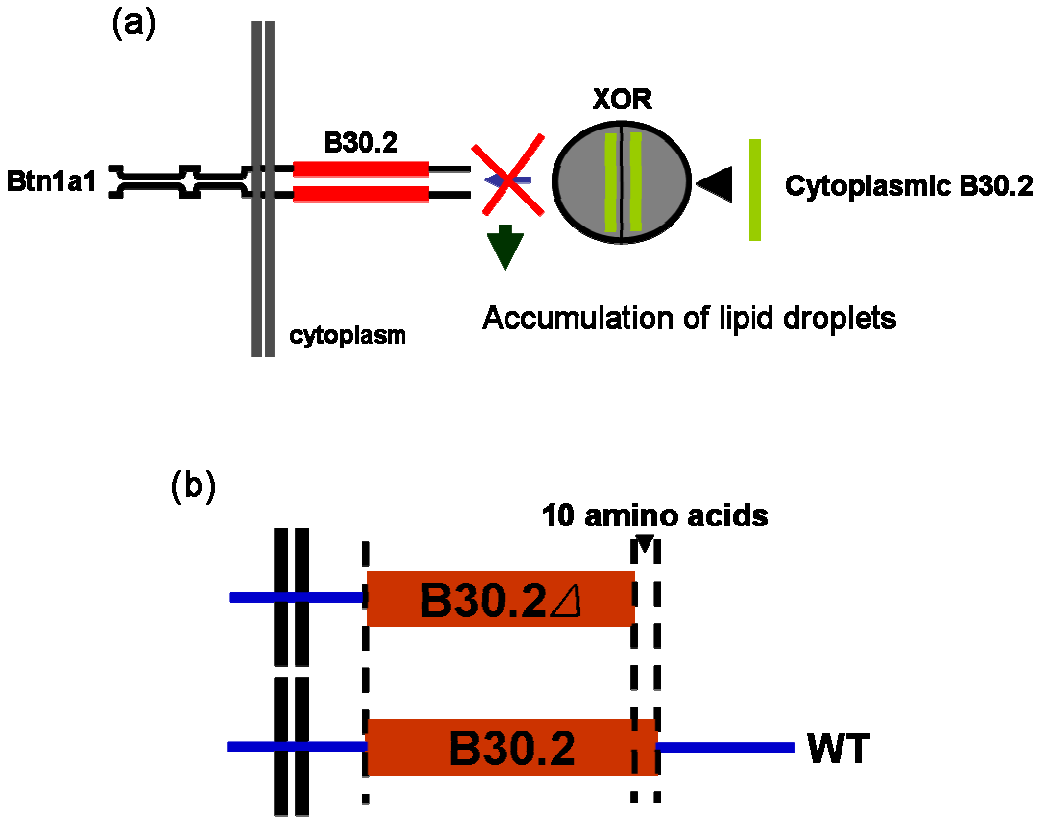


**Fig. 5.5. Experimental scheme to test whether over-expression of the mB30.2 domain acts as a dominant negative inhibitor *in vivo*.** (a) Schematic diagram showing how over-expression of cytosolic mB30.2 domain could inhibit the binding of XOR to endogenous BTN in the apical plasma membrane. (b) Diagram showing the structure of the mB30.2$\Delta_{10}$ and B30.2 domain. Mammary glands were transduced on the 18$^{th}$ day of pregnancy with adenoviral vectors separately encoding GFP and either the soluble mB30.2 or mB30.2$\Delta_{10}$ domain, and transduced tissues examined on day 2 of lactation.

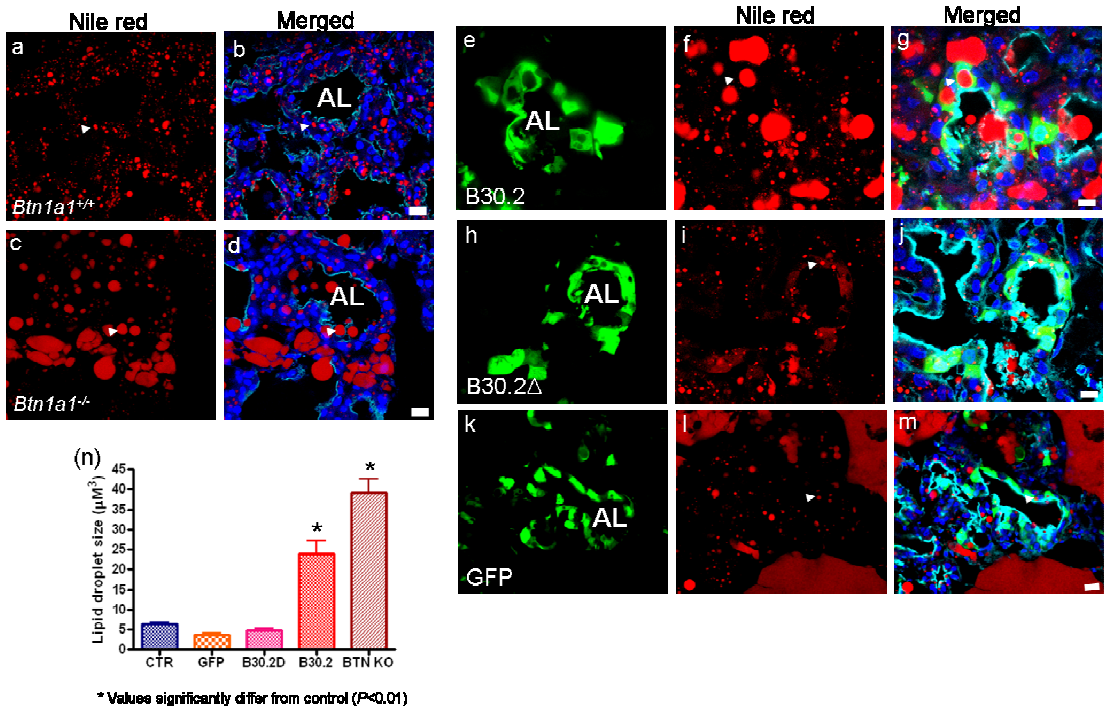


**Fig. 5.6. The mB30.2 domain acts as a dominant negative inhibitor when over-expressed in lactating mammary cells *in vivo*.** (a-d) Morphology of day 2-lactating mammary glands from Btn1a1$^{+/+}$ and *Btn1a1*$^{-/-}$ mice. (a, c) nile red stain for lipid droplets, (b, d) merged images; DAPI, blue (nuclei); WGA-Alexa 633, blue-green; white arrowhead, intracellular lipid droplets. (e-m) The mammary glands of day 17-pregnant mice were transduced with adenoviral vectors separately encoding (e-g) mB30.2+EGFP, (h-j) mB30.2$\Delta_{10}$+EGFP, and (k-m) EGFP. Tissue sections were fixed in 4% paraformaldehyde, and prepared as described in the legend to Fig. 4.6. (e) mB30.2 and EGFP, green; (h) mB30.2$\Delta_{10}$ and EGFP, green (k) EGFP, green; (f, i, l) nile red; (g, j, m) merged images; DAPI, blue. White arrowheads, intracellular lipid droplets; AL, alveolar lumen. (n) Measurement of intracellular lipid droplets. The cells marked with GFP were selected and the diameter of thirty-five intracellular lipid droplets per mouse was measured by Image-Pro plus (Version 6.2). (n=3), Bars, 10 μm.

BTN in the apical plasma membrane, and thus acts in a dominant negative manner.

### 5.5. Reducing fat content and lipid droplet size does not rescue the phenotype of *Btn1a1*$^{-/-}$ mice

Ablation of the BTN leads to accumulation of lipid droplets in the cytoplasm and inhibition of milk-lipid secretion from mammary epithelial cells (56). We postulated that this is because BTN is required for the envelopment of lipid droplets with apical plasma membrane as the droplets are secreted from the cell. However, the accumulation of lipid within the cells causes secondary structural damage to both cells and alveoli, potentially suggesting other more indirect inhibitory mechanisms. Therefore, we attempted to "rescue" the *Btn1a1*$^{-/-}$ mice by reducing the lipid-droplet size and the amount of lipid by feeding trans-10, cis-12 conjugated linoleic acid (CLA) in early lactation (Table 5.1). We reasoned that decreased lipid synthesis and droplet size would prevent forced secretion of large lipid droplets and maintain mammary structure. However, if BTN is required for milk-lipid secretion, then lipid droplets should still accumulate within the cells. Two groups of lactating mice (Btn1a1$^{+/+}$ and *Btn1a1*$^{-/-}$) were fed either a control diet containing oleic acid (20 g/kg), or a CLA diet, in which 6.67 g oleic acid was replaced with 6.67g CLA from day 6 to day 10 of lactation. On day 10 of lactation, milk samples were collected for estimation of milk-fat content. Pup weight was measured from day 6 to day 10 of lactation. Mammary tissue was collected

**Table 5.1. Four different sample groups used for CLA experiment.**

| Experimental groups | | | |
|---|---|---|---|
| WT | *Btn1a1*$^{-/-}$ | WT | *Btn1a1*$^{-/-}$ |
| Not fed with CLA | | Fed with CLA | |

Six mice were used for per group

and processed for microscopy.

As predicted, The CLA diet decreased milk-lipid content (%, wt/vol) by 40% and 30% in Btn1a1$^{+/+}$ and *Btn1a1*$^{-/-}$ mice, respectively (Fig. 5.7 a). The growth rate of pups was measured from day 6 to day 10 of lactation. As expected, Btn1a1$^{+/+}$ mice fed with CLA grew at 50% of the rate of Btn1a1$^{+/+}$ mice fed the control diet (Fig. 5.7 b). Likewise, the growth of *Btn1a1*$^{-/-}$ mice fed with CLA was reduced by about 50% compared with *Btn1a1*$^{-/-}$ control mice (Fig. 5.7 b). We expected that if reduced milk-fat content can rescue the phenotype of *Btn1a1*$^{-/-}$ mice, pup growth rate of CLA-fed *Btn1a1*$^{-/-}$ mice might be similar to *Btn1a1*$^{-/-}$ control mice. However, feeding a diet containing CLA in *Btn1a1*$^{-/-}$ mice reduced pup growth rate by about 40%, which indicates that feeding CLA in *Btn1a1*$^{-/-}$ mice does not rescue the phenotype of pup's growth rate (Fig. 5.7 b). To determine whether feeding CLA affects the size of intra-cellular lipid droplets and morphology of the mammary epithelial cells, the mammary gland was examined by either fluorescence or DIC microscopy. Feeding Btn1a1$^{+/+}$ mice a diet containing CLA reduced the size of lipid droplets compared with Btn1a1$^{+/+}$ mice (Fig. 5.7 c-d, g-h). However, CLA-fed *Btn1a1*$^{-/-}$ mice still accumulated of large lipid droplets in the lumen and in cells. (Fig. 5.7 e-f, i-j). Thus, CLA reduced the milk-fat content of Btn1a1$^{+/+}$ and *Btn1a1*$^{-/-}$ mice, and this reduction was accompanied by a decrease in the size of both intra-cellular and secreted lipid droplets in Btn1a1$^{+/+}$ mice. However, lipid droplets still accumulated in *Btn1a1*$^{-/-}$ mice fed CLA. Hence, reduction of milk-fat synthesis and lipid droplet size does not rescue the lactation

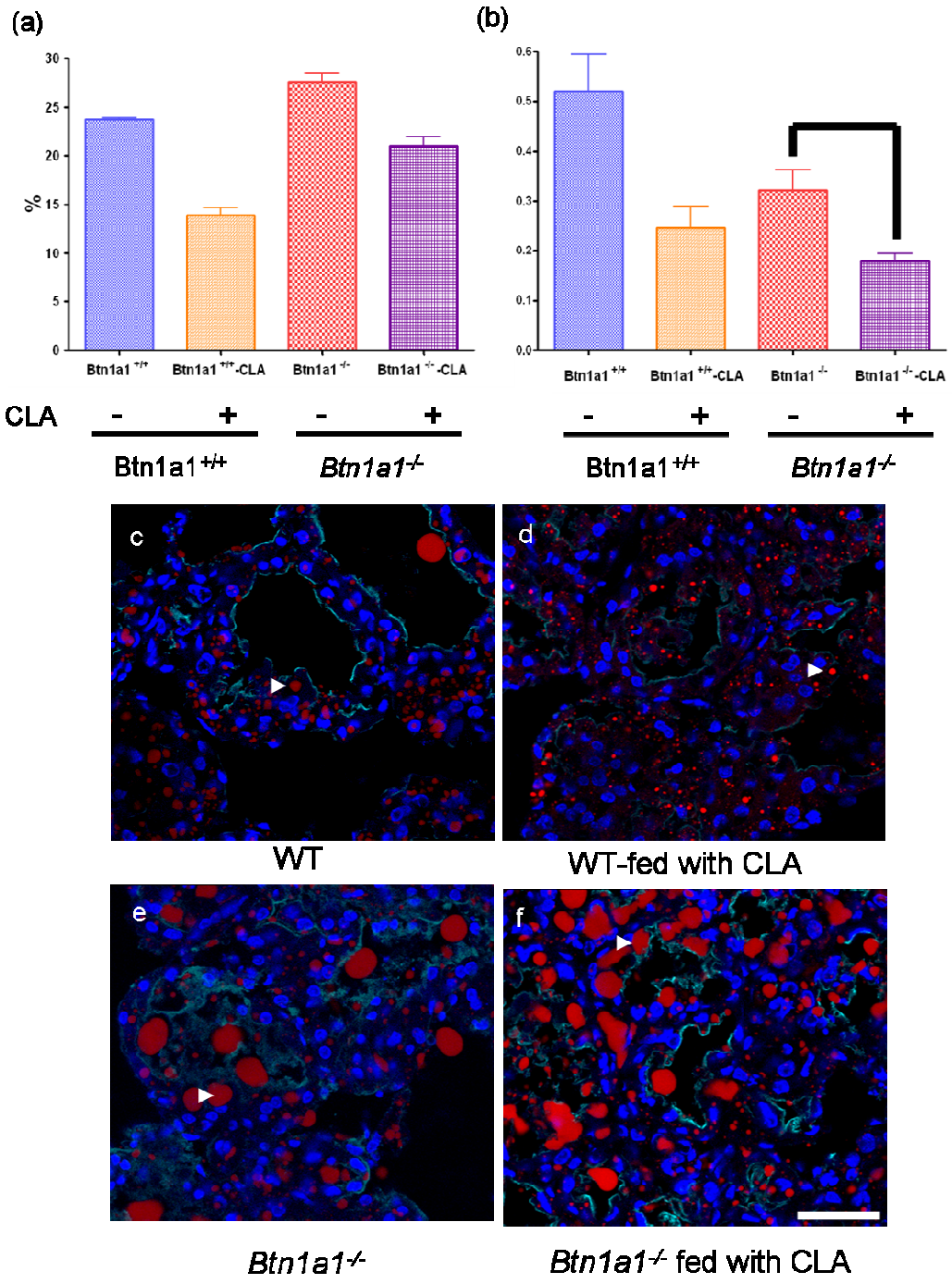
(a)
(b)
%
Btn1a1 +/+
Btn1a1 +/+-CLA
Btn1a1 -/-
Btn1a1 -/--CLA
CLA
-
+
Btn1a1 +/+
Btn1a1 -/-
c
d
WT
WT-fed with CLA
e
f
Btn1a1 -/-
Btn1a1 -/- fed with CLA

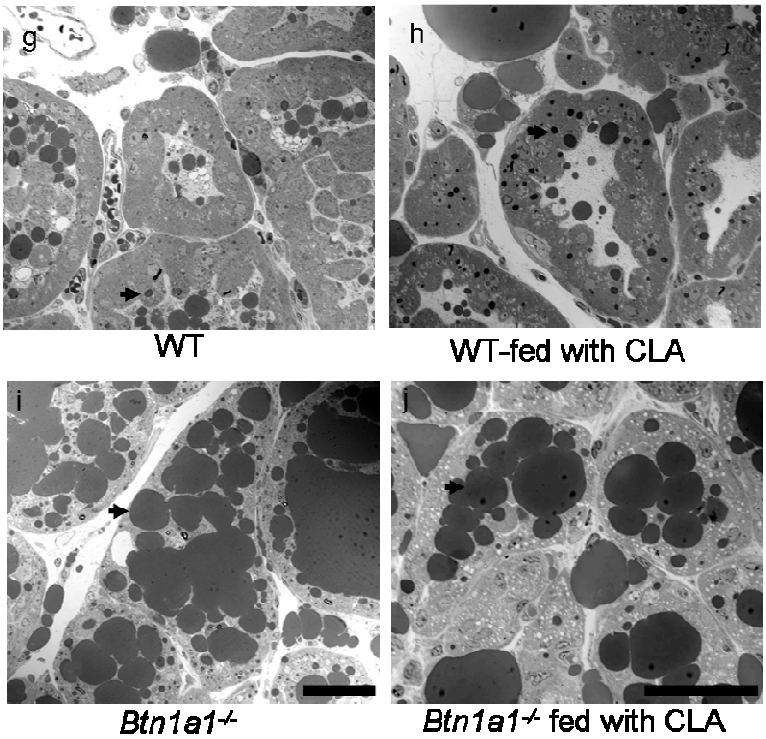


**Fig. 5.7. Reducing fat content does not rescue the phenotype of *Btn1a1*$^{-/-}$ mice.** (a-j) Two groups of lactating mice (Btn1a1$^{+/+}$ and *Btn1a1*$^{-/-}$) were fed either a control diet containing oleic acid (20 g/kg), or a CLA diet, in which 6.67 g/kg oleic acid was replaced with 6.67 g/kg CLA from day 6 to day 10 of lactation. (a) Milk samples were collected on day 10 of lactation and milk lipid percentage (*vol/vol*) was estimated by crematocrit. (72) (b) Pup weight was measured from day 6 to day 10 of lactation. (c-f) Mammary tissue sections from (c, d) day 10 lactating Btn1a1$^{+/+}$, and (e, f) *Btn1a1*$^{-/-}$ mice fed (c, e) without or (d, f) with CLA in the diet were stained with nile red for lipid droplets (red), WGA-Alexa 633 stain for apical plasma membrane (blue-green), DAPI stain for nuclei (blue). White arrowheads, intracellular lipid droplets. Bar, 50 μm. (g-j) Lactating mammary tissues were fixed simultaneously with 2.5% (w/v) glutaraldehyde and 2% (w/v) $OsO_4$ and embedded in Epon. Sections (1–2 μm) were observed directly by differential interference microscopy. (g) Btn1a1$^{+/+}$ mice, (h) CLA-fed Btn1a1$^{+/+}$ mice, (i) *Btn1a1*$^{-/-}$ mice, (j) CLA-fed *Btn1a1*$^{-/-}$ mice. Black arrow, intracellular lipid droplets. (Collaboration with Dr. A. K. G. Kadegowda)

phenotype of *Btn1a1*$^{-/-}$ mice, thus suggesting that BTN may play a direct role in milk-lipid secretion.

### 5.6. Loss of BTN causes apoptosis in the lactating mammary gland

As shown above, the loss of BTN causes accumulation of XOR in mammary epithelial cells and degeneracy in the apical plasma membrane. We therefore tested the possibility that apoptosis is induced in *Btn1a1*$^{-/-}$ mice, because of either accumulation of large lipid droplets or increased XOR levels. Day-10 lactating mammary glands from Btn1a1$^{+/+}$ and *Btn1a1*$^{-/-}$ mice were examined by the TUNEL assay, and compared with day 3 involuting mammary glands as positive controls. There was no evidence of apoptosis in wild-type controls (Fig. 5.8 a-b, g). However, about 10% of the mammary epithelial cells in the *Btn1a1*$^{-/-}$ mice were apoptotic (Fig. 5.8 c-d, g), which is similar to cells in glands at day 2 of involution (Fig. 5.8 e, f, g). To confirm these data, the level of cleaved caspase-3 was examined by immunofluorescence microscopy. There was no evidence of cleaved caspase-3 in Btn1a1$^{+/+}$ mice in agreement with the TUNEL assay. (Fig. 5.8 h, i). However, about half of the mammary epithelial cells were positive for cleaved caspase-3 (Fig. 5.8 j, k). Thus, the data from TUNEL and cleaved caspase-3 assays indicate that loss of BTN causes apoptosis in the lactating mammary gland.

### 5.7. Accumulation of large lipid droplets does not cause cell apoptosis

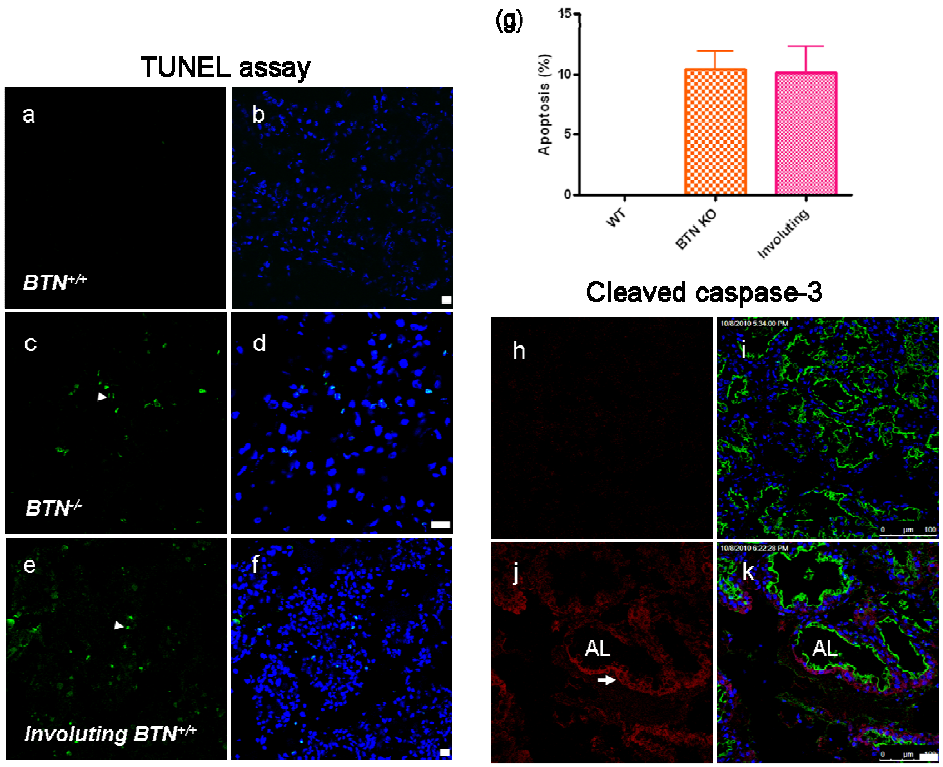


**Fig. 5.8. Loss of BTN causes apoptosis in the lactating mammary gland.** (a-f) Tissue sections from Btn1a1$^{+/+}$, *Btn1a1*$^{-/-}$, mice at day 10 of lactation and Btn1a1$^{+/+}$ mice at day 2 of involution were analyzed by the TUNEL assay to identify apoptotic cells. Tissue sections were fixed in 4% paraformaldehyde, and prepared as described in the manufacture's manual (In situ Cell Death Dectection Kit, Fluorescein; Roche). (a, b) Btn1a1$^{+/+}$ at day 10 lactation, (c, d) *Btn1a1*$^{-/-}$ at day 10 lactation, (e, f) Btn1a1$^{+/+}$ mice at day 2 of involution. (a, c, e), TUNEL assay; (b, d, f) merged images with DAPI, blue (nuclei). Bars, 10 μm. (g) Quantification of data from 3 mice (1,000 cells/mouse). (h-k) Mammary tissue at day 10 of lactation was fixed as described in the legend to Fig. 4.6 and cut into 10 μm frozen sections. (h, i) Btn1a1$^{+/+}$, and (j, k) Btn1a1$^{-/-}$ mice. Sections were incubated with specific antibody to mouse cleaved caspase-3, followed by goat anti-(rabbit IgG-Alexa568) as secondary detecting agent. (h, j), cleaved caspase-3; (i, k), merged images with DAPI, blue (nuclei); WGA-Alexa 633 stain for apical plasma membrane, green. AL, aveolar lumen; white arrowheads, positive signal for TUNEL and cleaved caspase-3. Bars, 20 μm.

As shown above, over-expression of B30.2 domain acted as a dominant negative inhibitor, and caused accumulation of large lipid droplets. To test the possibility that over-expression of the B30.2 domain induces apoptosis in the lactating mammary glands of wild-type mice, the level of cleaved caspase-3 in mammary glands expressing either B30.2+EGFP or B30.2$\Delta_{10}$+EGFP was examined by immunofluorescence microscopy. Day 3 involuting mammary glands were used as positive controls (Fig. 5.9 i-k). As expected, there was no evidence of cleaved caspase-3 in cells expressing B30.2$\Delta_{10}$+EGFP (Fig. 5.9 a-d). In addition, only 0.4% of cells expressing B30.2+EGFP were positive with antibody to cleaved caspase-3 (Fig. 5.9 e-h). Thus, induction of apoptosis is a secondary effect, most likely caused by the accumulation of large lipid droplets in the cytoplasm, which damages cell structure and triggers apoptotic signaling cascades.

In summary, the results in this chapter show that BTN modulates the amount of soluble XOR in mammary epithelial cells during lactation, and that interaction between the two proteins is most likely required for the accretion and/or secretion of milk-lipid droplets.

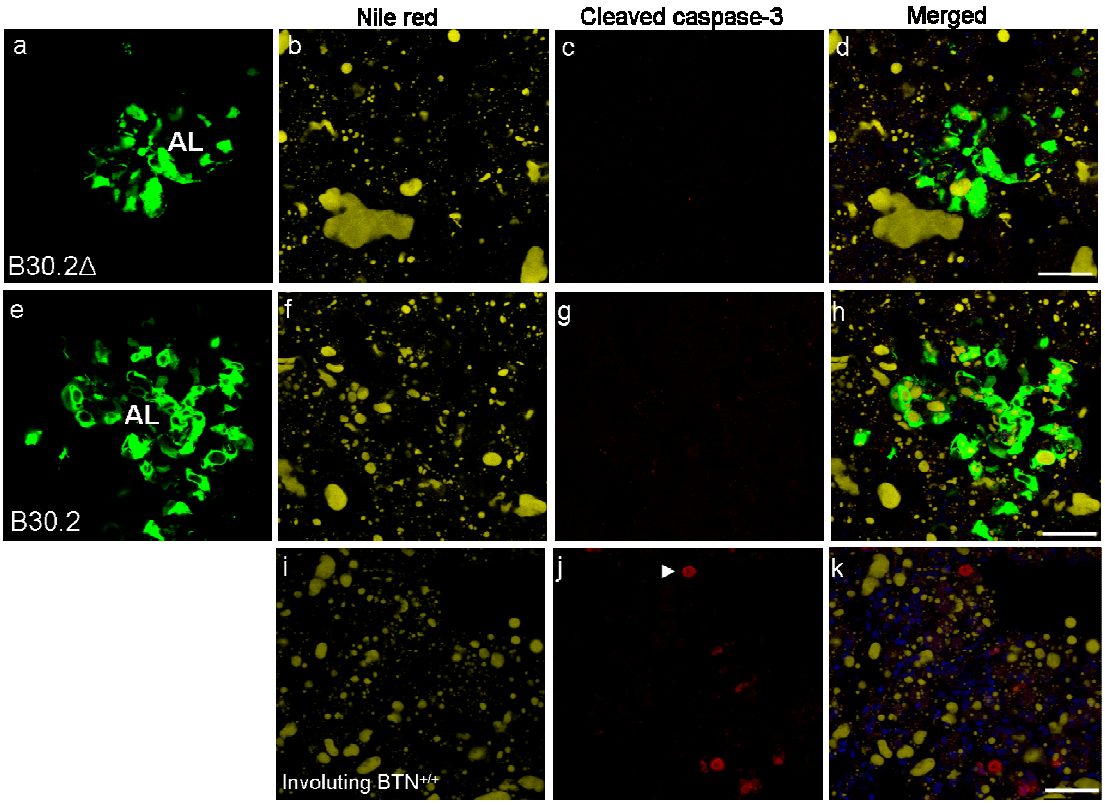


**Fig. 5.9. Accumulation of large lipid droplets does not cause cell apoptosis.** (a-h) Mammary tissue expressing B30.2$\Delta_{10}$+EGFP and B30.2+EGFP, as described in Fig 5.6, were cut into 10 μm frozen sections. (a-d) B30.2$\Delta_{10}$+EGFP, (e-h) B30.2+EGFP, and (i-k) day 3 involuting mammary gland. Sections were incubated with specific antibody to mouse cleaved caspase-3, followed by goat-anti(rabbit IgG)-Alexa633 as secondary detecting agent. (a) B30.2$\Delta_{10}$+EGFP, (e) B30.2+EGFP, (b, f, i) nile red, (c, g, j) cleaved caspase-3, (d, h, k) merged images with DAPI, blue. AL, alveolar lumen; white arrow head, positive signal for cleaved caspase-3 (n=3). Bars, 50 μm.

## Chapter 6: Discussion

Our objective was to investigate the potential functions of BTN and XOR in the mammary gland and in the secretion of lipid droplets during lactation. Preliminary evidence suggested that XOR binds to the cytoplasmic domain of mouse BTN in an *in vitro* binding assay (80, 81). Furthermore, BTN and XOR are the most abundant MFGM proteins in most species (6, 21, 23, 34, 82), and *Btn1a1*$^{-/-}$ and *Xdh*$^{+/-}$ mice have a similar lactation phenotype, so we hypothesized that BTN and XOR may bind to each other *in vivo* and function as a complex required for milk-lipid secretion during lactation. In this context, several major findings from this work are especially pertinent:-

(1) We showed that the cytoplasmic domain of BTN self-associates, probably via the stem region, which is predicted to comprise a short coiled-coil domain (55, 83) and that the cytoplasmic domain of BTN binds to XOR *in vitro* and *in vivo* with relatively high affinity. Furthermore, we identified the B30.2 domain of BTN as the region that binds to XOR in a pH- and salt-sensitive manner. Binding was independent of species; bovine or mouse XOR bound to the B30.2 domain of mouse, cow, or human BTN1A1. However, binding was not detected between XOR and the closely related paralogs, BTN2A1 and BTN3A1, or to the B30.2 domain of the unrelated RoRet (TRIM 38) protein even though the B30.2 domains are very similar to the B30.2 domain of BTN1A1. *In vitro* bead binding assays showed that bXOR binds to

the B30.2 domain of BTN with a monomeric binding ratio of 1:1, which is in agreement with the SPR data. These data are consistent with binding ratios for the B30.2 domain-containing proteins, GUSTAVUS and TRIM21, with their ligands (61, 62, 84, 85). Because bXOR is present as a homodimer in nature, presumably two B30.2 domains bind to one native XOR molecule. Thus, the binding specificity, stoichiometry, abundance and high levels of expression in the mammary gland suggest that BTN and XOR have specific functional roles in lactation.

The B30.2 domain is a conserved region of approx. 170 amino acids associated with several protein families including the BTN and TRIM families (83, 86), and the B30.2 domains have been identified in at least 86 human genes (83). Based on available 3D structural data, the B30.2 domain is assumed to function as a universal protein binding module (61, 62, 84, 85). The structure of the B30.2 domain comprises a conserved highly distorted core β-sandwich which is connected by variable loops (61, 85). In the available 3D structures, ligand binds to the B30.2 domains via the variable loops either by hydrogen bonding or hydrophobic interactions (61, 85). Comparison of the linear sequences of the B30.2 domain of human BTN1A1 with other family members (BTN2A1, BTN2A2, BTN2A3, BTN3A1, BTN3A2, and BTN3A3) shows that the most similar regions are the β-strands and that the loop regions are the most variable, suggesting that independent binding motifs are associated with the loops. The interaction of BTN with XOR shares

several common features with the binding characteristics of other B30.2 domain-containing proteins with their respective ligands. Thus, the dissociation constant ($K_D$) for the binding of BTN to XOR (27 nM in 20mM NaCl) is similar to those for GUSTAVUS (40 nM in 150mM NaCl) (84), and TRIM 21 (37 nM in 50 mM NaCl) (85), and in all cases, lower $K_D$ values (higher affinities) are associated with lower salt concentrations (79, 84, 85). However, because of the presumed discontinuous binding motifs of the B30.2 domain in the linear sequence, it is not possible to predict which residues in BTN are responsible for binding to XOR. Resolution of these structural issues will require analysis by x-ray crystallography.

(2) *In vivo* localization of BTN and XOR in the mammary gland revealed that BTN exclusively localizes in the apical plasma membrane, and that XOR is enriched at the same site. However, XOR freely diffuses in the cytoplasm in the absence of BTN in *Btn1a1*$^{-/-}$ mice, which suggests that BTN recruits XOR to the apical plasma membrane in wild-type mice. XOR was not detected on the surface of lipid droplets in either cultured cell lines or in lactating mammary tissue. Ablation of BTN gene expression in *Btn1a1*$^{-/-}$ mice dramatically increased the amount of XOR protein compared with wild-type mice, probably because XOR loses its binding partner protein, BTN, in the apical plasma membrane, and XOR cannot be secreted by the regular milk-lipid secretory mechanism. However, BTN may also regulate the amount of XOR by transcriptional or post-transcriptional mechanisms as the amount of

XOR mRNA is increased in *Btn1a1*$^{-/-}$ mice compared with wild-type mice, and over-expression of BTN in cultured cells reduces the amount of XOR protein. These data suggest that BTN negatively regulates the amount of XOR in cells (mRNA and protein) as well as serving as a membrane anchor that binds directly to XOR.

(3) Over-expression of cytosolic B30.2 domain acts as a dominant negative inhibitor, which induces a similar phenotype to that of *Btn1a1*$^{-/-}$ mice, i.e., the accumulation of large lipid droplets in the cytoplasm. The most facile explanation for this is that over-expression of the B30.2 domain inhibits the interaction between XOR and BTN in the apical plasma membrane, and thus inhibits milk-lipid secretion. These results are also consistent with data showing that XOR in the apical plasma membrane diffuses into the cytoplasm during milk stasis, at the time that large lipid droplets accumulate in the cells and lumen (23). However, during milk stasis, BTN remains in the apical plasma membrane, when XOR redistributes to the cytoplasm (23) potentially suggesting that milk stasis disrupts the binding between BTN and XOR by some unknown mechanism. One possibility is that the two proteins dissociate during stasis because the pH of the cytoplasm drops, and as we have shown, XOR does not bind to BTN below pH 6.0 (Fig. 3. 13 a).

As discussed in the introduction, three models have been proposed to explain how BTN and XOR may function in lipid secretion (6, 23, 43, 56, 69).

Mather and Keenan have suggested that BTN, as a transmembrane protein, binds to XOR. This interaction is required for the formation of the outer envelope of the MFGM and expulsion of the lipid droplets into the lumen (43, 56). In the process of lipid-droplet secretion, the lipid droplet remains a constant distance of about 10-20 nm from the outer apical membrane bilayer, which suggests that a protein coat including cytoplasmic XOR between the lipid droplets and outer apical membrane is responsible for secretion of the droplets (6). However, this model did not clarify where XOR is located, either on the lipid droplet surface, the apical plasma membrane, or sandwiched between both places. In an alternative model, McManaman et. al. have proposed that XOR is sandwiched between BTN in the apical plasma membrane and adipophilin (ADPH) on the surface of lipid droplet and is stabilized by disulfide bonds (23). In a radically different model, Robenek et. al. have suggested that milk-lipid secretion is regulated entirely by interactions between BTN molecules localized in both the apical plasma membrane and the surface of intracellular lipid droplets (69). Thus, each model gives rise to a set of predictions :-

| models | Predictions |
|---|---|
| Mather and Keenan | - BTN forms oligomers by self-association |
| (6, 43, 56) | - BTN localizes exclusively in the apical plasma membrane |
| | - Cytoplasmic XOR binds to either the surface of intracellular |

| | |
|---|---|
| | lipid droplets or the apical plasma membrane |
| McManaman et. al. (23) | - Both BTN and XOR localize in the apical plasma membrane<br>- Either BTN or XOR bind to ADPH |
| Robenek et. al. (69) | - BTN localizes in both the apical plasma membrane and on cytoplasmic lipid droplets and does not bind to XOR |
| All models | - BTN should be immobile in the plane of the lipid bilayer (Fig. 6.1) |

Our results reveal that BTN exclusively localizes in the apical plasma membrane, and XOR locates in the cytoplasm, but is enriched in the apical plasma membrane. In addition, XOR does not bind to the surface of lipid droplets in lactating mammary gland or on lipid droplets in cultured cells. Furthermore, XOR freely diffuses in the cytoplasm, and accumulates in the absence of BTN. Thus, BTN/XOR complexes localize to the apical plasma membrane, presumably because BTN functions as a binding scaffold for XOR as predicted by Mather and Keenan (6, 43, 56) and McManaman et. al. (23). However, the model suggested by Robenek et. al. (69) is not consistent with these data. Neither is Robenek's model consistent with our inability to detect BTN on intracellular lipid droplets, in either cultured cells or lactating mammary tissue.

In all proposed models, BTN should not be mobile in the bilayer membrane of MFGM (Fig. 6.1). However, BTN was freely mobile in the

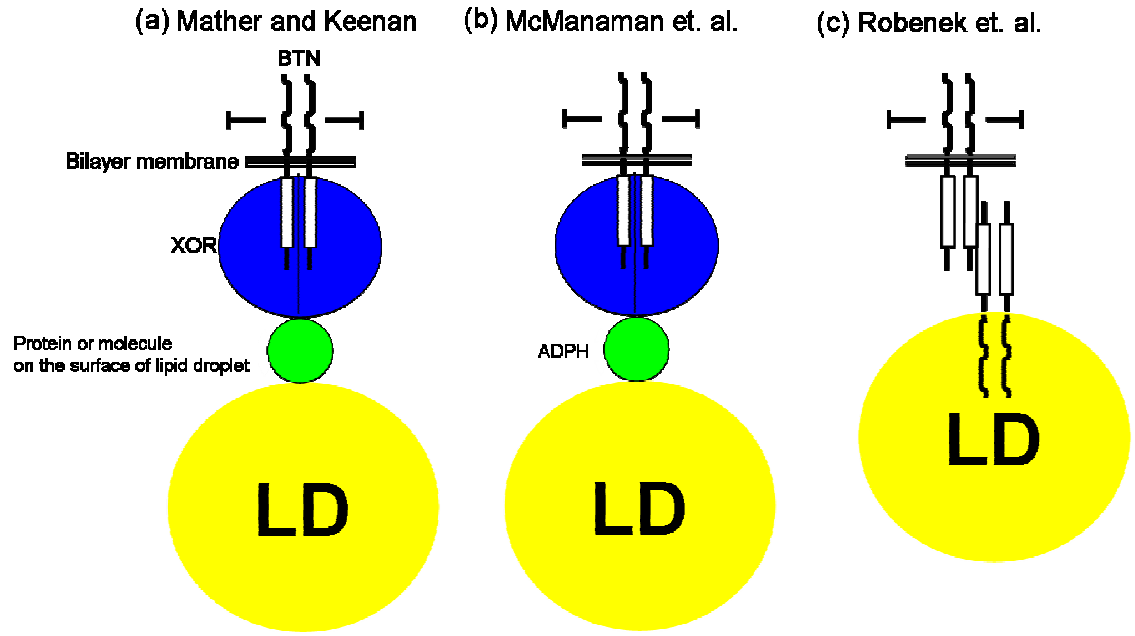


**Fig. 6.1. Predictions of mobility of BTN on the MFGM from three proposed models.** (a) Interactions between BTN/XOR complexes and other proteins or molecules on the surface of lipid droplet may inhibit the mobility of BTN in the bilayer membrane of MFGM (6, 43, 56). (b) Interactions between BTN/XOR complexes and ADPH on the surface of lipid droplet reduce the mobility of BTN in the bilayer membrane of MFGM (23). (c) Interactions between BTN molecules, localized to both the apical membrane and the surface of lipid droplets, prevent BTN from moving in the bilayer membrane of MFGM (69).

bilayer of droplets evenly coated with membrane (“continuous”) with diffusion coefficients of the same order as BTN in the plasma membrane of HC 11 cells. This suggests that BTN/XOR complexes are not anchored to proteins or molecules on the surface of lipid droplets in MFGM (Fig. 6.2). The difference in the mobility of mBTN-EGFP in “continuous” and “condensed” regions (Fig. 4.15) is almost certainly a reflection of the structural changes that occur to the MFGM after secretion (4, 38, 78). Immediately after secretion, the bilayer is continuous around droplets, but during storage in the gland, the membrane condenses into continents and islands, and the protein coat thickens between the bilayer and the surface of the droplets. The observation that mBTN-EGFP is freely mobile in droplets with a continuous membrane is important, because these droplets are freshly secreted, and have not undergone any structural change. All three models predict that mBTN-EGFP should be immobile, even in these nascent lipid droplets. Thus, the FRAP data are not consistent with any of the proposed models.

One possibility is that as in the models of Mather and Keenan (6, 43, 56), and McManaman et. al. (23), BTN binds to XOR in the apical plasma membrane (Fig. 6.3 a, b), and the complexes function in lipid droplet secretion. The complexes interact with proteins or molecules on the surface of lipid droplets (possibly ADPH) (Fig. 6.3 c) (23), and the lipid droplets are secreted into the lumen (Fig. 6.3 d). After secretion, proteins or molecules on the lipid droplet surface dissociate, and BTN/XOR complexes become freely

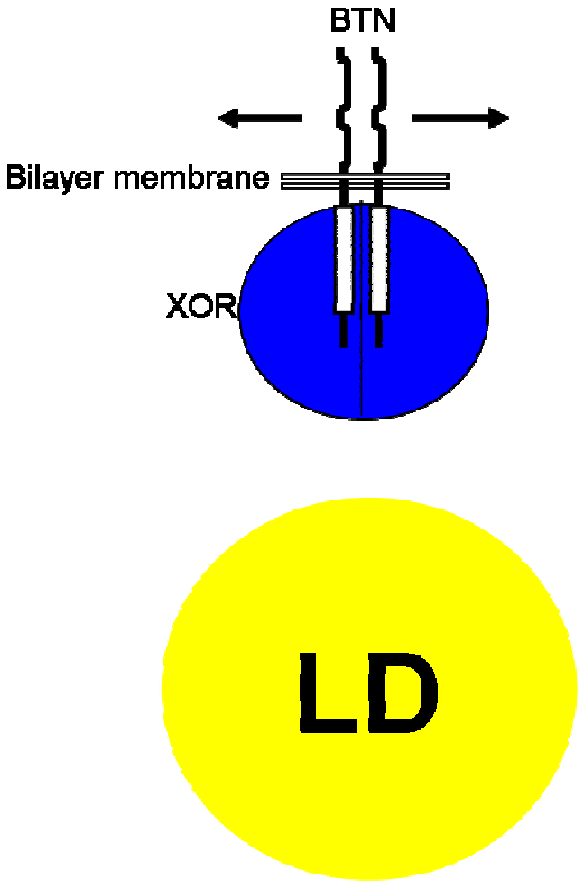


**Fig. 6.2. Mobility of BTN in milk-lipid droplets and in the plasma membrane of HC 11 cells.** BTN was freely mobile in the bilayer of the MFGM, and in the plasma membrane of HC 11 cells with same diffusion coefficient.

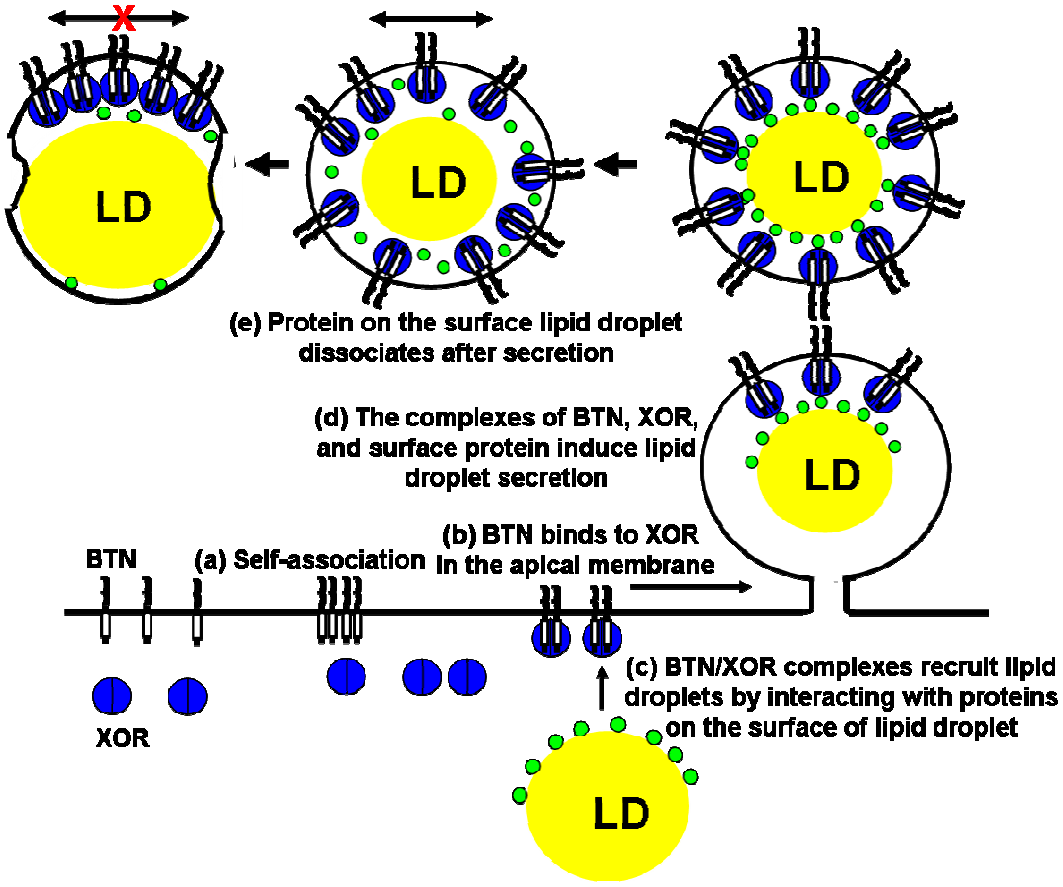


**Fig. 6.3. Working model for the function of BTN/XOR complexes in lipid droplet secretion.** (a) BTN self-associates and, (b) binds to XOR in the apical plasma membrane. (c, d) BTN/XOR complexes bind to proteins or molecules on the surface of lipid droplets, and lipid droplets are secreted into the lumen. (e) After secretion, the complex of BTN and XOR disengages from the droplet and is freely mobile in the bilayer membrane.

mobile (Fig. 6.3 e). Interference in the interaction between BTN and XOR, e.g., in knock-out mouse strains (56, 63) and after over-expression of the B30.2 domain (Fig. 5.6), causes the accumulation of lipid droplets, and XOR accumulates in the cytoplasm (Figs. 4.9, 5.3).

Interestingly, the loss of BTN caused cell apoptosis in lactating mammary gland. In appropriate physiological contexts, XOR, either as a dehydrogenase or an oxidase can generate ROS, including $H_2O_2$ and superoxide radical, which may act on downstream targets and regulate gene expression (87). Stress activated p56 MAP kinase induces gene expression of XOR, following the increase of XOR-derived ROS, and induces cell apoptosis (72, 73, 87). Since the accumulation of XOR causes cell death, the cells have to regulate the amount of XOR at sub-apoptotic levels. Consistently, XOR levels dramatically increase and apoptosis is induced in *Btn1a1*$^{-/-}$ mice (Fig. 5.8).

Therefore, this raises the possibility that the primary function of BTN is to maintain mammary secretory cells in a fully differentiated state either as a regulator of XOR levels or as part of a signaling complex with XOR. If this were the case, then interference of XOR binding to BTN by over-expression of the B30.2 domain should induce apoptosis; first, and then only secondarily cause the accumulation of large lipid droplets in the cytoplasm. However, over-expression of cytosolic B30.2 domain induced the accumulation of large lipid droplets, and evidence of apoptosis was minimal (Fig. 5.9). Thus, cell

apoptosis in the BTN knock-out mouse appears to be a secondary effect caused by the accumulation of large lipid droplets and consequent structural damage when lipid secretion is inhibited. Elevated levels of XOR and ROS may also contribute to cell damage. Further experiments will be required to explain how the loss of BTN induces cell apoptosis in lactating mammary gland.

In summary, the results, presented in this thesis, show that BTN binds to XOR with high affinity through the B30.2 domain, and that interaction between the two proteins *in vivo* is essential for the regulated accretion and/or secretion of lipid droplets from mammary cells during lactation.

## Chapter 7. References


(1) McManaman, J. L., and Neville, M. C. (2003) Mammary physiology and milk secretion. *Adv Drug Deliv Rev*. 55, 629-641

*(2)* Brisken, C. (2002) Hormonal control of alveolar development and its implications for breast carcinogenesis. *J. Mammary Gland Biol. Neopl. 7, 39-48*

*(3)* Alberts, B., Johnson, A., Lewis, J. (2008) Molecular Biology of the Cell. 5th edition. New York, 1426.

*(4)* Wooding, F, B, P. (1971) The mechanism of secretion of the milk fat globule. *J. Cell Sci.* 9, 805-821

*(5)* Wooding, F, B, P. (1973) Formation of the milk fat globule membrane without participation of the plasmalemma. *J. Cell Sci.* 13, 221-235

(6) Mather. I. H. and Keenan, T. W. (1998) Origin and secretion of milk lipids. *J. Mammary Gland Biol. Neopl.* 3, 259-273

(7) Olins, G. M. and Bremel, R. D. (1984). Oxytocin-stimulated myosin phosphorylation in mammary myoepithelial cells: roles of calcium ions and cyclic nucleotides. *Endocrinology.* 114, 1617-1626.

(8) Shennan, D. B., and Peaker, M. (2000) Transport of milk constituents by the mammary gland. *Physiol. Rev.* 80, 925-951

(9) Ollivier-Bousquet, M (1998). Transferrin and prolactin transcytosis in the lactating mammary epithelial cell. *J. Mammary Gland Biol. Neopl.* 3, 303-313

(10) Valivullah, H. M., Bevan, D. R., Peat, A., and Keenan, T. W. (1988) Milk lipid globules: control of their size distribution. *Proc. Natl. Acad. Sc.i U.S.A.* 85, 8775-8779

(11) Cooper, S, M. and Grigor, M, R. (1980) Fatty acid specificities of microsomal acyltransferases esterifying positions-1 and -2 of acylglycerols in mammary glands from lactating rats. *Biochem. J*. 187,289-295

(12) Stein, O. and Stein, Y. (1967) Lipid synthesis, intercellular transport, and secretion. *J. Cell Biol*. 34, 1967

(13) Dylewski, D, P, Dapper, C, H, Valivullah, H, M, Deeney, J, T, Keenan, T, W. (1984) Morphological and biochemical characterization of

possible intracellular precursors of milk lipid globules. *Eur. J. Cell Biol*. 35, 99-111

(14) Deeney, J, T, Valivullah, H, M, Dapper, C, H, Dylewski, D, P, Keenan, T, W (1985) Microlipid droplets in milk secreting mammary epithelial cells: evidence that they originate from endoplasmic reticulum and are precursors of milk lipid globules. *Eur. J. Cell Biol*. 38, 16-26

(15) Ghosal, D., Shappell, N, W., and Keenan, T, W. (1994) Endoplasmic reticulum lumenal proteins of rat mammary gland. Potential involvement in lipid droplet assembly during lactation. *Biochim. Biophys. Acta.* 6, 175-81

(16) Martin, S and Parton, R. G. (2006) Lipid droplets: a unified view of a dynamic organelle. *Nat. Rev.* 7, 373-378

(17) Zaczek, M., and Keenan, T, W. (1990) Morphological evidence for an endoplasmic reticulum origin of milk lipid globules obtained using lipid-selective staining procedures. *Protoplasma* 159, 179-183

(18) Valivullah, H, M., Bevan, D, R., Peatt, A., AND Keenan, T, W. (1988) Milk lipid globules: Control of their size distribution. *Proc. Nati. Acad. Sci. U.S.A*. 85, 8775-8779

(19) Keon, B, H., Ghosal, D., Keenan, T, W. (1993) Association of cytosolic lipids with fatty acid synthase from lactating mammary gland. *Int. J. Biochem*. 25, 533-43

(20) Keon, B, H., Ankrapp, D, P., Keenan, T, W. (1994) Cytosolic lipoprotein particles from milk-secreting cells contain fatty acid synthase and interact with endoplasmic reticulum. *Biochim. Biophys. Acta*. 1215, 327-36

(21) Franke, W, W., Heid, H, W., Grund, C., Winter, S., Freudenstein, C., Schmid, E., Jarasch, D., and Keenan, T, W. (1981) Antibodies to the major insoluble milk fat globule membrane-associated protein : Specific location in apical regions of lactating epithelial cells. *J. Cell Biol*. 89, 485-494

(22) Johnson, V, G., Mather, I, H. (1985) Monoclonal antibodies prepared against PAS-I butyrophilin and GP-55 from guinea-pig milk-fat-globule membrane bind specifically to the apical pole of secretory-epithelial cells in lactating mammary tissue. *Exp. Cell Res*. 158, 144-

158
(23) McManaman, J, C., Palmer, C, A., Wright, R, M., and Neville, M, C. (2002) Functional regulation of xanthine oxidoreductase expression and localization in the mouse mammary gland: evidence of a role in lipid secretion. *J. Physiol.* 545, 567–579
(24) Nickerson, S, C. and Keenan, T, W. (1979) Distribution and orientation of microtubules in milk secreting epithelial cells of rat mammary gland. *Cell Tiss. Res.* 202, 303-312
(25) Ohtsubo, T., Rovira, I. I., Starost, M. F., Liu, C., Finkel, T. (2004) Xanthine oxidoreductase is an endogenous regulator of cyclooxygenase-2. *Circulation Res.* 95, 1118-1124
(26) Patton, S. (1974) Reversible suppression of lactation by colchicine. *FEBS* 48, 85-87
(27) Patton S, Stemberger, B, H, Knudson, C, M. The suppression of milk fat globule secretion by colchicine: an effect coupled to inhibition of exocytosis. *Biochim. Biophys. Acta*. 499, 404-10
(28) Nickerson, S, C. and Keenan, T, W. (1980) Role of microtubules in milk secretion — Action of colchicine on microtubules and exocytosis of secretory vesicles in rat mammary epithelial cells. *Cell Tiss. Res.* 207, 361-376
(29) Henderson, A, J and Peaker, M. (1980) The effects of colchicine on milk secretion, mammary metabolism and blood flow in the goat. *Quant. J. Exp. Physiol.* 65, 367-378.
(30) Daudet, F., Augeron, C., Ollivier-Bousquet, M. (1981) Early action of colchicine, ammonium chloride and prolactin, on secretion of milk lipids in the lactating mammary gland. *Eur. J. Cell Biol*. 24, 197-202
(31) Amato, P, A., and Loizzi, R, F. The identification and localization of actin and actin-like filaments in lactating guinea pig mammary gland alveolar cells. *Cell Motility Cytoskel.* 1, 329 – 347
(32) Du, Y., Weed, S. A., Xiong, W. C., Marshall, T. D., and Parsons, J. T. (1998) Identification of a novel cortactin SH3 domain-binding protein and its localization to growth cones of cultured neurons. *Mol. Cell Biol*. 18, 5838-5851.
(33) Loizzi, R, F., de Pont, J, J., Bonting, S,L. (1975) Inhibition by cyclic

AMP of lactose production in lactating guinea pig mammary gland slices. *Biochim. Biophys. Acta.* 392, 20-25.

(34) Patton, S., and Keenan, T, W. (1975) The milk fat globule membrane. *Biochim. Biophys. Acta*. 415, 273-309

(35) Cavaletto, M., Giuffrida, M, G., and Conti, A. (2004) The proteomic approach to analysis of human milk fat globule membrane. *Clin. Chim. Acta*. 347, 41-48

(36) Mather, I, H., Jack, L, J, W., Madara, P, J., Johnson, V, G. (2001) The distribution of MUC1, an apical membrane glycoprotein, in mammary epithelial cells at the resolution of the electron microscope: implications for the mechanism of milk secretion. *Cell Tiss. Res.* 304, 91–101

(37) Keenan, T, W., Olson, D, E and Mollenhauer, H, H. (1970) Origin of the milk fat globule membrane. *J. Dairy Sci*. 54, 295-199

(38) Wooding. F.B.P. (1971). The mechanism of secretion of the milk fat globule. *J. Cell Sci*. 9, 805-821.

(39) Wooding, F. B. P. (1971). The structure of the milk fat globule membrane. *J. Ultrastruct. Res.* 37, 388-400.

(40) Freudenstein, C., Keenan, T. W., Eigel, W. N., Sasaki, M., Stadler, J., and Franke, W.W. (1979). Preparation and characterization of the inner coat associated with fat globule membranes from bovine and human milk. *Exp. Cell Res*. 118, 277–294.

(41) Buchheim, W. (1982). Paracrystalline arrays of milk fat globule membrane-associated proteins as revealed by freeze-fracture. *Naturwissenschaft*. 69, 505-507.

(42) Wu, C, C., Howell, K, E., Neville, M, C., Yates III, J, R., Mcmanaman, J, L. (2000) Proteomics reveal a link between the endoplasmic reticulum and lipid secretory mechanisms in mammary epithelial cells. *Electrophoresis* 21, 3470-3482

(43) Keenan, T, W. and Mather, I, H. (2006) Intracellular origin of milk fat globules and the nature of the milk fat globule membrane. *Adv. Dairy Chem.* 2, 137-171

(44) Spicer, A, P., Rowse, G, J., Lidner, T, K., and Gendler, S, J. (1995) Delayed Mammary Tumor Progression in Muc-1 Null Mice. *J. Biol.*

*Chem*. 270, 30093–30101

(45) Pallesen, L, T., Berglund, L., Rasmussen, L, K., Petersen, T, E., and Rasmussen, J, T. (2002) Isolation and characterization of MUC15, a novel cell membrane-associated mucin. *Eur. J. Biochem*. 269, 2755–2763

(46) Pallesen, L. T., Berglund, L., Rasmussen, L. K., Petersen, T. E., and Rasmussen, J. T. (2002) Isolation and characterization of MUC15, a novel cell membrane-associated mucin. *Eur. J. Biochem*. 269, 2755–2763

(47) Huang, J., Che, M., Huang, Y., Shyu, M., Huang, Y., Wu, Y., Lin, W., Huang, P., Liang, J., Lee, P., and Huang, M. (2009) Overexpression of MUC15 activates extracellular signal-regulated kinase 1/2 and promotes the oncogenic potential of human colon cancer cells. *Carcinogenesis.* 30, 1452–1458.

(48) Harrison R. (2002) Structure and function of xanthine oxidoreductase: where are we now? *Free Radic. Biol. Med.* 15, 774-797

(49) Vorbach, C., Capecchi, M, R., Penninger, J, M. (2006) Evolution of the mammary gland from the innate immune system? *BioEssays.* 28, 606–616

(50) Mather, I, H., Weber, K., and Keenan, T, W. (1976) Membranes of mammary gland. XII. Loosely associated proteins and compositional heterogeneity of bovine milk fat globule membrane. *J. Dairy Sci*. 60, 393-402

(51) Spitsberg, V, L., Matitashvili, E., and Gorewit, R, C. (1995) Association and coexpression of fatty-acid-binding protein and glycoprotein CD36 in the bovine mammary gland. *Eur. J. Biochem*. 230, 872-878

(52) Ghosh, A., Li, W., Febbraio, M., Espinola, R. G., McCrae, K. R., Cockrell, E., Silverstein, R. L. (2008) Platelet CD36 mediates interactions with endothelial cell-derived microparticles and contributes to thrombosis in mice. *J. Clin. Invest.* 118, 1934-43.

(53) Tahar, H., Xiao, X. H., Arend, B., and Abumrad, N. A. (2002) Defective fatty acid uptake modulates insulin responsiveness and metabolic responses to diet in CD36-null mice. *J. Clin. Invest.* 109,

1381–1389
(54) Victor, A. D., Mohammad, A., Fatiha, N., Nicholas, O. D., Andromeda, M. N., Daisy, S., Patrick, T., and Abumrad, N. A. (2005) CD36 deficiency impairs intestinal lipid secretion and clearance of chylomicrons from the blood. *J Clin Invest.* 115, 1290–1297.
(55) Banghart, L, R., Chamberlain, C. W., Velarde, J., Korobko, I. W., Ogg, S. L., Jack, L. J. W., Vakharia, V. N., and Mather, H. I. (1998) Butyrophilin is expressed in mammary epithelial cells from a single-sized messenger RNA as a type I membrane glycoprotein. *J. Biol. Chem.* 273, 4171–4179
(56) Ogg, S. L., Weldon, A. K., Dobbie, L., Smith, A. J. H., and Mather, I. H. (2004) Expression of butyrophilin (Btn1a1) in lactating mammary gland is essential for the regulated secretion of milk-lipid droplets. *Proc. Natl. Acad. Sci. U.S.A.* 101, 10084-10089
(57) Nguyen, T., Liu, X. K., Zhang, Y., and Dong, C. (2006) BTNL2, a butyrophilin-like molecule that functions to inhibit T cell activation. *J. Immunol.* 176, 7354-7360
(58) Guggenmos, J., Schubart, A. S., Ogg, S. L., Andersson, M., Olsson, T., Mather, I. H., and Linington, C. (2004) Antibody cross-reactivity between myelin oligodendrocyte glycoprotein and the milk protein butyrophilin in multiple sclerosis. *J. Immunol.* 172, 661-668
(59) Smith, I. A., Knezevic, B. R., Ammann, J. U., Rhodes, D. A., Aw, D., Palmer, D. B., Mather, I. H. and Trowsdale, J. (2010) BTN1A1, the mammary gland butyrophilin, and BTN2A2 are both inhibitors of T cell activation. *J. Immunol.* 184, 3514-3525
(60) Tazi-Ahnini, R., Henry, J., Offer, C., Bouissou-Bouchouata, C., Mather, I. H., and Pontarotti, P. (1997) Cloning, localization, and structure of new members of the butyrophilin gene family in the juxta-telomeric region of the major histocompatibility complex. *Immunogenetics* 47, 55-63
(61) Woo, J. S., Imm, J, H., Min, C, K., Kim, K, J., Cha, S. S. and Oh, B. H. (2006) Structural and functional insights into the B30.2/SPRY domain. *EMBO J.* 25, 1353–1363
(62) Leo C. J., Anthony H. K., Zahra K., Rhodes, D. A., and Trowsdale, J.

(2007) Structural basis for PRYSPRY-mediated tripartite motif (TRIM) protein function. *Proc. Natl. Acad. Sci. U.S.A.* 104, 6200-6205

(63) Vorbach, C., Scriven, A., and Capecchi, M. R. (2002) The housekeeping gene xanthine oxidoreductase is necessary for milk fat droplet enveloping and secretion: gene sharing in the lactating mammary gland. *Genes Dev.* 16, 3223-3235

(64) Hong, Y. E., and Serrero, G. (1998) Stimulation of adipose differentiation related protein (ADRP) expression by ibuprofen and indomethacin in adipocyte precursors and in adipocytes. *Biochem. J*. 330, 803-809

(65) Brasaemle, D. L., Barber, T., Wolins, N. E., Serrero, G., Blanchette-Mackie, E. J., Londos, C. (1997) Adipose differentiation-related protein is an ubiquitously expressed lipid storage droplet-associated protein. *J. Lipid Res.* 38, 2249–2263.

(66) Russell, T, D., Palmer, C, A., Orlicky, D, J., Fischer, A., Rudolph, M, C., Neville, M, C., and McManaman, J, L. (2007) Cytoplasmic lipid droplet accumulation in developing mammary epithelial cells: roles of adipophilin and lipid metabolism. *J. Lipid Res.* 48, 1463-1475

(67) Atabai, K., Fernandez, R., Huang, X., Ueki, I., Li, Y., Sadatmansoori, S., Smith-Steinhart, C., Zhu, W., Werb, Z. R., and Sheppard, D. (2005) Mfge8 is critical for mammary gland remodeling during involution. *Mol. Biol. Cell* 16, 5528–5537

(68) Jinushi, M., Nakazaki, Y., Dougan, M., Carrasco, D. R., Mihm, M., and Dranoff, G. (2007) MFG-E8-mediated uptake of apoptotic cells by APCs links the pro- and antiinflammatory activities of GM-CSF. *J Clin Invest*. 117, 1902-13.

(69) Robenek, H., Hofnagel, O., Buers, I., Lorkowsky, S., Schnoor, M., Robenek, M. J., Heid, H., Troyer, D., and Severs, N. J. (2006) Butyrophilin controls milk fat globule secretion. *Proc. Natl. Acad. Sci. U.S.A.* 103, 10385-10390

(70) Kreis, T.E. (1986). Microinjected antibodies against the cytoplasmic domain of vesicular stomatitis virus glycoprotein block its transport to the cell surface. *EMBO J*. 5, 931–941.

(71) Russell, T. D., Fischer, A., Beeman, N. E., Freed, E. F., Neville, M. C.,

and Schaack, J. (2003). Transduction of the mammary epithelium with adenovirus vectors *in vivo*. *J. Virol*. 77, 5801-5809

(72) Lucas, A., Gibbs, J. A. H., Lyster, R. L. J., and Baum, J. D. (1978) Creamatocrit: simple clinical technique for estimating fat concentration and energy value of human milk. *Brit. Med. J*. 1, 1018-1020

(73) Sullivan CH, Mather IH, Greenwalt DE, Madara PJ. (1982) Purification of xanthine oxidase from the fat-globule membrane of bovine milk by electrofocusing. *Mol. Cell. Biochem*. 1982 Apr 16;44(1):13-22.

(74) Katherine J. S., Laura E. R, Mehdi A. F, Lisa A. P, Tatiana L. O., and Richard M. W. (2006) Stress activation of mammary epithelial cell xanthine oxidoreductase is mediated by p38 MAPK and CCAAT/enhancer-binding protein-beta. *J. Biol. Chem.* 281, 8545-8558

(75) Kurosaki, M., Zanotta, S., Calzi, M. L., Garattini, E., and Terao, T. (1996) Expression of xanthine oxidoreductase in mouse mammary epithelium during pregnancy and lactation: regulation of gene expression by glucocorticoids and prolactin. *Biochem J*. 319, 801–810.

(76) Russell, T. D., Palmer, C. A., Orlicky, D. J., Fischer, A., Rudolph, M. C., Neville, M. C., and McManaman, J. L. (2007) Cytoplasmic lipid droplet accumulation in developing mammary epithelial cells: roles of adipophilin and lipid metabolism. *J. Lipid Res.* 48, 1463-1475

(77) Orlicky, D. J., and Schaack, J. (2001) Adenovirus transduction of 3T3-L1 cells. *J. Lipid Res.* 42, 460-466

(78) Wooding, F. B. P. (1971) The structure of the milk fat globule membrane. *J. Ultrastruct. Res*. 37, 388-400

(79) Jeong, J., Rao, A, U., Xu, J., Ogg, S, L., Hathout, Y., Fenselau, C., and Mather, I, H. (2009) The PRY/SPRY/B30.2 domain of butyrophilin 1A1 (BTN1A1) binds to xanthine oxidoreductase: Implications for the function of BTN1A1 in the mammary gland and other tissues*. J. Biol. Chem.* 284, 22444-22456

(80) Ishii, T., Aoki, N., Noda, A., Adachi, T., Nakamura, R., and Matsuda,

T. (1995) Carboxyl-terminal cytoplasmic domain of mouse butyrophilin specifically associated with a 150 kDa protein of mammary epithelial cells and milk fat globule membrane. *Biochim. Biophys. Acta* 1245, 285–292

(81) Rao, A. U. (2003) Structural and functional characterization of the cytoplasmic domain of mouse butyrophilin. *Thesis dissertation of University of Maryland*.

(82) Jarasch, E. D., Grund, C., Bruder, G., Heid, H. W., Keenan, T. W., Franke, W. W. (1981) Localization of xanthine oxidase in mammary-gland epithelium and capillary endothelium. *Cell*. 25, 67-82.

(83) Henry, J., Mather, I. H., McDermott, M. F., and Pontarotti, P. (1998) B30.2-like domain proteins: update and new insights into a rapidly expanding family of proteins. *Mol. Biol. Evol.* 15, 1696-1705.

(84) Woo. J., Suh. H., Park. S., and Oh. B (2006) Structural basis for protein recognition by B30.2/SPRY domains. *Mol. Cell*, 24, 967-976

(85) James. L, C., Keeble. A, H., Khan. Z., Rhodes. D, A., and Trowsdale. J. (2007) Structural basis for PRYSPRY-mediated tripartite motif (TRIM) protein function. *Proc. Natl. Acad. Sci. U.S.A. 104,* 6200–6205.

(86) Song, B., Gold, B., O'hUigin, C., Javanbakht, H., Li, X., Stremlau, M., Winkler, C., Dean, M., and Sodroski, J. (2005) The B30.2(SPRY) domain of the retroviral restriction factor TRIM5α exhibits lineage-specific length and sequence variation in primates *J. Virol*. 79**,** 6111-6121

(87) Le, A., Damico, R., Damarla, M., Boueiz, A., Pae, H. H., Skirball, J., Hasan, E., Peng, X., Chesley, A., Crow, M. T., Reddy, S. P., Tuder, R. M., Hassoun, P. M. (2008) Alveolar cell apoptosis is dependent on p38 MAP kinase-mediated activation of xanthine oxidoreductase in ventilator-induced lung injury. *J. Appl. Physiol.* 105, 1282-90.